

N71-28861

NASA TECHNICAL  
MEMORANDUM



NASA TM X-2287

NASA TM X-2287

CASE FILE  
COPY

AERODYNAMIC CHARACTERISTICS  
OF WING-BODY AND LIFTING-BODY  
CONFIGURATIONS OF HYPERSONIC  
CRUISE AIRCRAFT AT MACH 2.30 TO 4.63

*by Lloyd S. Jernell*  
*Langley Research Center*  
*Hampton, Va. 23365*

1. Report No. NASA TM X-2287		2. Government Accession No.		3. Recipient's Catalog No.	
4. Title and Subtitle AERODYNAMIC CHARACTERISTICS OF WING-BODY AND LIFTING-BODY CONFIGURATIONS OF HYPERSONIC CRUISE AIRCRAFT AT MACH 2.30 TO 4.63				5. Report Date July 1971	
				6. Performing Organization Code	
7. Author(s) Lloyd S. Jernell				8. Performing Organization Report No. L-7229	
9. Performing Organization Name and Address NASA Langley Research Center Hampton, Va. 23365				10. Work Unit No. 722-01-10-07	
				11. Contract or Grant No.	
12. Sponsoring Agency Name and Address National Aeronautics and Space Administration Washington, D.C. 20546				13. Type of Report and Period Covered Technical Memorandum	
				14. Sponsoring Agency Code	
15. Supplementary Notes					
16. Abstract  An investigation has been conducted to determine the effects of wing area and body-cross-section ellipticity ratio on the aerodynamic characteristics of a series of delta-planform wing-body configurations representing some of the principal features of a hypersonic cruise aircraft. The effects of body cross-section shape were also investigated for several lifting-body configurations. Data were obtained at angles of attack to approximately 24° for angles of sideslip of 0° and 3°. The Reynolds number was $9.8 \times 10^6$ per meter ( $3 \times 10^6$ per ft).					
17. Key Words (Suggested by Author(s)) Hypersonic aircraft Body cross-section shape Wing-area effects			18. Distribution Statement Unclassified - Unlimited		
19. Security Classif. (of this report) Unclassified		20. Security Classif. (of this page) Unclassified		21. No. of Pages 79	22. Price* \$3.00

\* For sale by the National Technical Information Service, Springfield, Virginia 22151

AERODYNAMIC CHARACTERISTICS OF WING-BODY AND LIFTING-BODY  
CONFIGURATIONS OF HYPERSONIC CRUISE AIRCRAFT

AT MACH 2.30 TO 4.63

By Lloyd S. Jernell  
Langley Research Center

SUMMARY

An investigation has been conducted at Mach numbers from 2.30 to 4.63 to determine the effects of wing area and body-cross-section ellipticity ratio on the aerodynamic characteristics of a series of delta-planform wing-body models which represent some of the principal features of a hypersonic cruise aircraft. The effects of body cross-section shape were also investigated for several lifting-body configurations.

For relatively large wing area, body ellipticity ratio had little effect on either the static longitudinal stability margin or the lift-curve slope. As wing area was decreased, however, increased ellipticity ratio led to substantial decreases in the static margin and to significant increases in the lift-curve slope. Similarly, for large wing area there was little effect of body shape on the lateral aerodynamic characteristics. Decreases in wing area, however, generally led to increases in the directional stability derivative and to increases in the effective dihedral with increased ellipticity ratio. Although the zero-lift drag coefficients of the wing-body and lifting-body configurations were not significantly affected by body cross-section shape, increased ellipticity ratio did lead to improved lift-drag ratios.

INTRODUCTION

Preliminary studies of the feasibility of hypersonic cruise aircraft indicate that the first generation of such aircraft will probably be designed to cruise at a Mach number near 6.0 (ref. 1). At this early stage of consideration, an optimum configuration for such a vehicle has not been determined. It is generally believed, however, that the aircraft will be characterized by an air-breathing propulsion system which utilizes liquid-hydrogen fuel. Although this fuel has favorable heat-sink characteristics and high energy content per unit weight, its low density will necessitate provisions for relatively large fuel-tank volume.

Generalized models of large-volume configurations which are considered amenable to hypersonic cruise flight have been investigated in a number of small wind tunnels at

relatively low Reynolds number. The purpose of this investigation is to provide complementary aerodynamic data obtained at considerably higher Reynolds numbers on model configurations which represent some of the principal features of a hypersonic cruise vehicle. The primary model series considered in the investigation was a relatively large-volume delta-planform wing-body configuration. The model had interchangeable wings and bodies such that the effects of wing area and body cross-section shape on the longitudinal and lateral aerodynamic characteristics could be considered. Also investigated was a series of lifting-body configurations of varying cross-section ellipticity ratio.

The wing-body and lifting-body models were tested in the Langley Unitary Plan wind tunnel at Mach numbers from 2.30 to 4.63 and at a Reynolds number of  $9.8 \times 10^6$  per meter ( $3 \times 10^6$  per ft). Although the maximum Mach number of the tests ( $M = 4.63$ ) is somewhat below the probable hypersonic design Mach number of 6.0, the aerodynamic trends presented should be useful in the design of future hypersonic vehicles.

## SYMBOLS

The aerodynamic characteristics in pitch and sideslip are referred to the stability-axis and body-axis systems, respectively. The moment centers for the wing-body models are located at the 50-percent root-chord station (model center line) of the respective wings. The moment centers of the lifting bodies have the same longitudinal location as those for the small-wing configurations. (See figs. 1(a) and 1(b).) Also, the force and moment coefficients of the lifting bodies are based on the reference area and dimensions of the small wing.

$A_b$	fuselage base area
$a$	major axis of elliptic-body cross section
$\frac{a}{b}$	ellipticity ratio
$b$	minor axis of elliptic-body cross section
$b_w$	wing span
$C_D$	drag coefficient, $\frac{\text{Drag}}{qS}$
$C_{D,0}$	zero-lift drag coefficient
$C_L$	lift coefficient, $\frac{\text{Lift}}{qS}$

$C_{L\alpha}$	lift-curve slope at $\alpha \approx 0$ , $\frac{\partial C_L}{\partial \alpha}$ , per degree
$C_l$	rolling-moment coefficient, $\frac{\text{Rolling moment}}{qSb_w}$
$C_{l\beta}$	effective dihedral parameter, $\frac{\Delta C_l}{\Delta \beta}$ , per degree
$C_m$	pitching-moment coefficient, $\frac{\text{Pitching moment}}{qS\bar{c}}$
$C_{mC_L}$	static margin, $\frac{\partial C_m}{\partial C_L}$
$C_n$	yawing-moment coefficient, $\frac{\text{Yawing moment}}{qSb_w}$
$C_{n\beta}$	directional stability parameter, $\frac{\Delta C_n}{\Delta \beta}$ , per degree
$C_Y$	side-force coefficient, $\frac{\text{Side force}}{qS}$
$C_{Y\beta}$	side-force parameter, $\frac{\Delta C_Y}{\Delta \beta}$ , per degree
$c_r$	wing root chord
$\bar{c}$	wing mean geometric chord
L/D	lift-drag ratio
$(L/D)_{\max}$	maximum lift-drag ratio
$l$	fuselage length
M	Mach number
q	dynamic pressure
S	wing area
$S_p$	wing-body or lifting-body planform area

x	distance from fuselage nose
$\alpha$	angle of attack, referred to body center line, degrees
$\beta$	angle of sideslip, referred to body center line, degrees

Designations of model components:

B <sub>1</sub>	circular cross-section fuselage, $\frac{a}{b} = 1$
B <sub>2</sub>	elliptic cross-section fuselage, $\frac{a}{b} = 2$
B <sub>3</sub>	elliptic cross-section fuselage, $\frac{a}{b} = 3$
B <sub>4</sub>	elliptic cross-section lifting body, $\frac{a}{b} = 2.175$
B <sub>5</sub>	elliptic cross-section lifting body, $\frac{a}{b} = 3.025$
B <sub>6</sub>	elliptic cross-section lifting body, $\frac{a}{b} = 3.822$
V	vertical tail
W <sub>1</sub>	large wing
W <sub>2</sub>	intermediate-size wing
W <sub>3</sub>	small wing

## APPARATUS AND METHODS

### Models

Drawings of the wing-body models are shown in figure 1(a). The three mating fuselages, shown superimposed on each wing, had cross sections ranging from circular to elliptic, with the elliptic sections having ellipticity ratios of 2 and 3. The wings, which were of delta planform, had a leading-edge sweep angle of  $70^\circ$  and double-wedge airfoil sections with a maximum thickness of 4 percent of the local chord at the 50-percent-chord station. The wings were sized to represent wing loadings of 1915, 3352, and 4788 N/m<sup>2</sup> (40, 70, and 100 lb/ft<sup>2</sup>) at  $M = 6$  and an altitude of 30 480 meters (100 000 ft). Drawings of the lifting-body models, which had elliptic cross sections with ellipticity ratios of 2.175, 3.025,

and 3.822, are shown in figure 1(b). Details of the vertical tail (used for all models) are provided in figure 1(c). The tail was positioned vertically so that the leading edge of the root chord coincided with each body surface. Pertinent geometric parameters for both the wing-body and lifting-body configurations are tabulated in table I. The major- and minor-axis coordinates used for the construction of the wing-body fuselages and the lifting bodies are provided in tables II and III, respectively. A photograph depicting a typical model installation is shown in figure 2.

### Tunnel

The investigation was conducted in both the low and high Mach number test sections of the Langley Unitary Plan wind tunnel, which is a continuous-flow, variable-pressure facility. The test sections are 1.22 meters (4 ft) square by approximately 2.13 meters (7 ft) in length. The nozzles leading to the test sections are of the asymmetric sliding-block type which permits a continuous variation in Mach number from about 1.5 to 2.9 and 2.3 to 4.7 in the low and high Mach number test sections, respectively.

### Measurements, Corrections, and Tests

The aerodynamic forces and moments were measured by means of a sting-supported, six-component strain-gage balance housed within the model body. Base pressure measurements obtained from static orifices located within the base cavity were used to adjust drag coefficient to a condition of free-stream static pressure at the model base. The angles of attack and sideslip were corrected for the deflection of the model support system due to aerodynamic load. The angle of attack was also corrected for tunnel flow angularity.

The tests were conducted at Mach numbers from 2.30 to 4.63 and a Reynolds number of  $9.84 \times 10^6$  per meter ( $3.0 \times 10^6$  per ft). The dewpoint was maintained below  $239^\circ \text{K}$  ( $-30^\circ \text{F}$ ) to prevent tunnel moisture condensation effects. The angle-of-attack range was from approximately  $-4^\circ$  to  $24^\circ$  for angles of sideslip of  $0^\circ$  and  $3^\circ$ . A limited number of tests were also conducted for an angle-of-sideslip range from about  $-4^\circ$  to  $6^\circ$  for angles of attack of  $0^\circ$  and  $8^\circ$ .

Boundary-layer transition strips composed of either carborundum or sand embedded in a plastic adhesive were placed 30.5 millimeters (1.20 in.) rearward of the nose apex and 10 millimeters (0.4 in.) rearward (streamwise) of the wing and tail leading edges. For the investigations in the low Mach number test section ( $M = 2.36$  and  $2.86$ ), 1.6-millimeter-wide (0.06-in.) strips of No. 50 carborundum grains having an average diameter of approximately 0.33 millimeter (0.013 in.) were used. The investigations in the high Mach number test section ( $M = 2.30, 2.96, 3.95,$  and  $4.63$ ) were conducted using No. 35 sand grains having an average diameter of approximately 0.56 millimeter

(0.022 in.). The sand particles were placed individually with a spacing perpendicular to the free stream of approximately 3 particle diameters.

## DISCUSSION

The basic longitudinal aerodynamic characteristics of the wing-body configurations are presented in figures 3 to 5. The pitching-moment coefficient is essentially linear for the large-wing-area configuration but becomes progressively nonlinear as wing area is decreased. This nonlinearity is further aggravated by increasing the ellipticity ratio of the body cross section. The lift curves (variation of  $C_L$  with  $\alpha$ ) exhibit near-linear variations, particularly those for the larger wing area configurations and at the lower Mach numbers. The basic longitudinal characteristics of the lifting-body configurations are presented in figure 6. Both the pitching-moment coefficient and lift curves exhibit abrupt changes in slope in the region near  $\alpha = 4^\circ$ , especially at the lower Mach numbers.

The summary of the static margin (fig. 7) indicates only small effects of ellipticity ratio on the static margin of the large-wing ( $W_1$ ) configurations. However, these effects become prominent as wing area is decreased, and a considerable decrease in static margin is obtained as  $a/b$  is increased. There is essentially no effect of body shape on the static margin of the lifting bodies. The effects of ellipticity ratio on the lift-curve slope  $C_{L\alpha}$  are negligible for the large-wing configurations but become significant as wing area is decreased, with the lift-curve slope increasing as the magnitude of ellipticity ratio is increased. (See fig. 8.) The values of the lift-curve slope show the expected decrease as Mach number is increased. The lifting bodies show considerable increase in  $C_{L\alpha}$  as  $a/b$  is increased but little effect due to Mach number.

The zero-lift drag coefficients for both the wing-body and lifting body show only small effects due to body shape but show the expected decrease with increasing Mach number. (See fig. 9.)

As expected, the configurations with the greater wing areas exhibit larger maximum lift-drag ratios. (See fig. 10.) The maximum lift-drag ratio is further enhanced by the flatter fuselages (larger values of  $a/b$ ). At the higher Mach numbers the wing-body configurations show the usual decrease in lift-drag ratio as Mach number is increased; however,  $(L/D)_{\max}$  for the lifting-body configurations reaches maximum values at Mach numbers of about 4.0 to 4.3.

Some of the basic lateral aerodynamic characteristics are presented in figures 11 to 16 for angles of attack of  $0^\circ$  and  $8^\circ$ . These data were obtained primarily to ascertain the degree of linearity of the basic parameters when used as a function of the sideslip angle  $\beta$ . With few exceptions, these data are essentially linear within the range of  $\beta$

considered. Hence, the remaining lateral data are evaluated in terms of the stability derivatives obtained from  $\alpha$  polars at  $\beta = 0^\circ$  and  $3^\circ$ .

The large wing configuration shows little effect of body shape on the lateral aerodynamic characteristics (fig. 17). However, as wing area is decreased (figs. 18 and 19) there is generally an increase in  $C_{n\beta}$  and a decrease in  $C_{l\beta}$  (increase in effective dihedral) as cross-section ellipticity ratio is increased. The effects of body cross-section shape on the lateral stability derivatives of the lifting-body configurations (fig. 20) are relatively small.

## CONCLUSIONS

An investigation has been conducted to determine the effects of wing area and body cross-section shape on the aerodynamic characteristics of a series of wing-body configurations representing a range of hypersonic cruise aircraft. The effects of body cross-section shape were also investigated for several lifting-body configurations. The conclusions are summarized as follows:

1. The effects of body-cross-section ellipticity ratio on the static margin of the large-wing configuration are small. However, these effects become prominent as wing area is decreased, and a decrease in static margin is obtained as ellipticity ratio is increased.
2. The effects of body-cross-section ellipticity ratio on the lift-curve slope are negligible for the large-wing configuration but become significant as wing area is decreased, with the lift-curve slope increasing as the magnitude of ellipticity ratio is increased.
3. The zero-lift drag coefficients for both the wing-body and lifting body show only small effects due to body shape.
4. The maximum lift-drag ratios of all configurations increase as ellipticity ratio is increased.
5. The large-wing configuration shows little effect of body shape on the lateral aerodynamic characteristics. However, as wing area is decreased there is generally an increase in the directional stability parameter and a decrease in the effective dihedral parameter (increase in effective dihedral) as the ellipticity ratio is increased.

Langley Research Center,  
National Aeronautics and Space Administration,  
Hampton, Va., May 26, 1971.

## REFERENCE

1. Jarlett, F. E.: Performance Potential of Hydrogen Fueled, Airbreathing Cruise Aircraft. Vol. 2 - Phase I Studies. Rep. No. GD/C DCB66-00412 (Contract NAS 2-3180), Gen. Dyn./Convair Div., May 6, 1966.

TABLE I.- MODEL GEOMETRIC PARAMETERS

$$[A_b = 0.0062 \text{ m}^2 \text{ (0.067 ft}^2\text{)}]$$

Configuration	a/b	S		S <sub>p</sub>		$\bar{c}$		b <sub>w</sub>		c <sub>r</sub>	
		m <sup>2</sup>	ft <sup>2</sup>	m <sup>2</sup>	ft <sup>2</sup>	cm	in.	cm	in.	cm	in.
B <sub>1</sub> W <sub>1</sub>	1	0.2928	3.152	0.3127	3.366	59.79	23.54	65.30	25.71	89.69	35.31
B <sub>2</sub> W <sub>1</sub>	2	↓	↓	.3228	3.475	↓	↓	↓	↓	↓	↓
B <sub>3</sub> W <sub>1</sub>	3	↓	↓	.3336	3.591	↓	↓	↓	↓	↓	↓
B <sub>1</sub> W <sub>2</sub>	1	0.1578	1.699	0.2002	2.155	43.89	17.28	47.93	18.87	65.84	25.92
B <sub>2</sub> W <sub>2</sub>	2	↓	↓	.2208	2.377	↓	↓	↓	↓	↓	↓
B <sub>3</sub> W <sub>2</sub>	3	↓	↓	.2382	2.564	↓	↓	↓	↓	↓	↓
B <sub>1</sub> W <sub>3</sub>	1	0.1080	1.163	0.1616	1.739	36.32	14.30	39.65	15.61	54.48	21.45
B <sub>2</sub> W <sub>3</sub>	2	↓	↓	.1884	2.028	↓	↓	↓	↓	↓	↓
B <sub>3</sub> W <sub>3</sub>	3	↓	↓	.2093	2.253	↓	↓	↓	↓	↓	↓
B <sub>4</sub>	2.175	<sup>1</sup> 0.1080	<sup>1</sup> 1.163	0.1456	1.567	<sup>1</sup> 36.32	<sup>1</sup> 14.30	<sup>1</sup> 39.65	<sup>1</sup> 15.61		
B <sub>5</sub>	3.025	↓	↓	.1717	1.848	↓	↓	↓	↓		
B <sub>6</sub>	3.822	↓	↓	.1930	2.077	↓	↓	↓	↓		

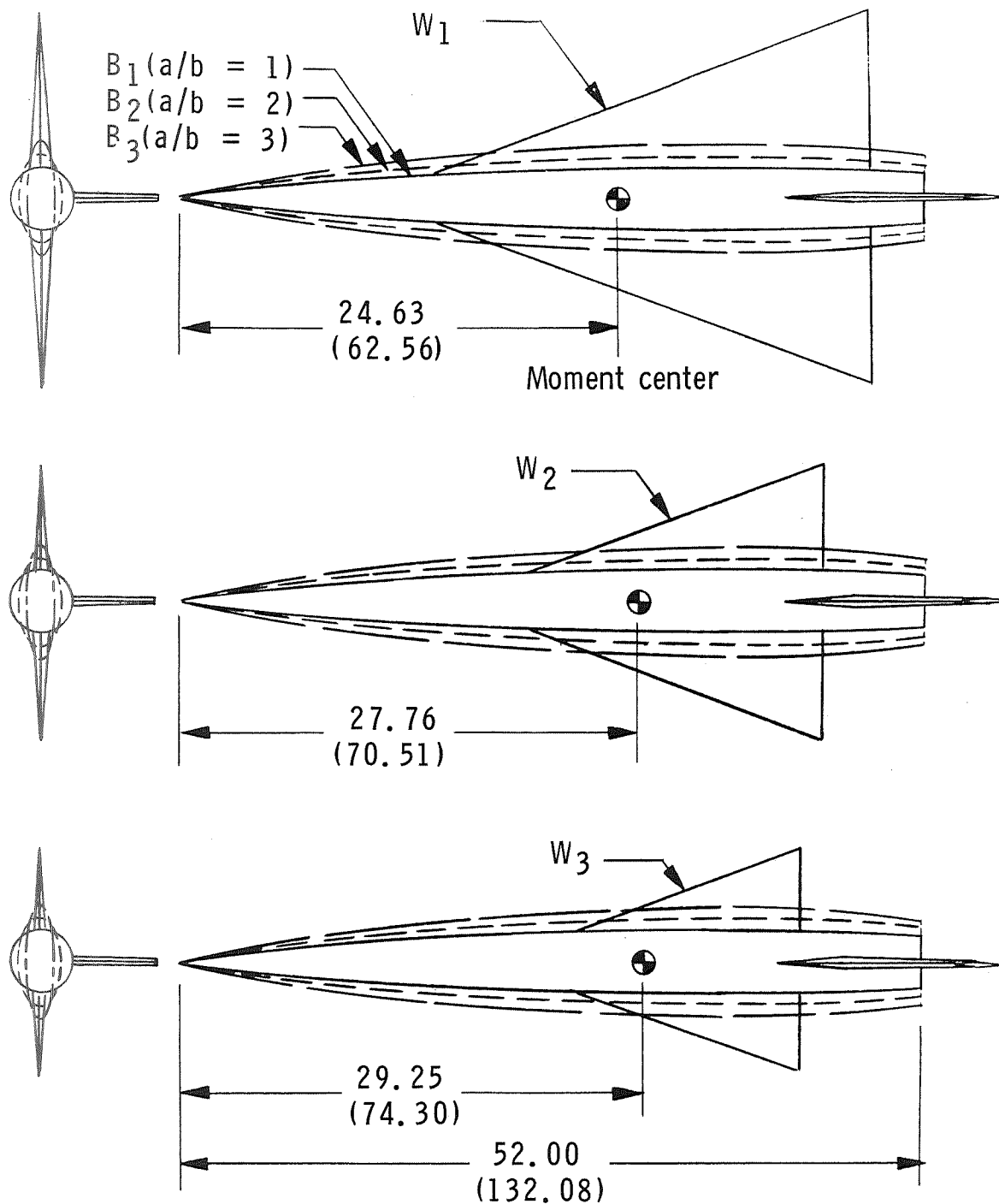
<sup>1</sup>W<sub>3</sub> wing geometry used.

TABLE II.- BODY COORDINATES FOR WING-BODY MODELS

x/l	$\frac{a}{b} = 1$	$\frac{a}{b} = 2$		$\frac{a}{b} = 3$	
	$\frac{a}{l} = \frac{b}{l}$	a/l	b/l	a/l	b/l
0	0	0	0	0	0
.0350	.0056	.0079	.0040	.0097	.0032
.0700	.0095	.0134	.0067	.0165	.0055
.1400	.0157	.0222	.0111	.0272	.0091
.2100	.0209	.0296	.0148	.0362	.0121
.2800	.0257	.0364	.0182	.0411	.0148
.3500	.0295	.0417	.0209	.0511	.0170
.4200	.0331	.0468	.0234	.0573	.0191
.4900	.0362	.0511	.0256	.0626	.0209
.5600	.0387	.0547	.0274	.0670	.0223
.6300	.0406	.0575	.0287	.0704	.0235
.6650	.0413	.0584	.0292	.0715	.0238
.7000	.0417	.0589	.0295	.0722	.0241
.8216	.0417	.0589	.0295	.0722	.0241
.8269	.0416	.0588	.0294	.0720	.0240
.8402	.0414	.0585	.0292	.0716	.0239
.8536	.0410	.0579	.0290	.0709	.0236
.8669	.0405	.0572	.0286	.0701	.0234
.8935	.0392	.0554	.0277	.0679	.0226
.9201	.0377	.0533	.0267	.0653	.0218
.9467	.0361	.0511	.0255	.0626	.0209
.9601	.0354	.0500	.0250	.0613	.0204
.9734	.0347	.0490	.0245	.0601	.0200
.9867	.0342	.0483	.0242	.0592	.0197
1.0000	.0338	.0478	.0239	.0585	.0195

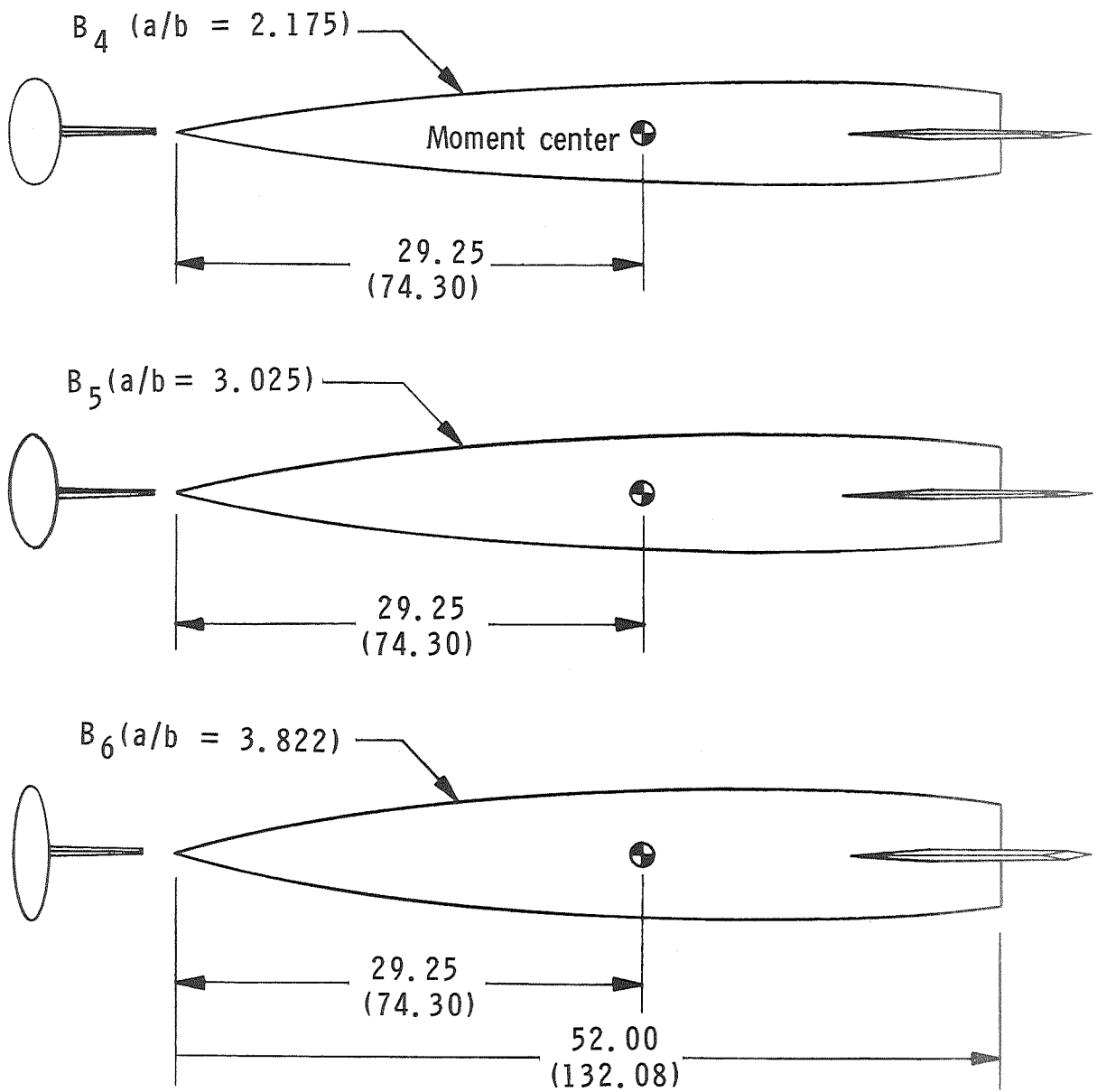
TABLE III.- BODY COORDINATES FOR LIFTING-BODY MODELS

x/l	$\frac{a}{b} = 2.175$		$\frac{a}{b} = 3.025$		$\frac{a}{b} = 3.822$	
	a/l	b/l	a/l	b/l	a/l	b/l
0	0	0	0	0	0	0
.0041	.0082	.0038	.0097	.0032	.0109	.0029
.0822	.0138	.0063	.0162	.0054	.0182	.0048
.1643	.0230	.0106	.0271	.0090	.0305	.0080
.2465	.0308	.0142	.0364	.0120	.0409	.0107
.3286	.0377	.0173	.0444	.0147	.0499	.0131
.4108	.0435	.0200	.0513	.0170	.0577	.0151
.4930	.0489	.0225	.0577	.0191	.0648	.0170
.5751	.0534	.0246	.0630	.0208	.0708	.0185
.6573	.0570	.0262	.0673	.0222	.0756	.0198
.7394	.0599	.0275	.0707	.0234	.0794	.0208
.8216	.0614	.0283	.0725	.0240	.0815	.0213
.8269	.0613	.0282	.0723	.0239	.0813	.0213
.8402	.0610	.0280	.0719	.0238	.0808	.0212
.8536	.0604	.0278	.0712	.0236	.0801	.0210
.8669	.0597	.0274	.0704	.0223	.0791	.0207
.8935	.0578	.0266	.0682	.0225	.0766	.0200
.9201	.0556	.0256	.0656	.0217	.0737	.0193
.9467	.0533	.0245	.0628	.0208	.0706	.0185
.9601	.0522	.0240	.0615	.0203	.0691	.0181
.9734	.0512	.0235	.0603	.0199	.0678	.0177
.9867	.0504	.0232	.0594	.0196	.0668	.0175
1.0000	.0498	.0229	.0587	.0194	.0660	.0173



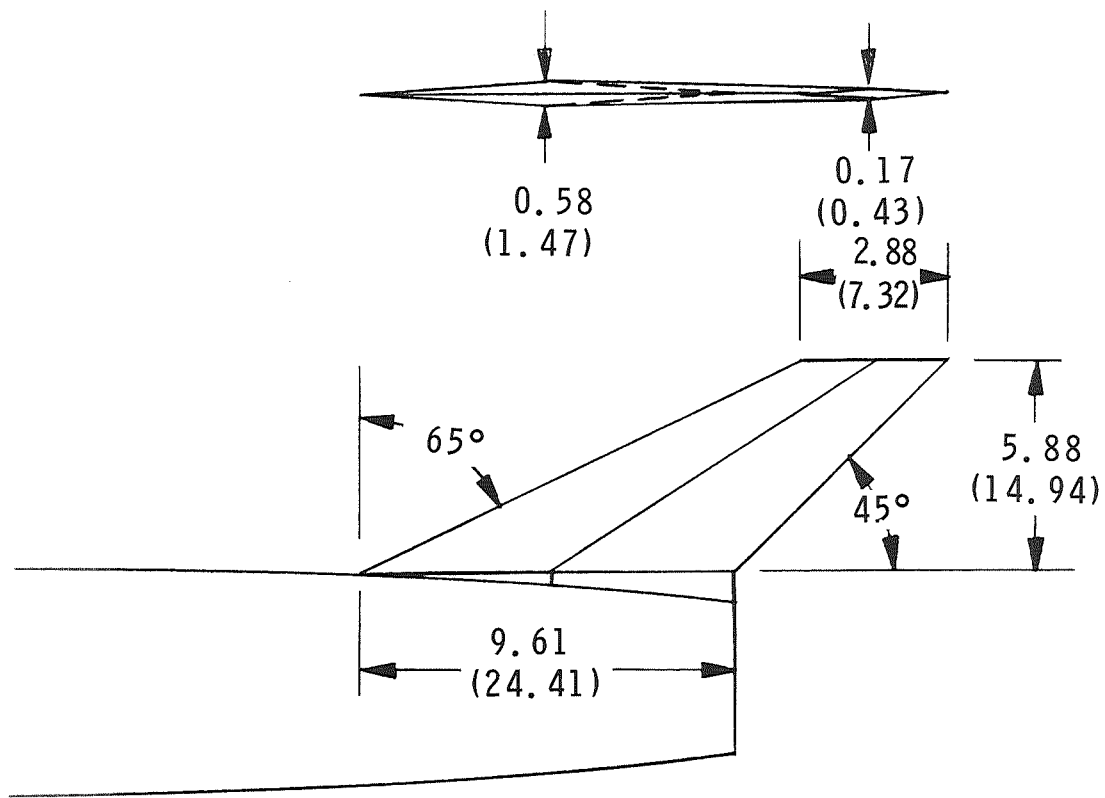
(a) Wing-body models.

Figure 1.- Model drawings for hypersonic cruise vehicle. Linear dimensions are given in inches and parenthetically in centimeters.



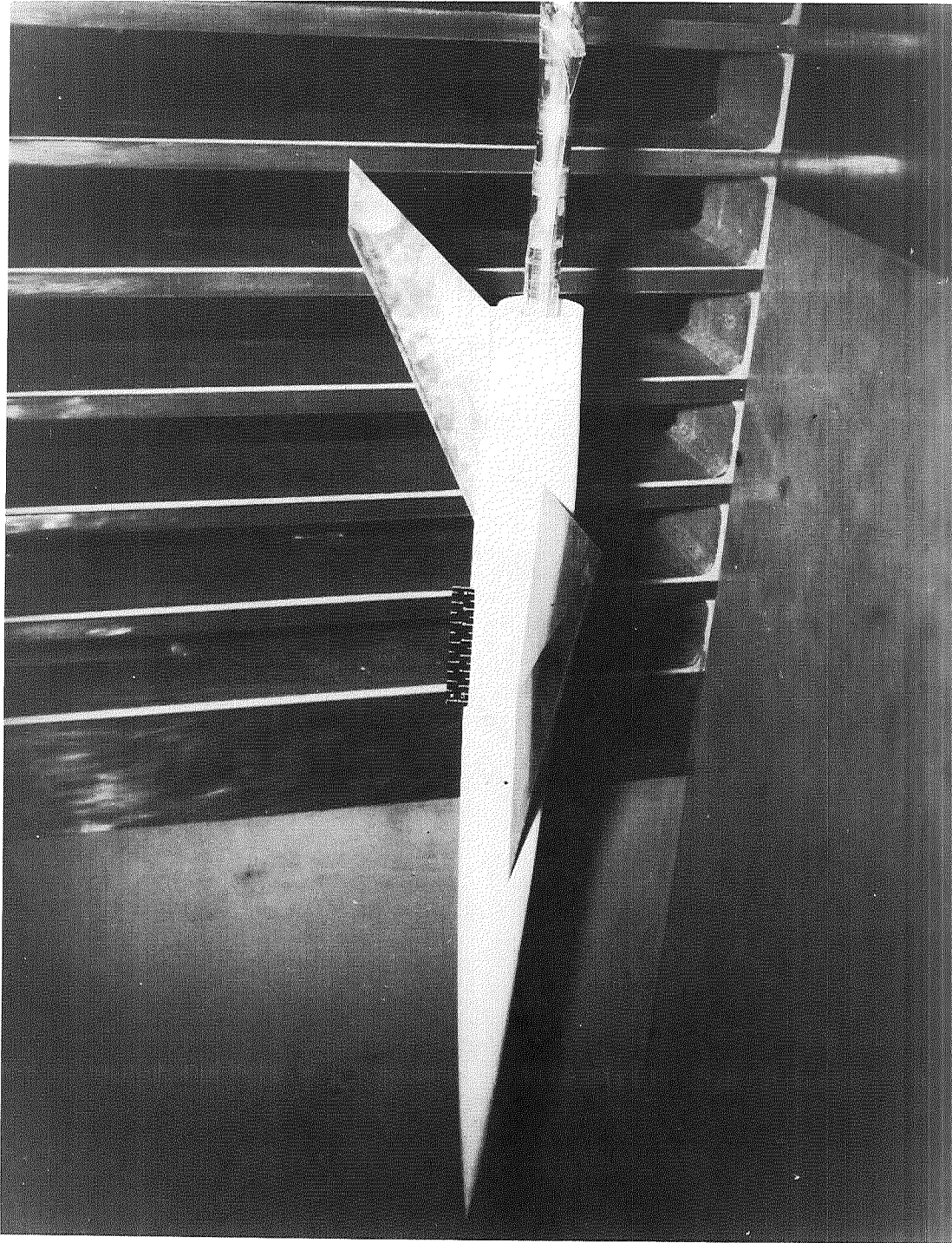
(b) Lifting-body models.

Figure 1.- Continued.



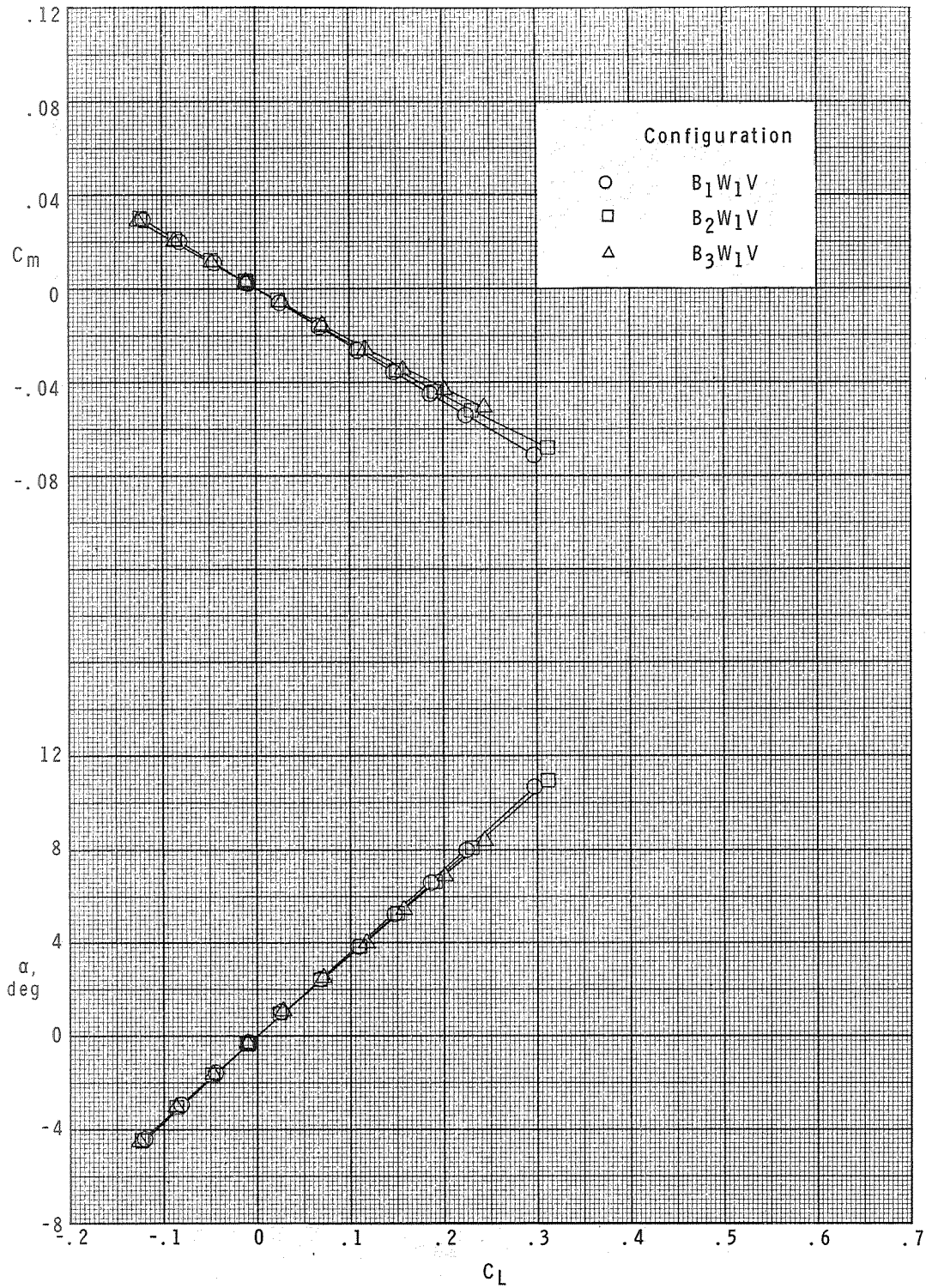
(c) Vertical tail.

Figure 1.- Concluded.



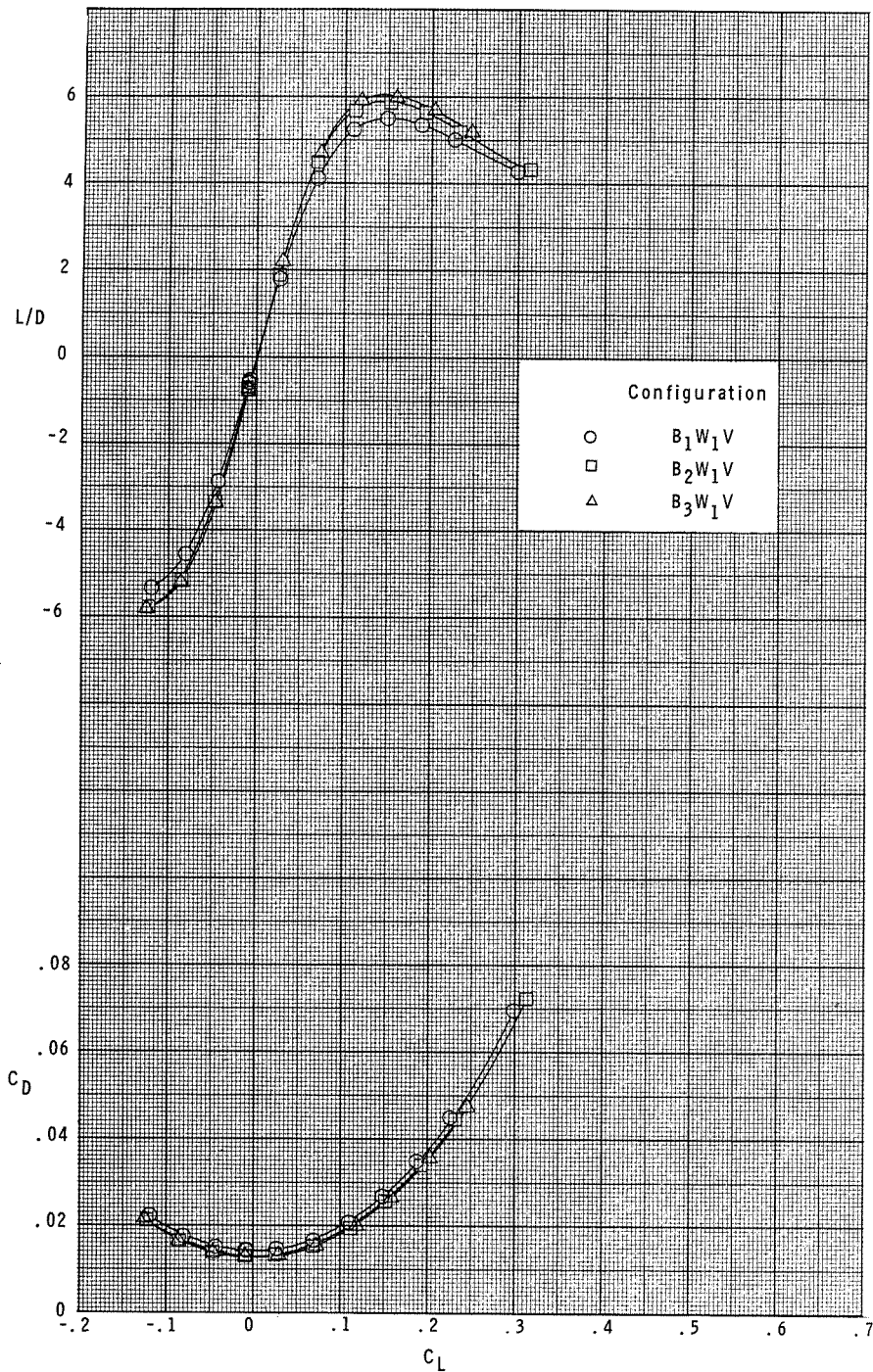
L-67-4538

Figure 2.- Typical model installation (configuration B<sub>1</sub>W<sub>2</sub>V).



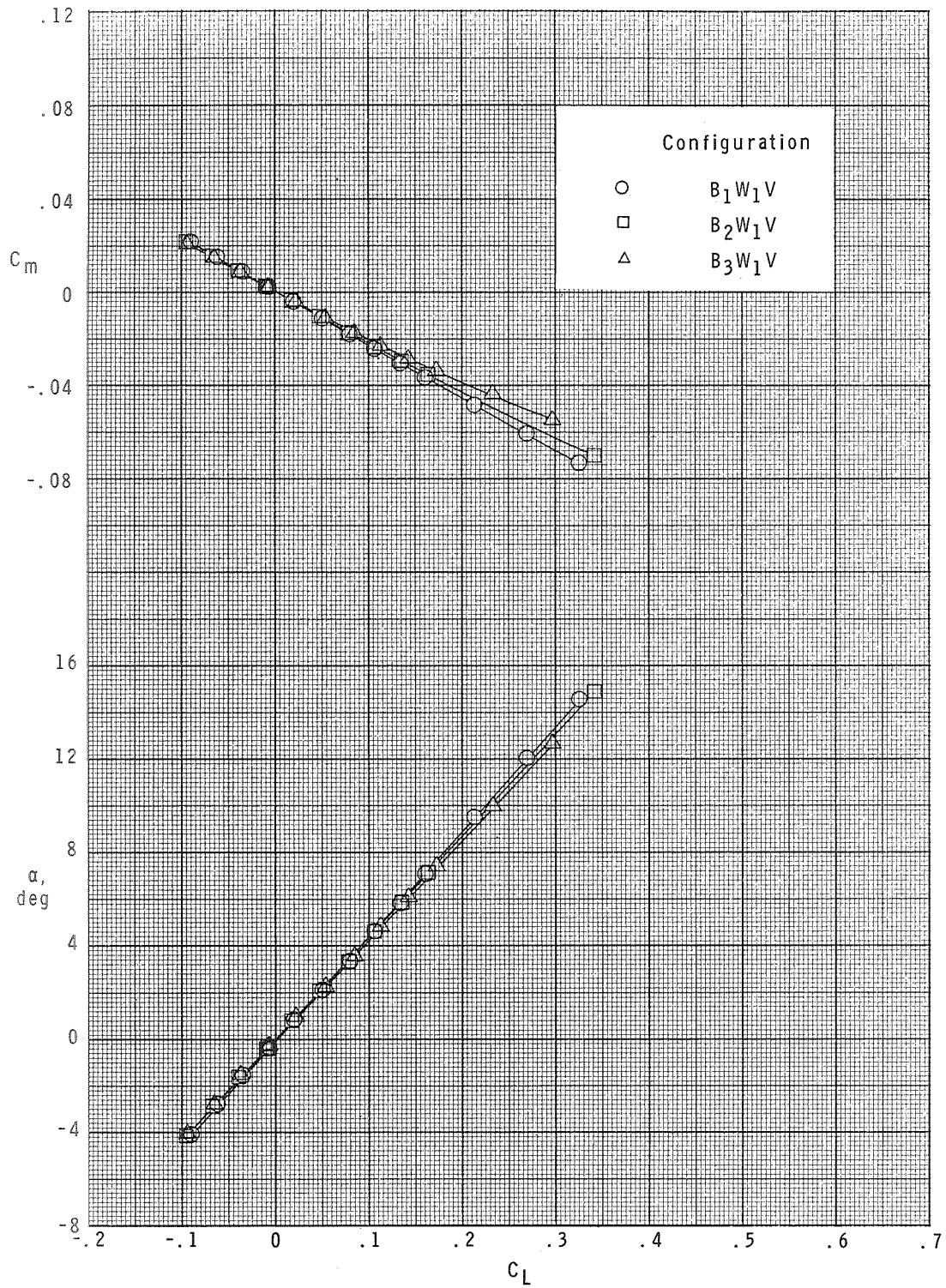
(a)  $M = 2.30$ .

Figure 3.- Longitudinal aerodynamic characteristics of model with large ( $W_1$ ) wing.



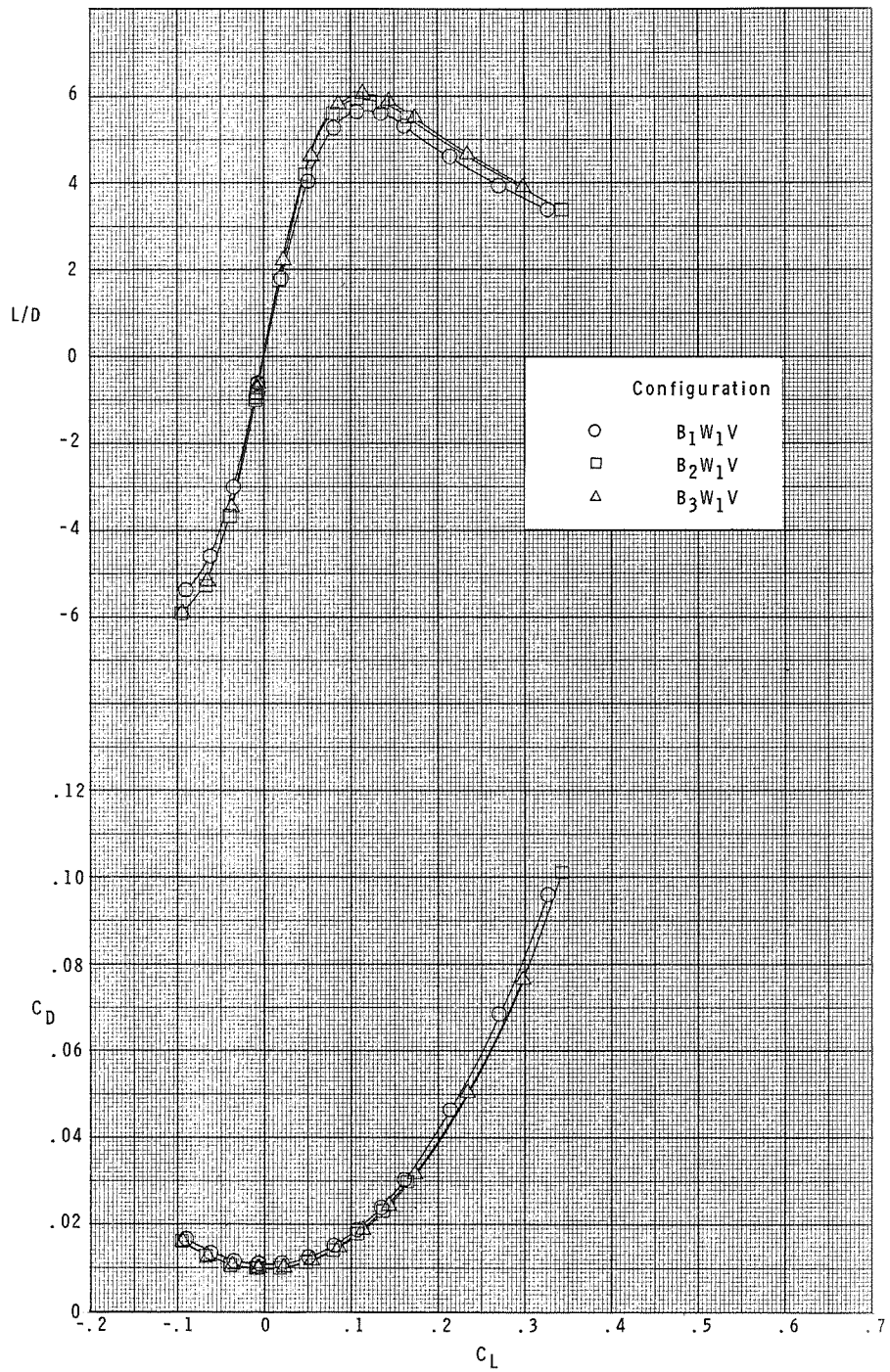
(a)  $M = 2.30$ . Concluded.

Figure 3.- Continued.



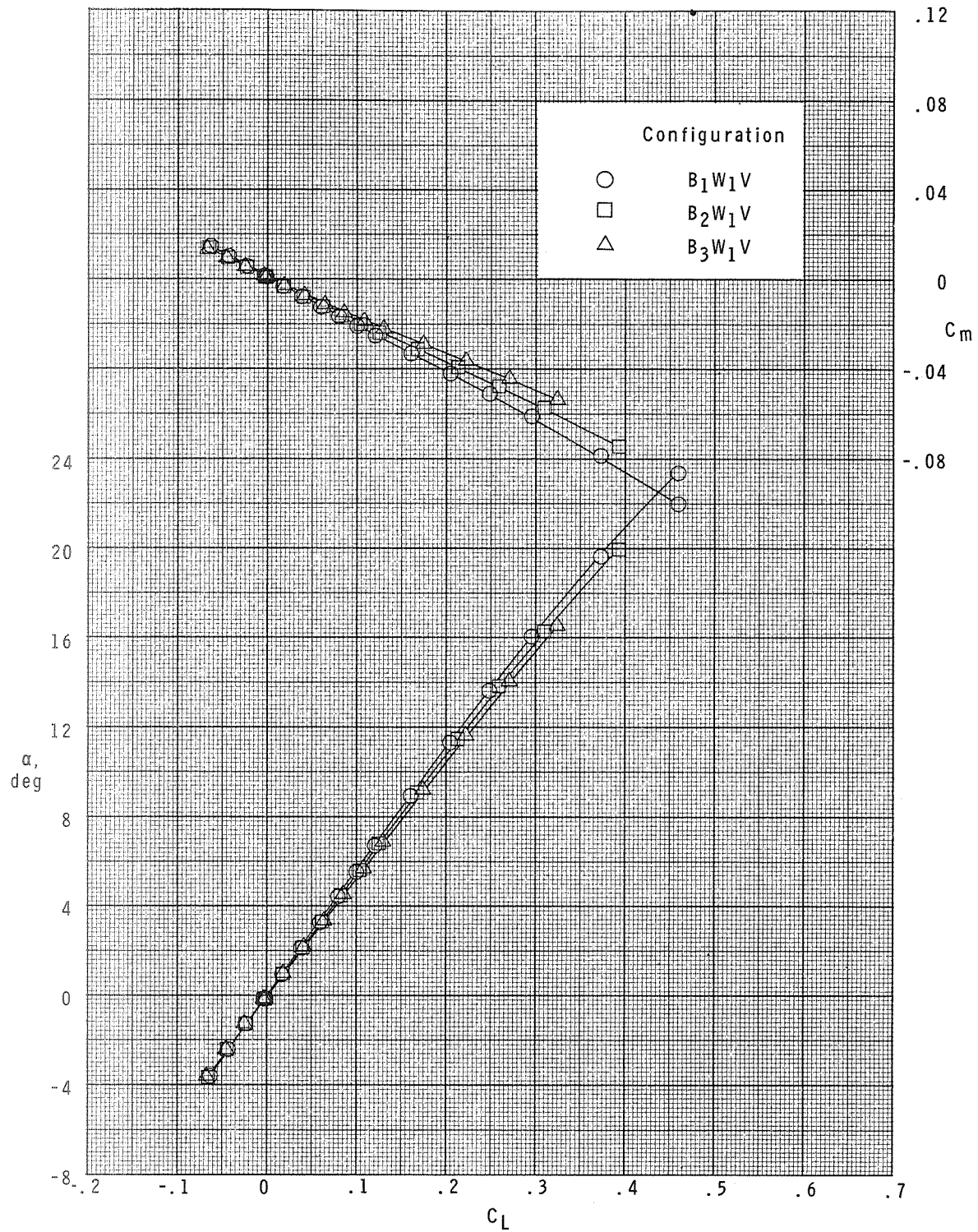
(b)  $M = 2.96$ .

Figure 3.- Continued.



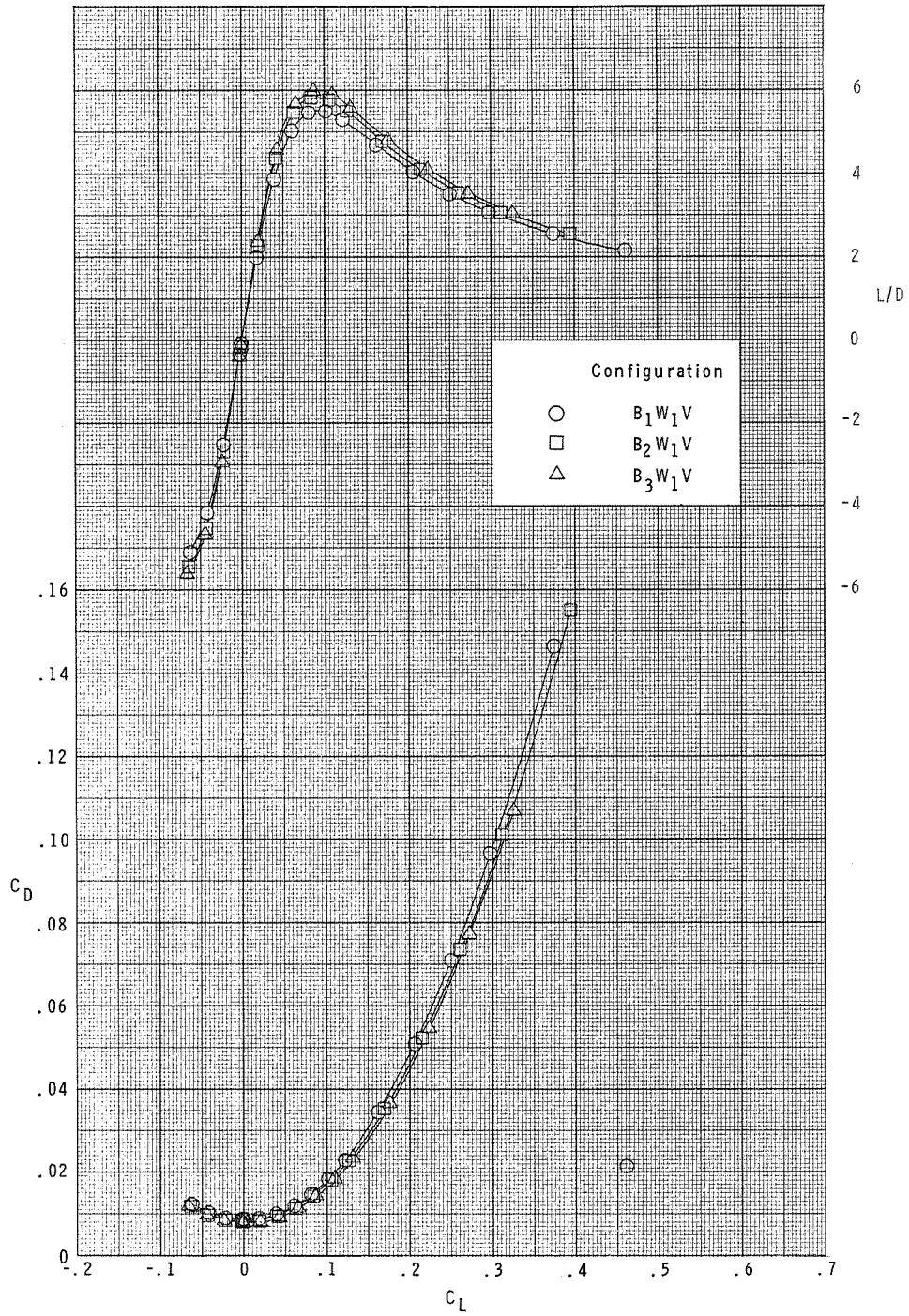
(b)  $M = 2.96$ . Concluded.

Figure 3.- Continued.



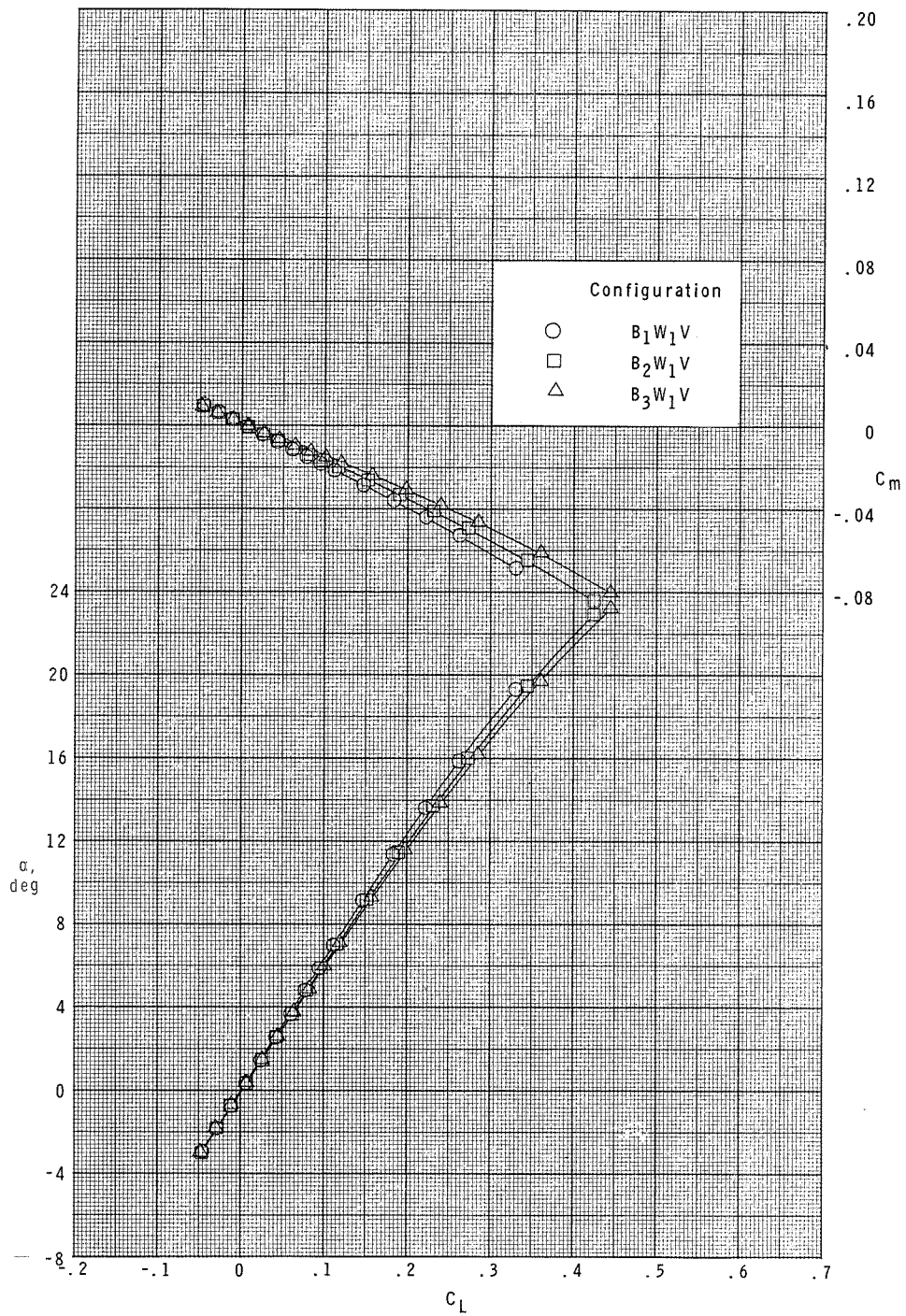
(c)  $M = 3.95$ .

Figure 3.- Continued.



(c)  $M = 3.95$ . Concluded.

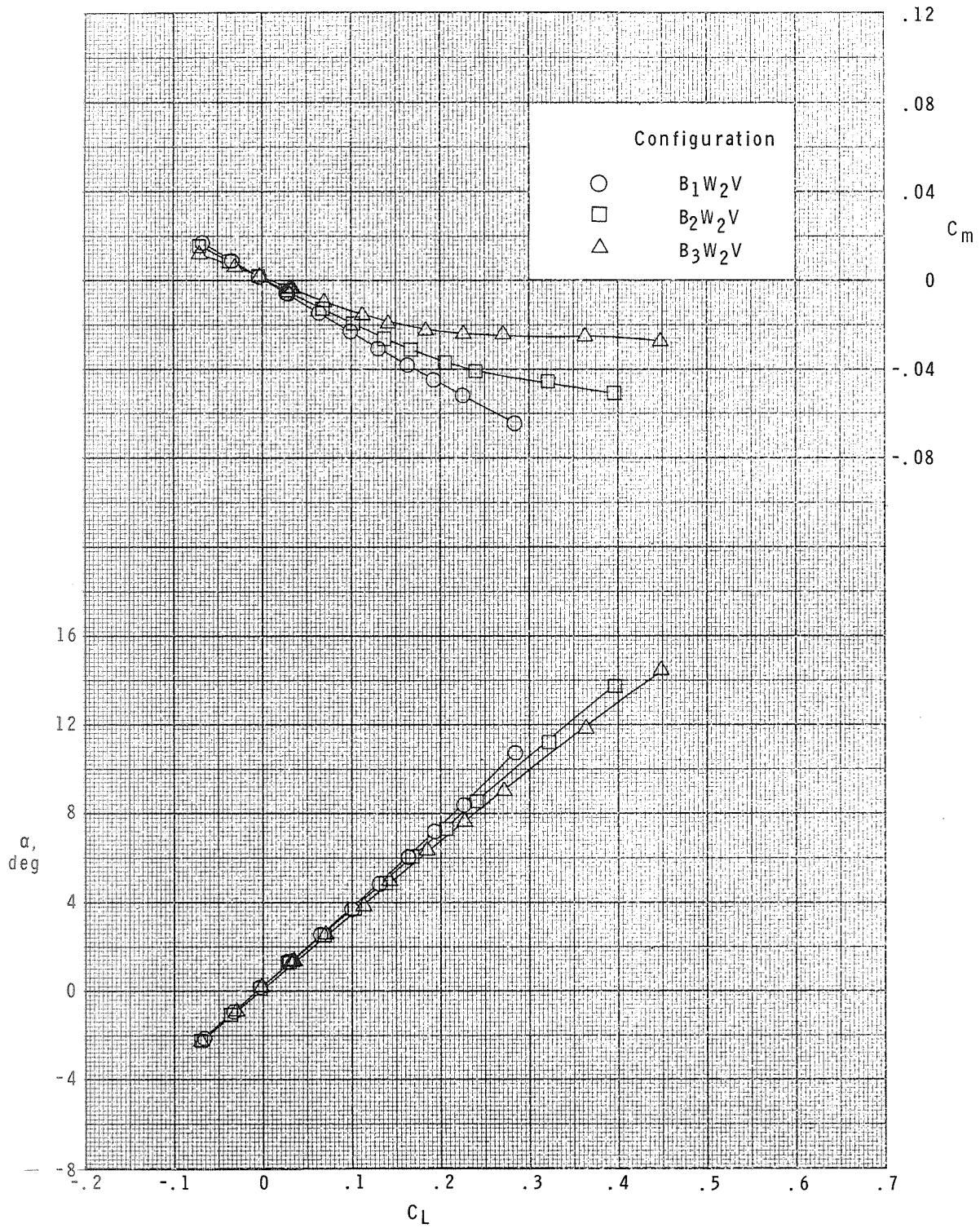
Figure 3.- Continued.



(d)  $M = 4.63$ .

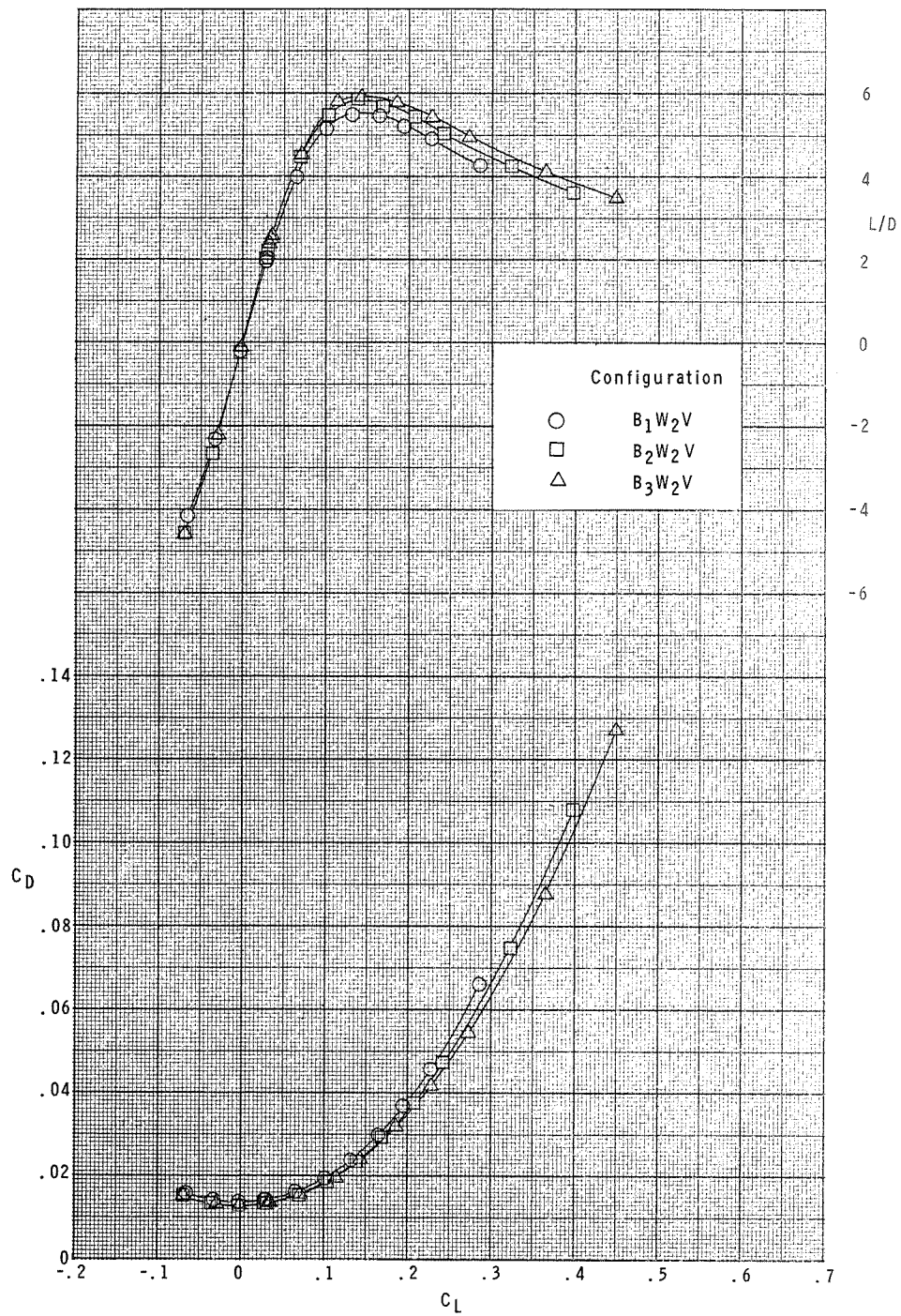
Figure 3.- Continued.





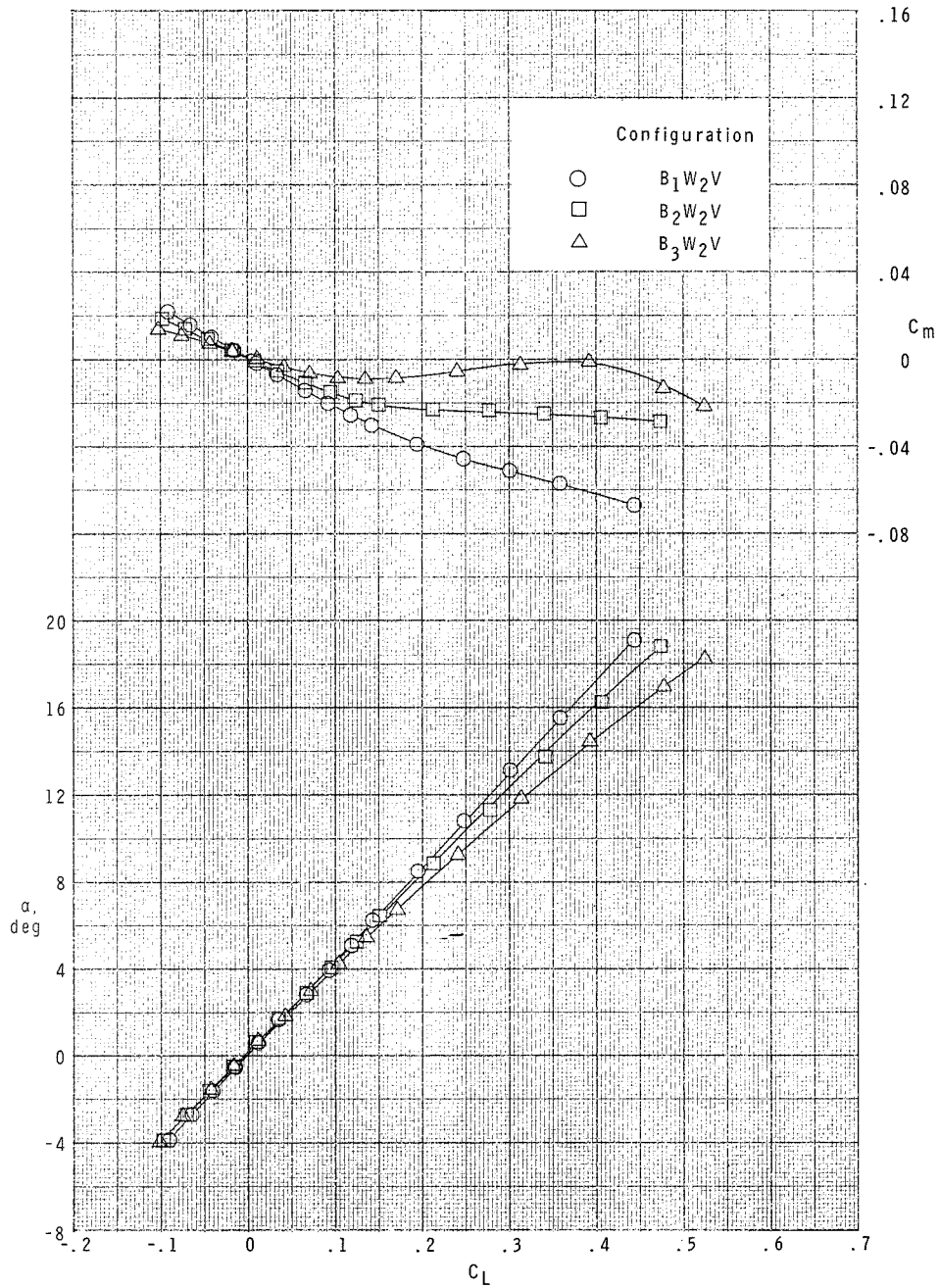
(a)  $M = 2.36$ .

Figure 4.- Longitudinal aerodynamic characteristics of model with intermediate-size ( $W_2$ ) wing.



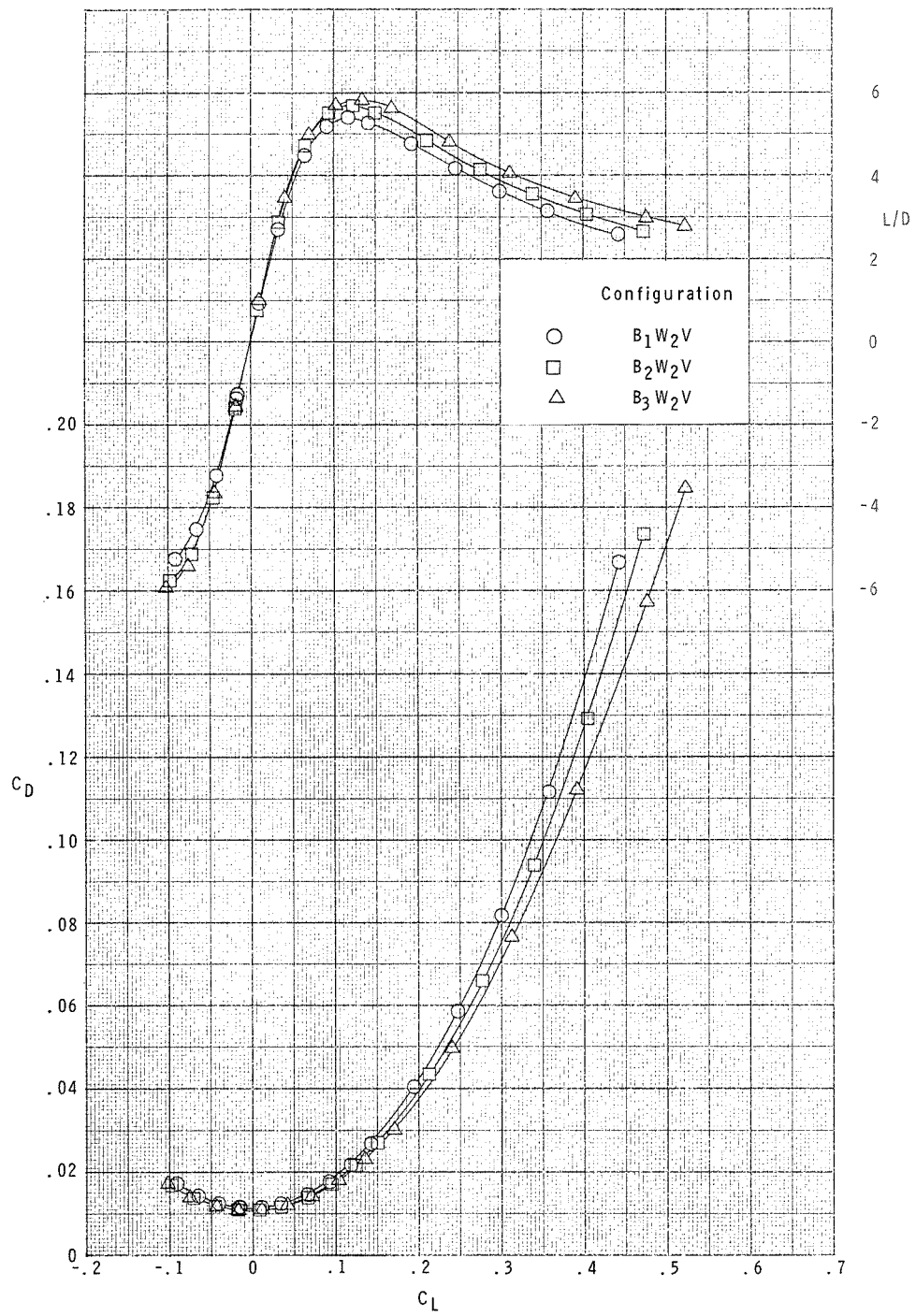
(a)  $M = 2.36$ . Concluded.

Figure 4.- Continued.



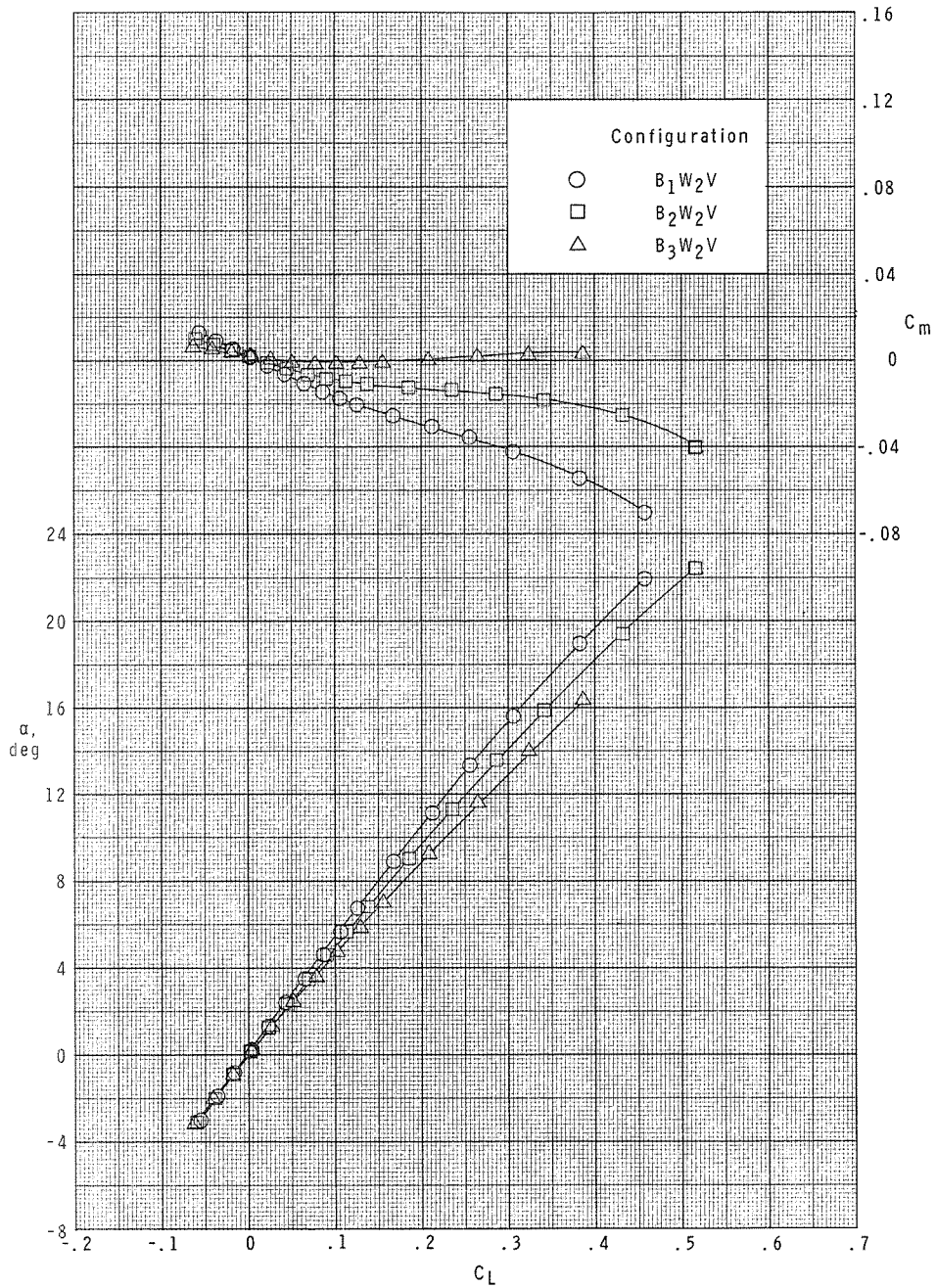
(b)  $M = 2.86$ .

Figure 4.- Continued.



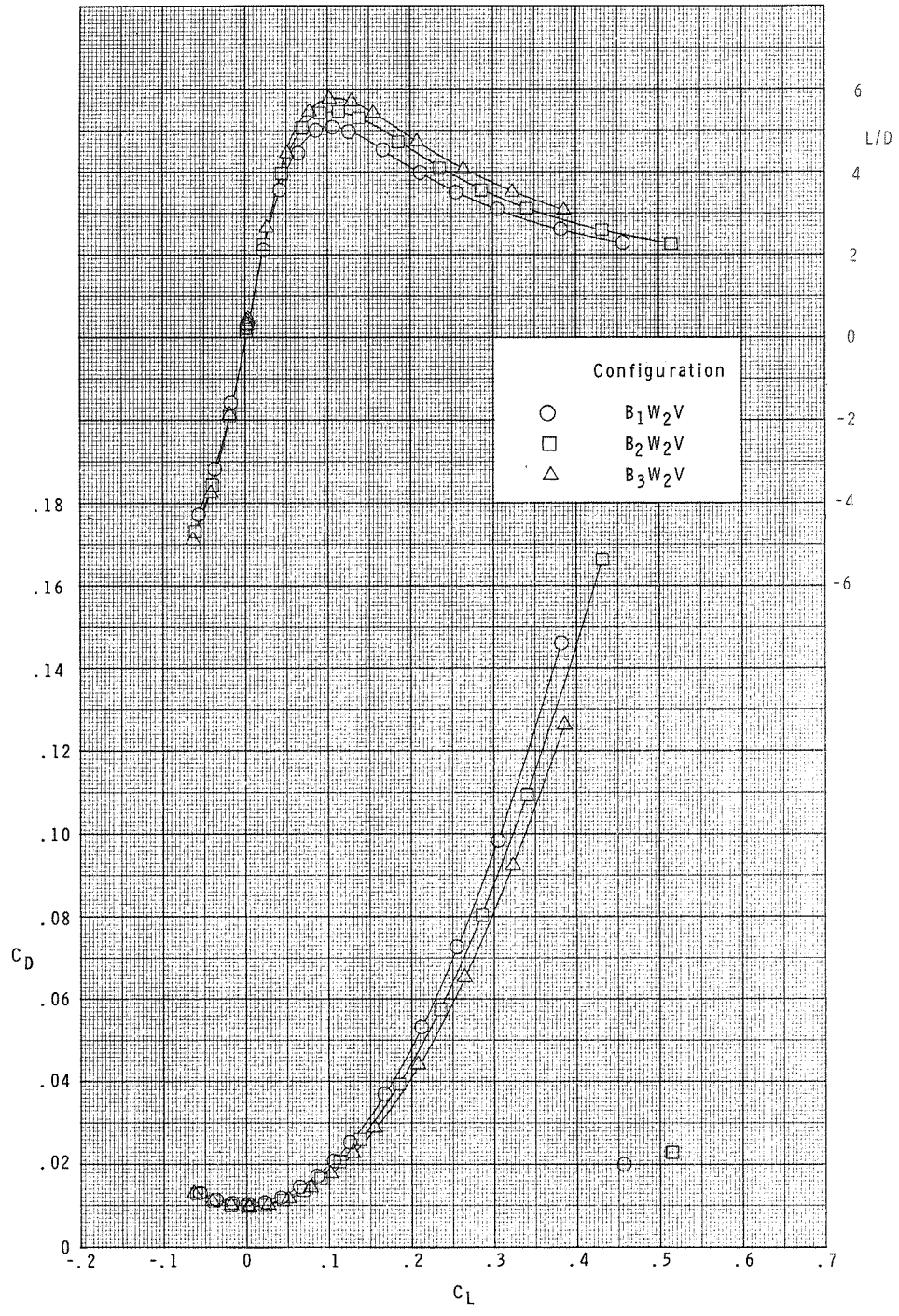
(b)  $M = 2.86$ . Concluded.

Figure 4.- Continued.



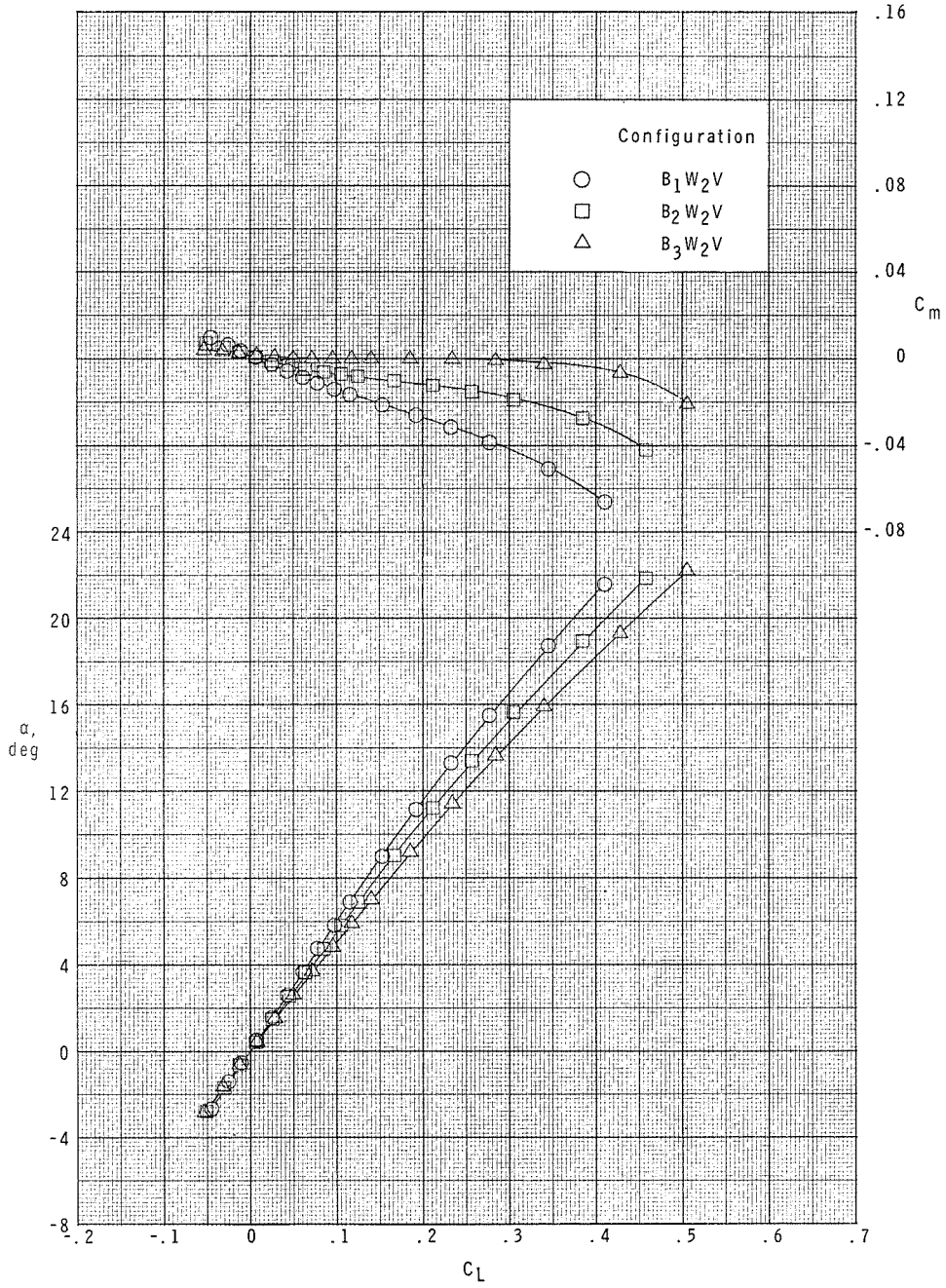
(c)  $M = 3.95$ .

Figure 4.- Continued.



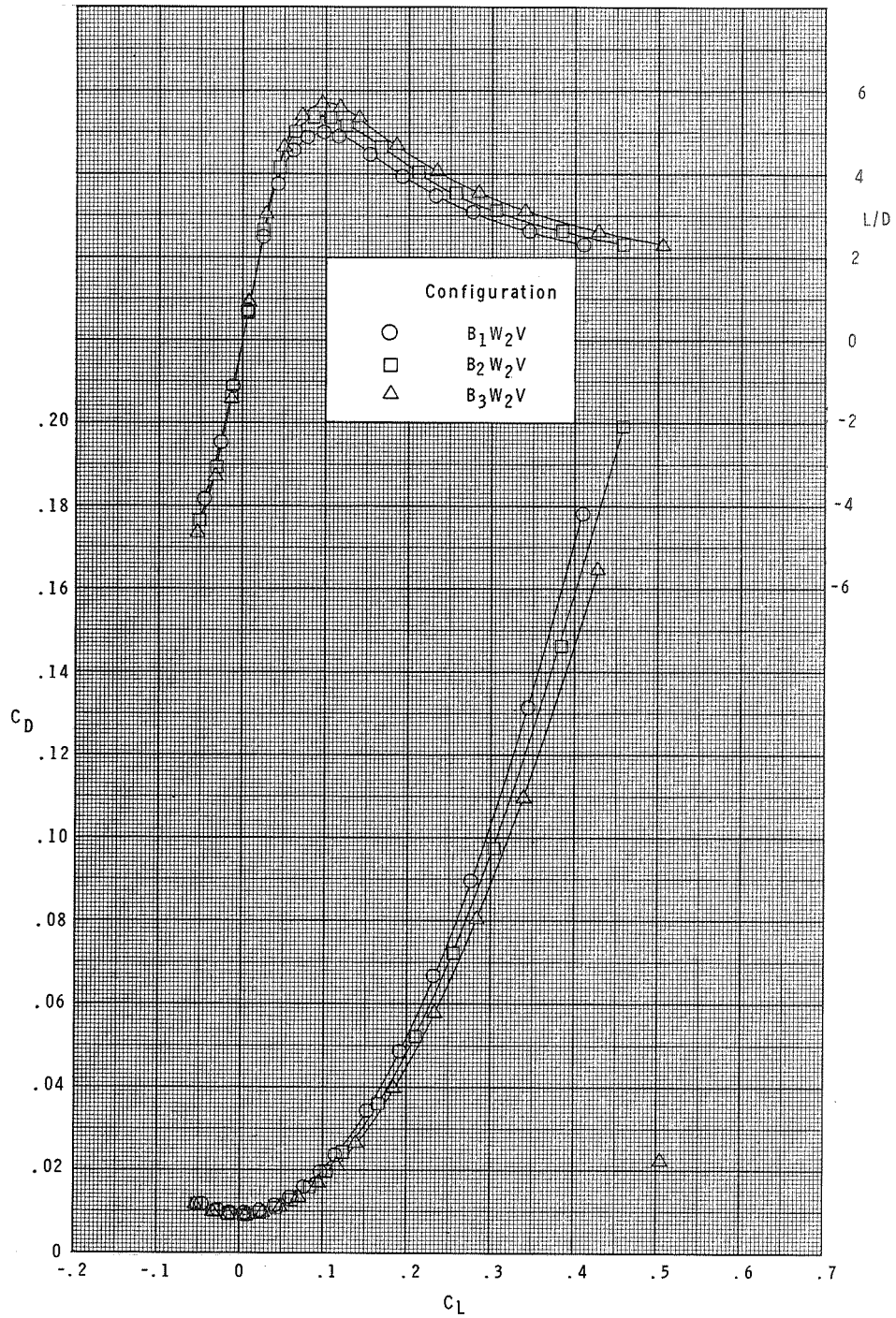
(c)  $M = 3.95$ . Concluded.

Figure 4.- Continued.



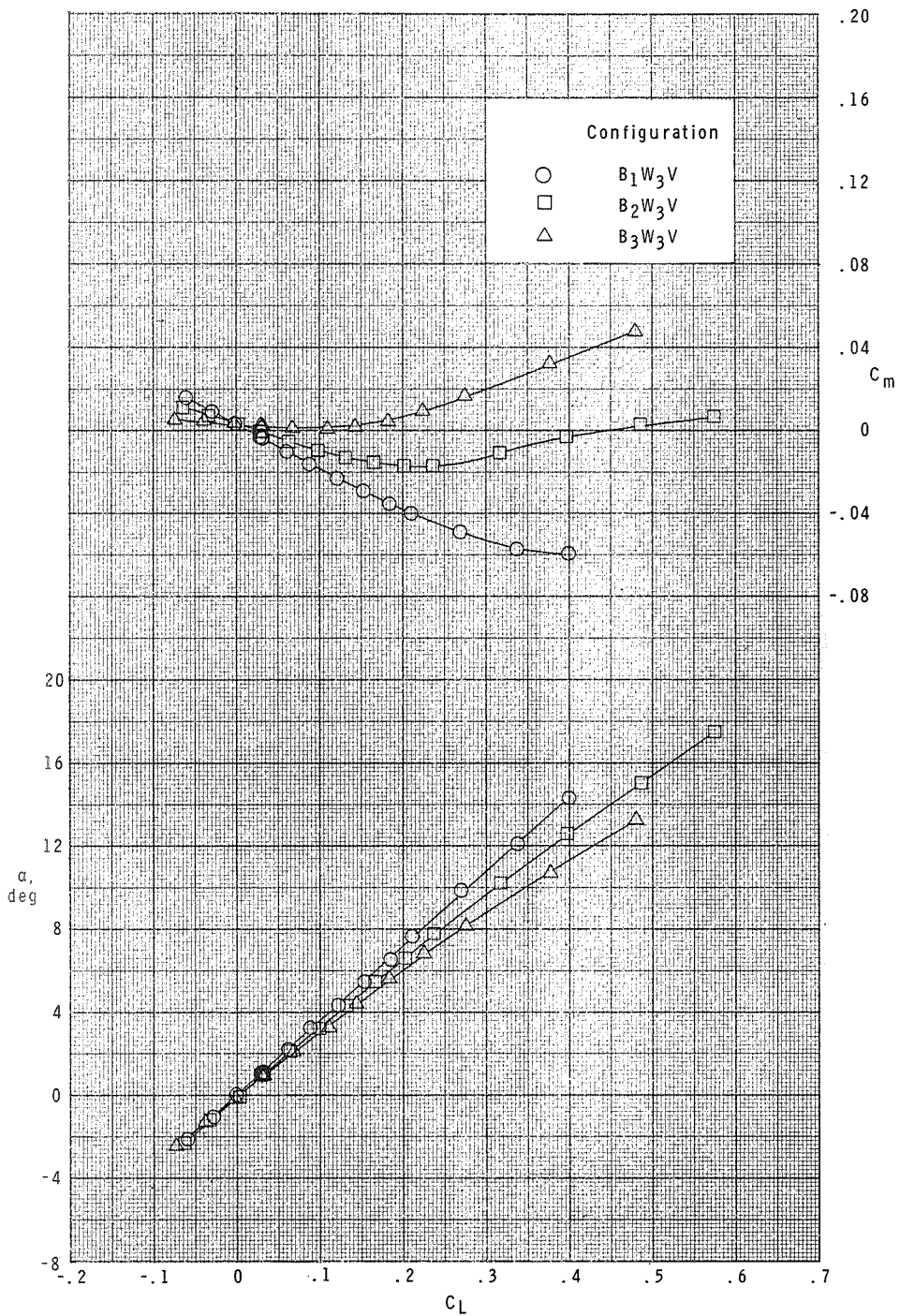
(d)  $M = 4.63$ .

Figure 4.- Continued.



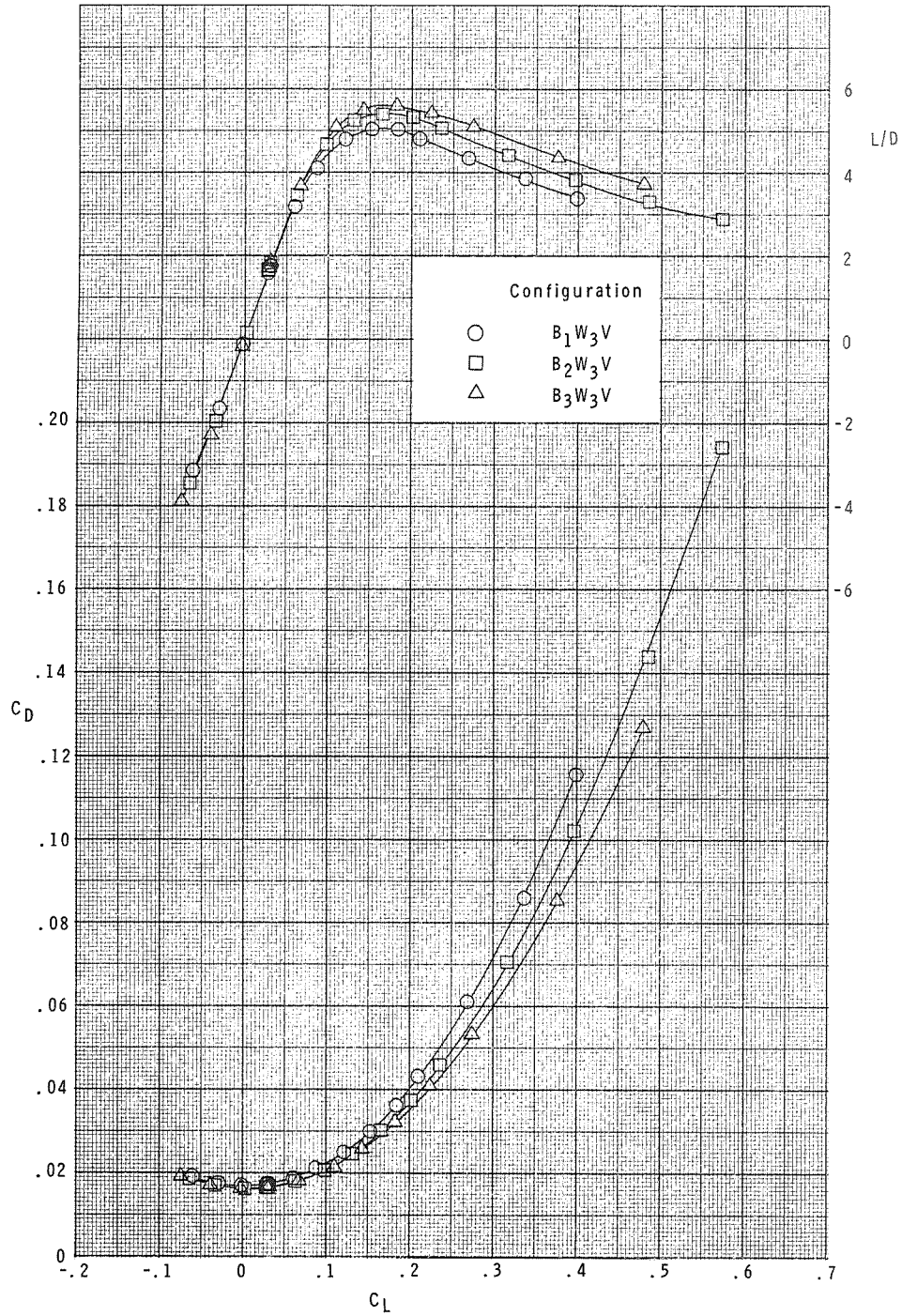
(d)  $M = 4.63$ . Concluded.

Figure 4.- Concluded.



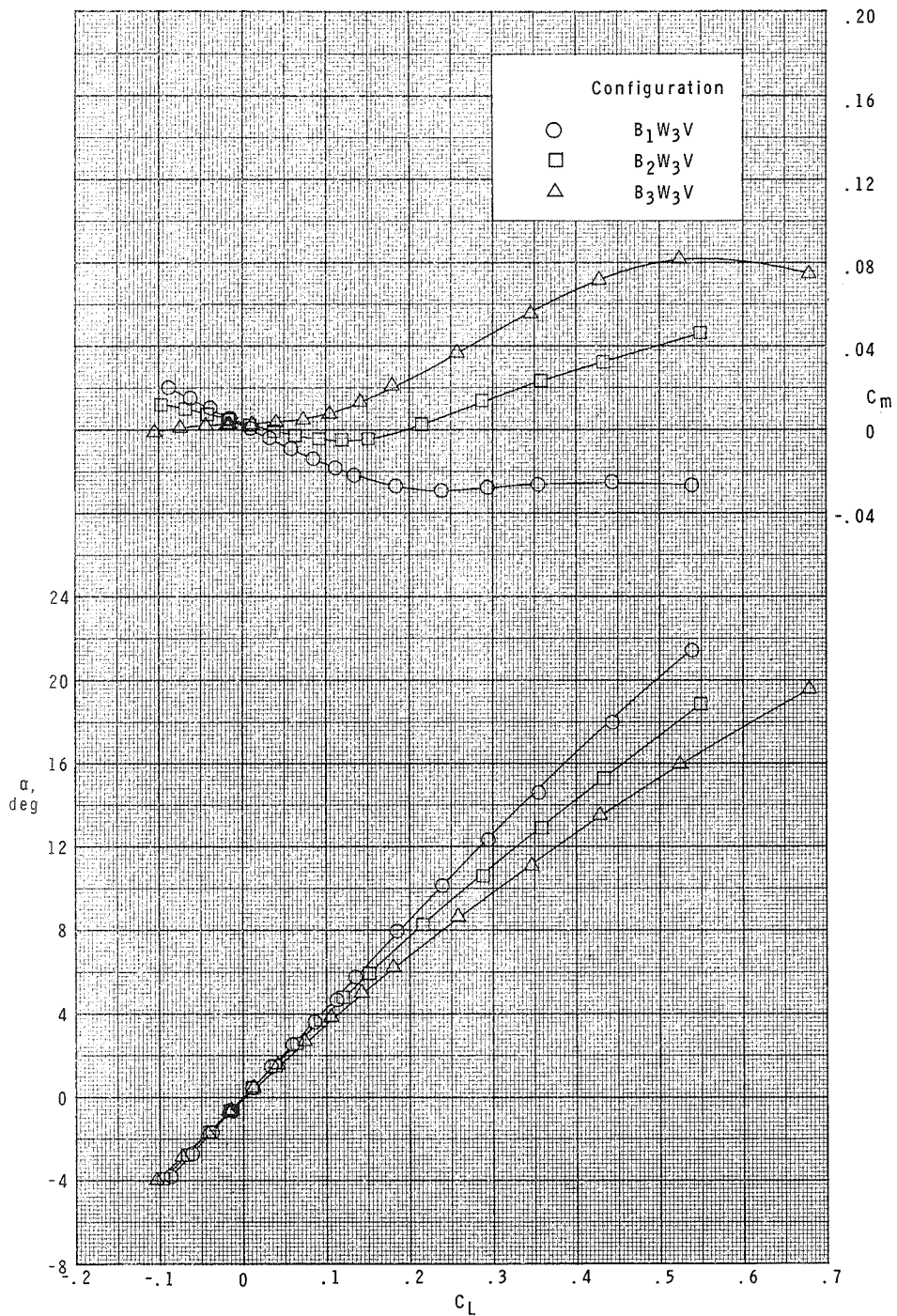
(a)  $M = 2.36$ .

Figure 5.- Longitudinal aerodynamic characteristics of model with small ( $W_3$ ) wing.



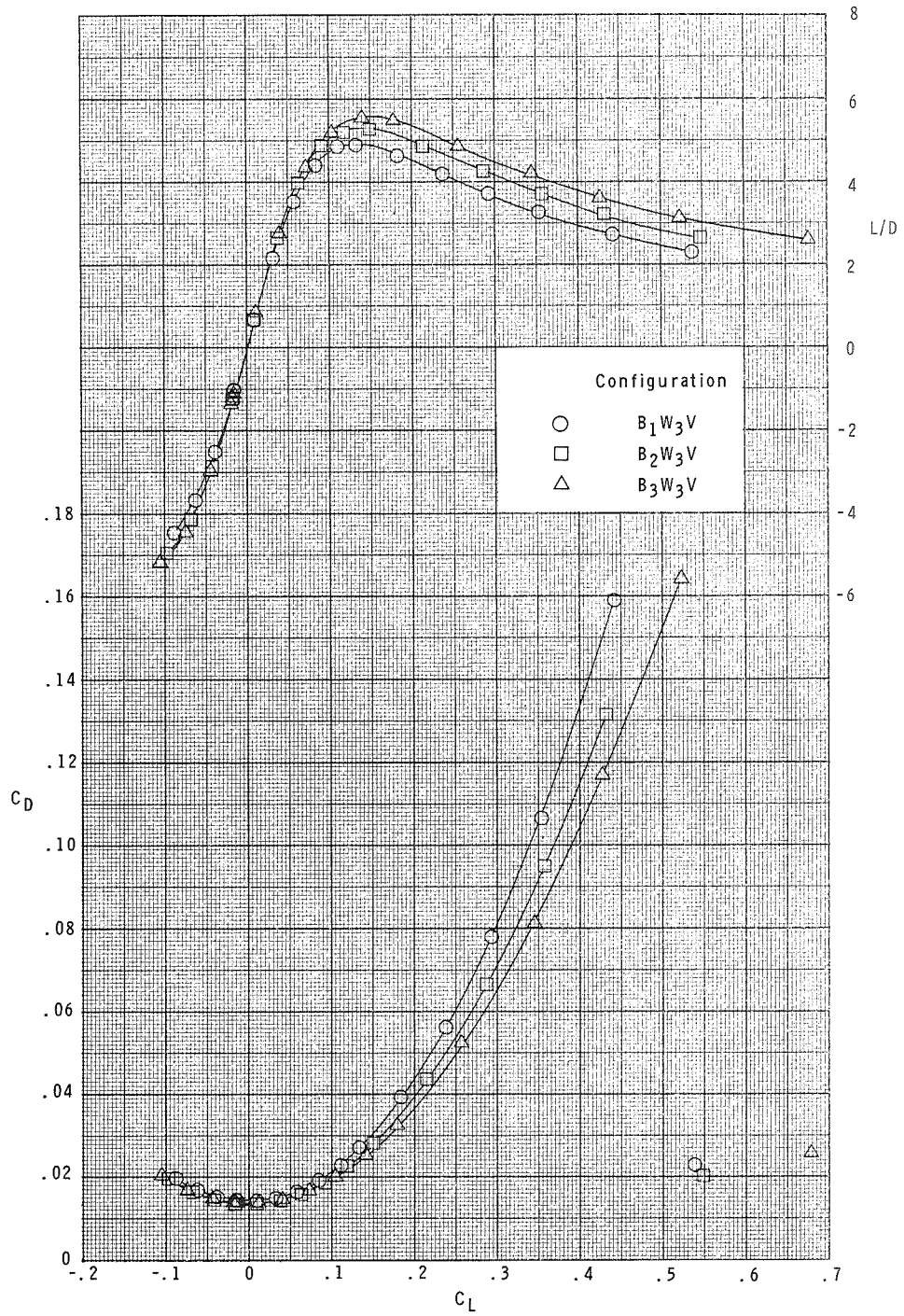
(a)  $M = 2.36$ . Concluded.

Figure 5.- Continued.



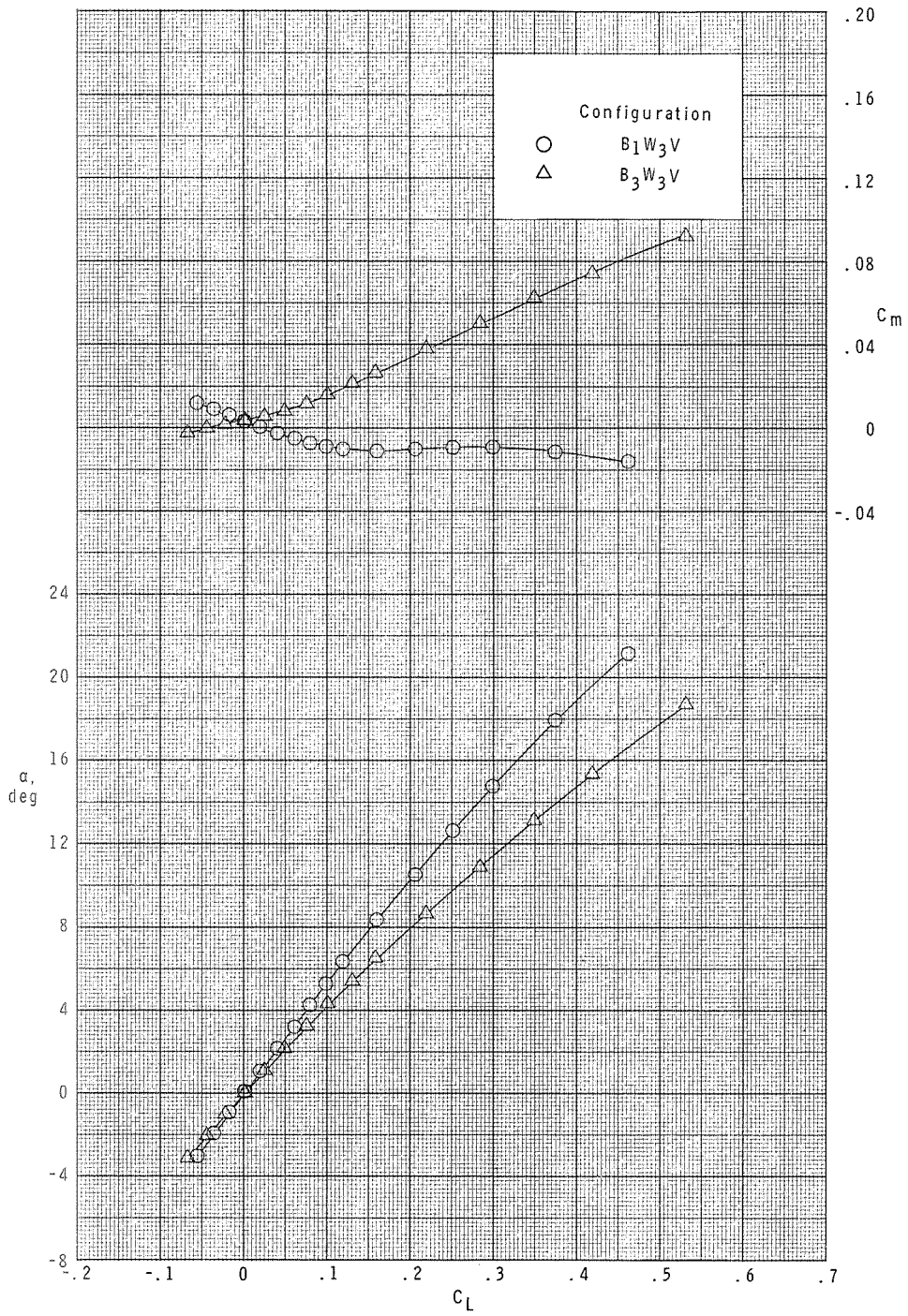
(b)  $M = 2.86$ .

Figure 5.- Continued.



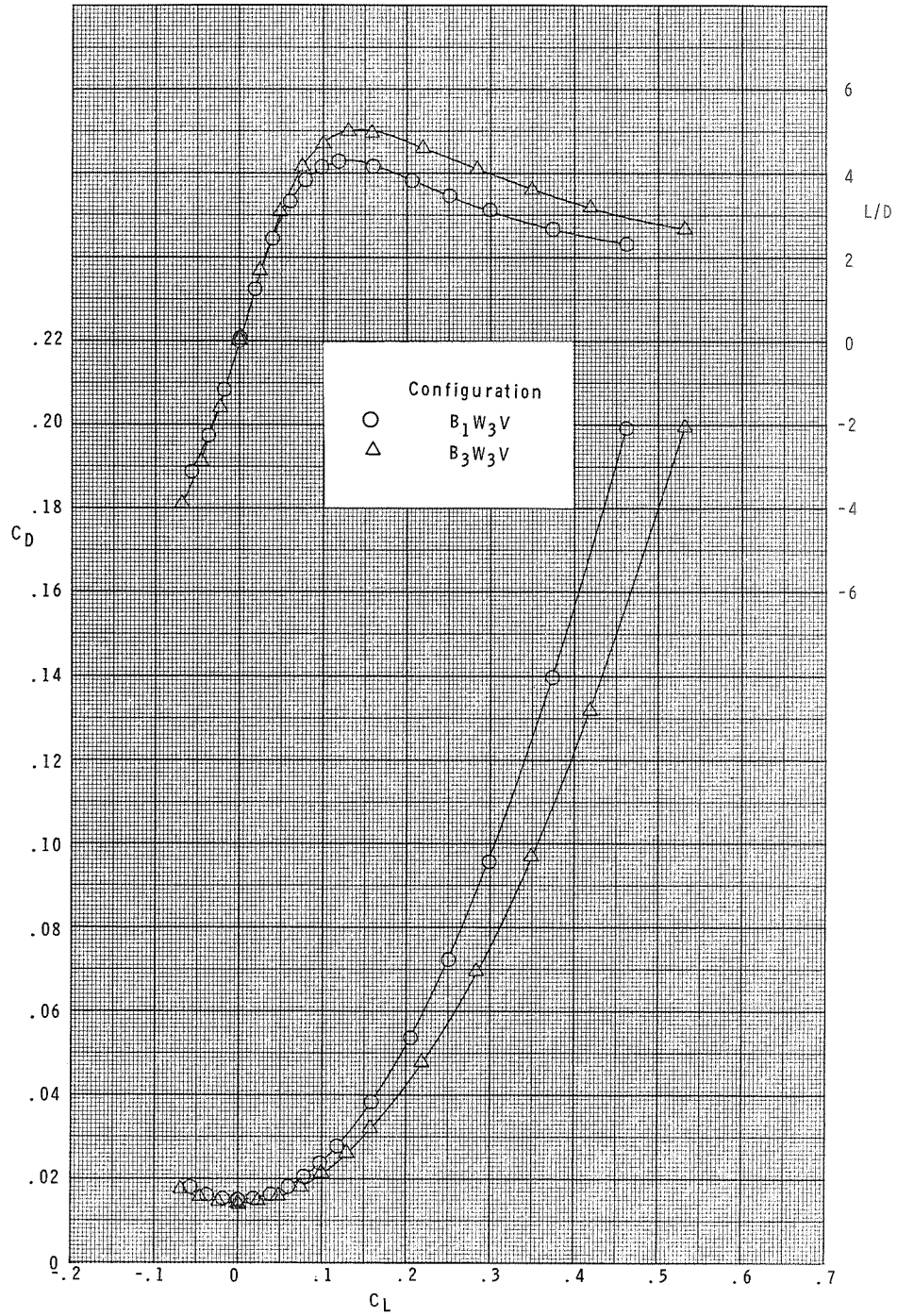
(b)  $M = 2.86$ . Concluded.

Figure 5.- Continued.



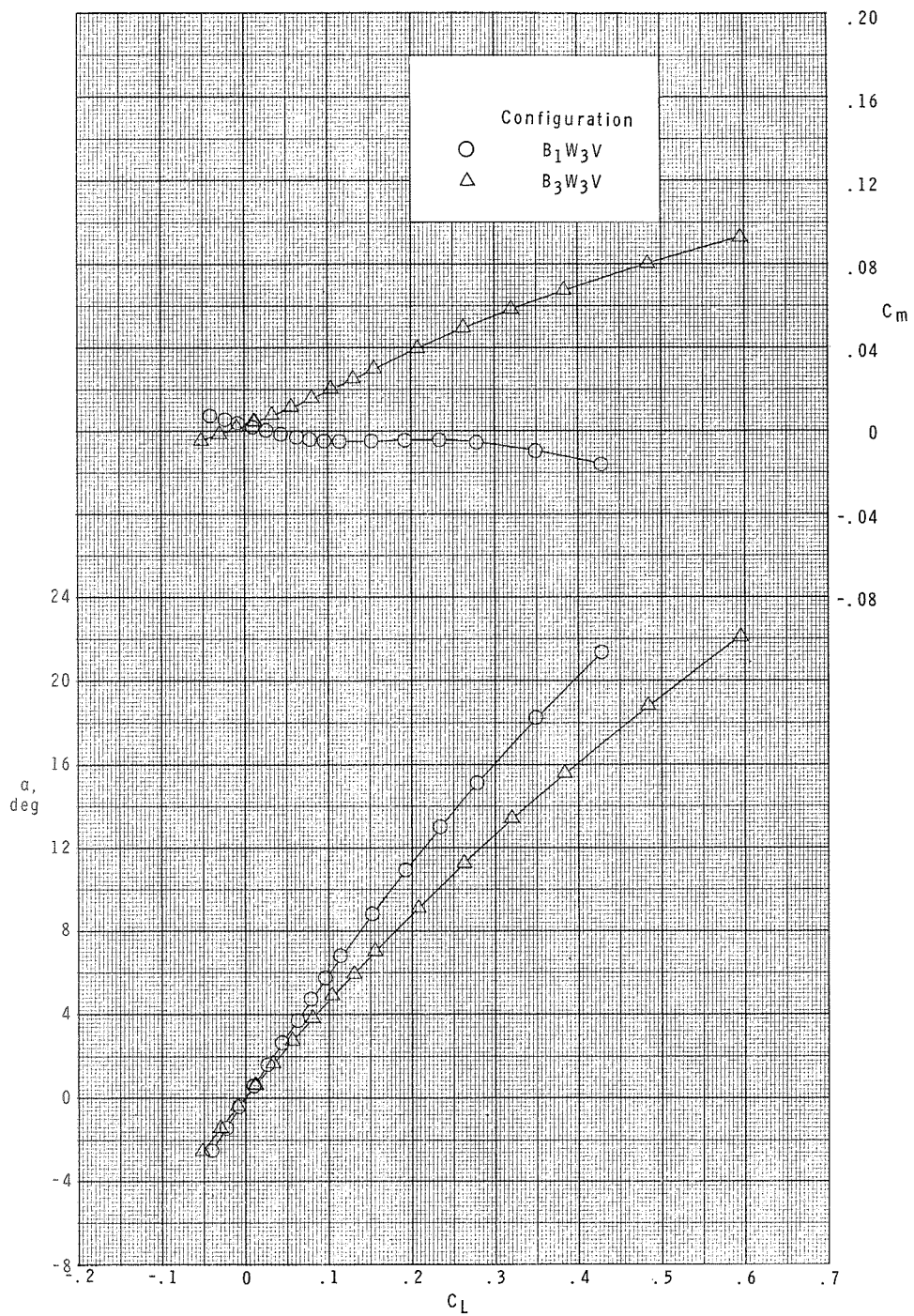
(c)  $M = 3.95$ .

Figure 5.- Continued.



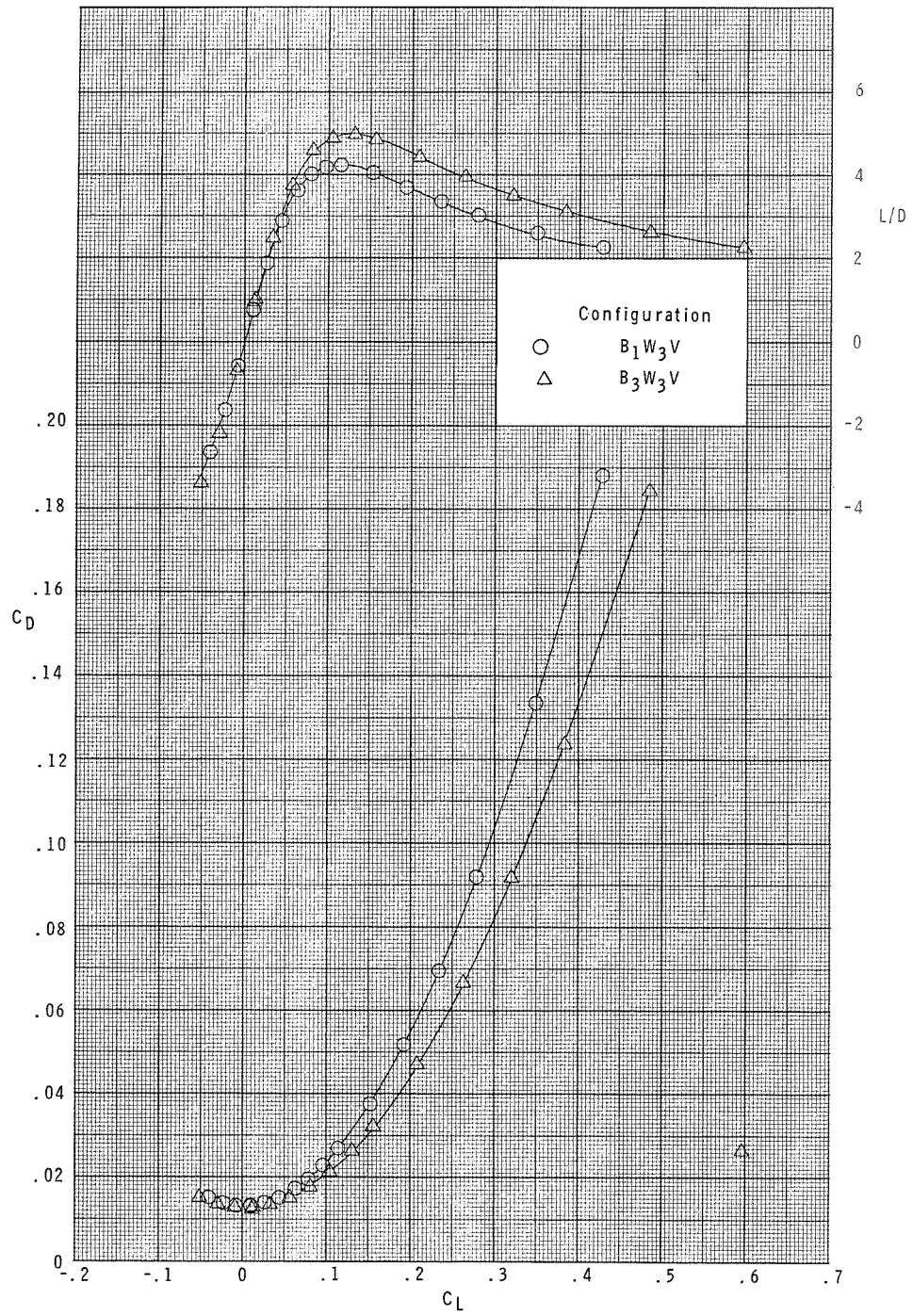
(c)  $M = 3.95$ . Concluded.

Figure 5.- Continued.



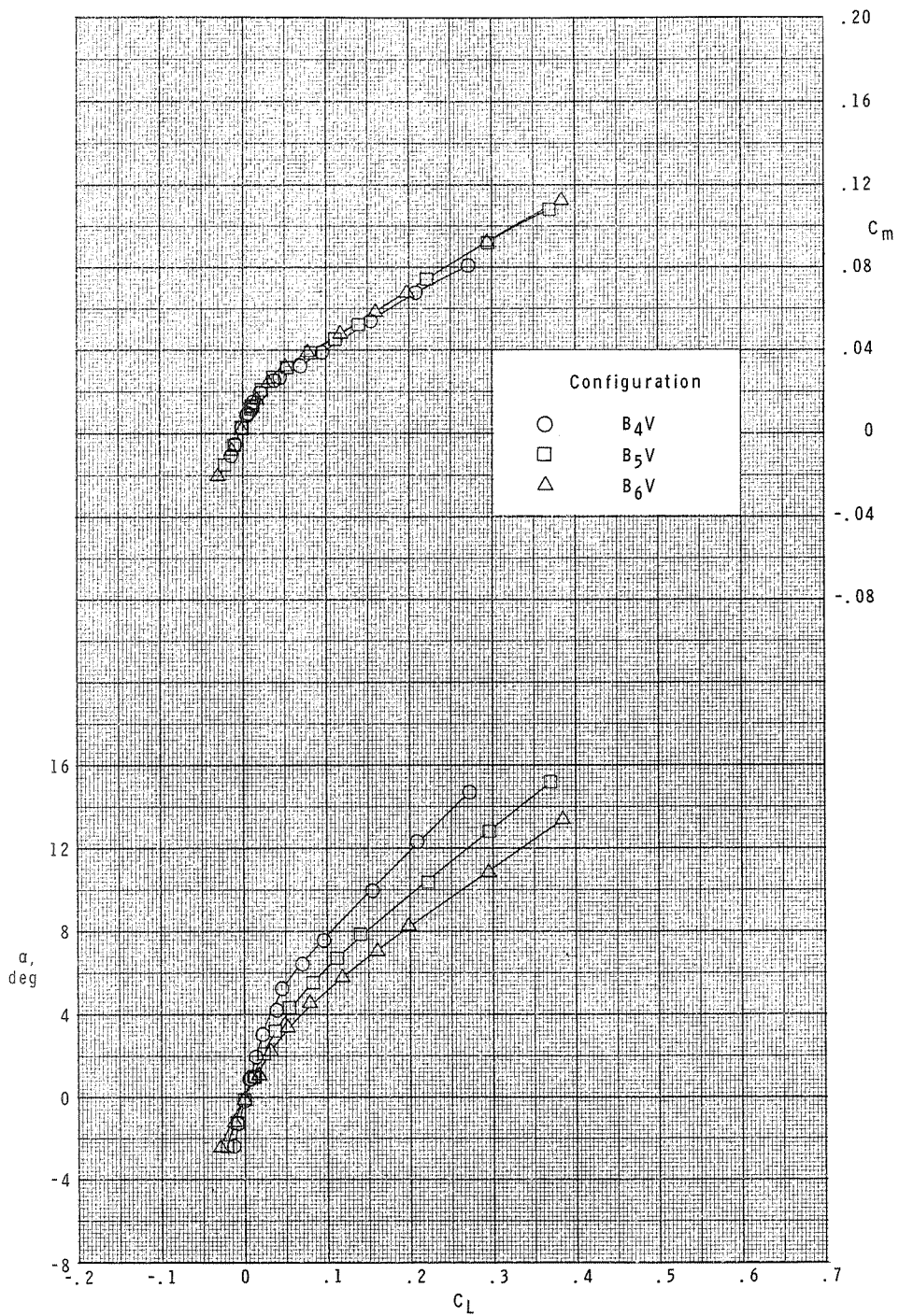
(d)  $M = 4.63$ .

Figure 5.- Continued.



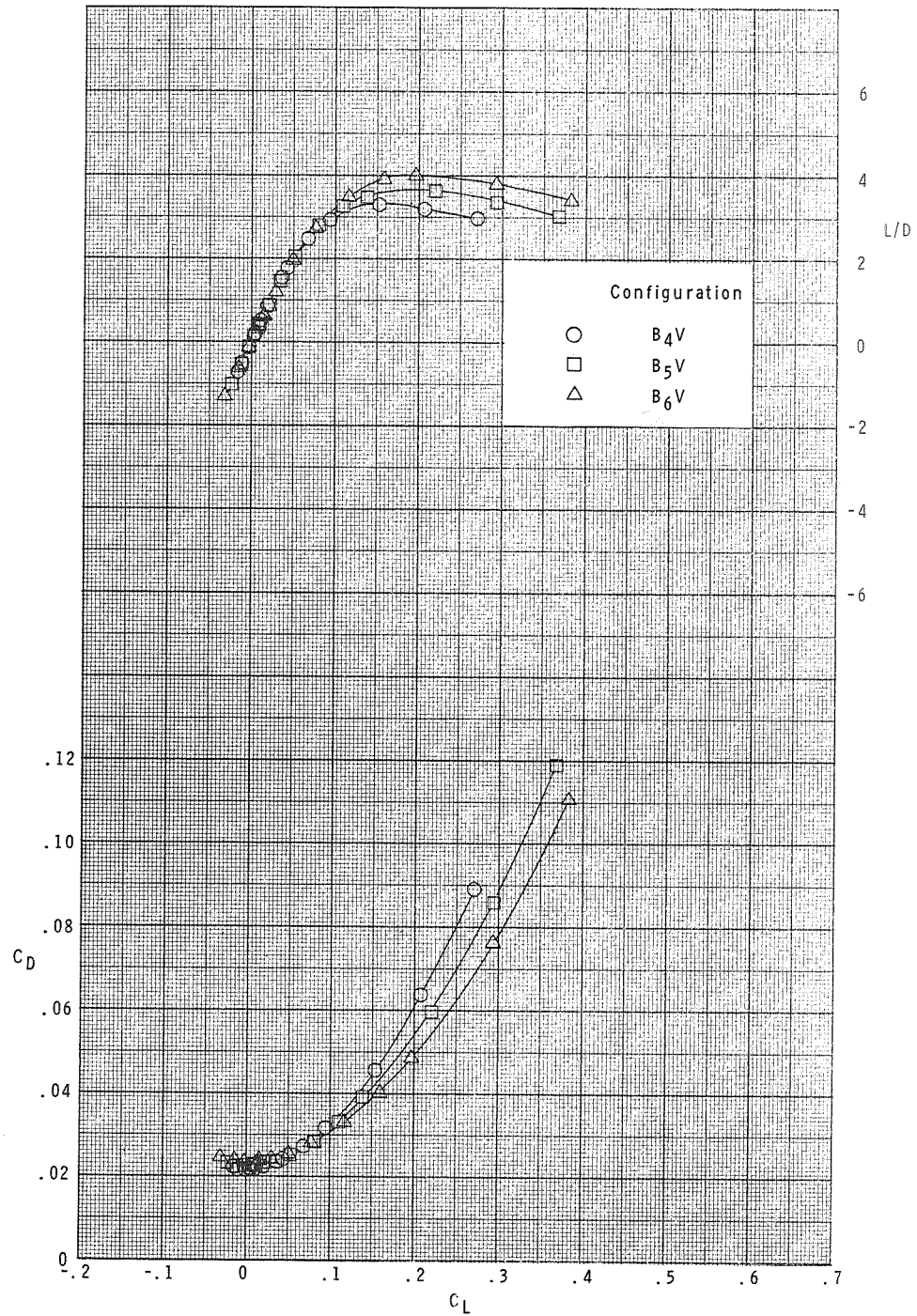
(d)  $M = 4.63$ . Concluded.

Figure 5.- Concluded.



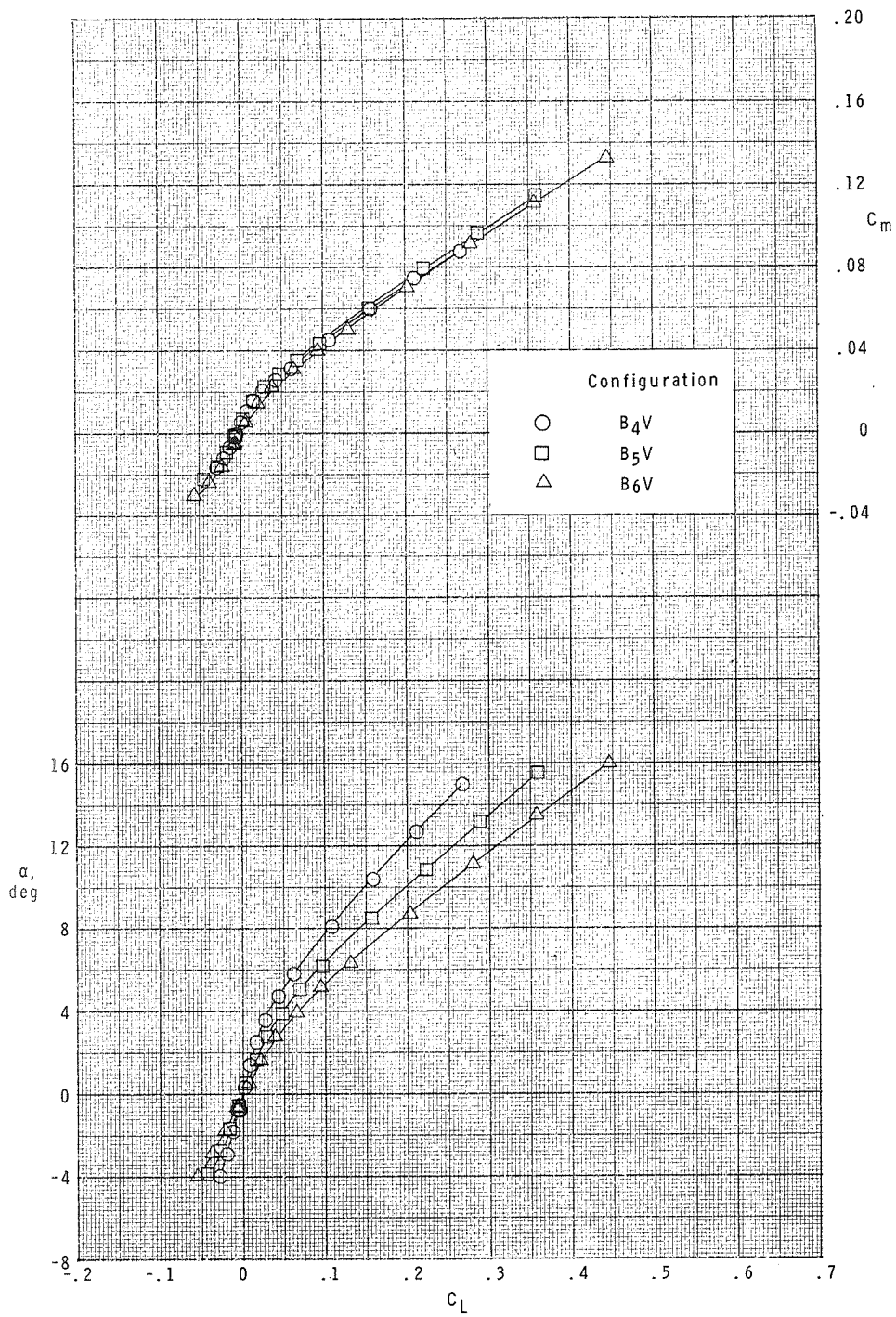
(a)  $M = 2.36$ .

Figure 6.- Longitudinal aerodynamic characteristics of lifting-body models.



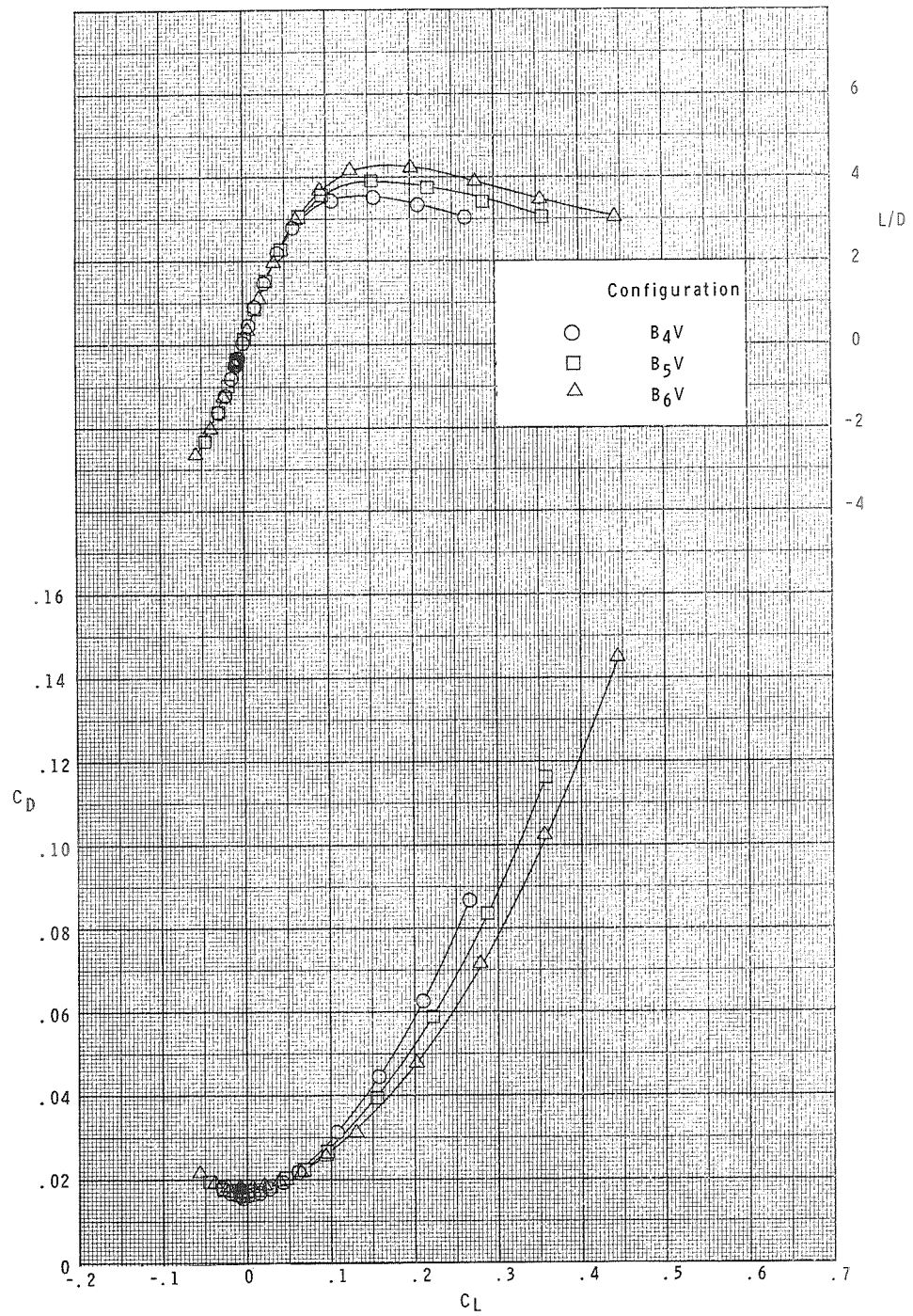
(a)  $M = 2.36$ . Concluded.

Figure 6.- Continued.



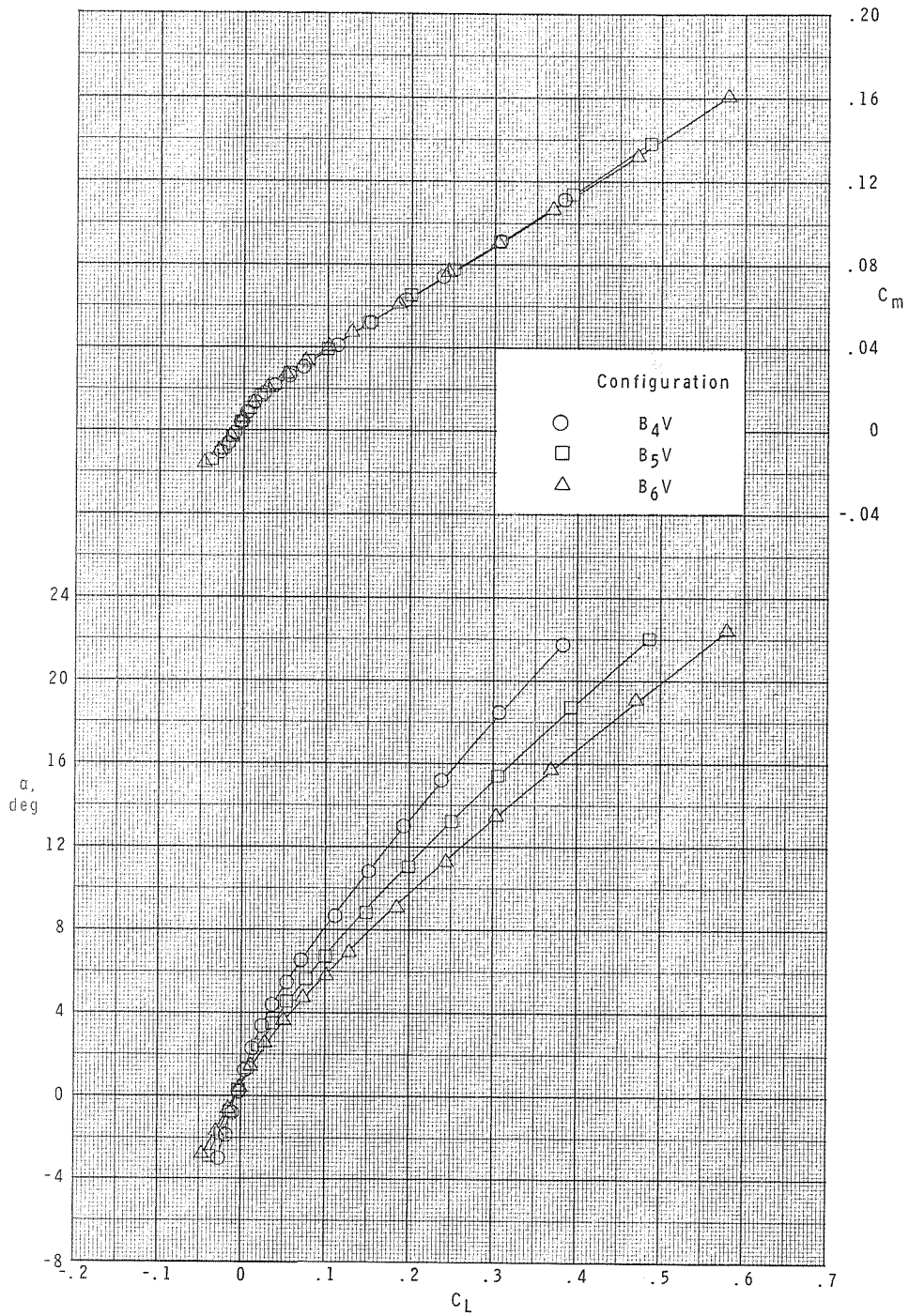
(b)  $M = 2.86$ .

Figure 6.- Continued.



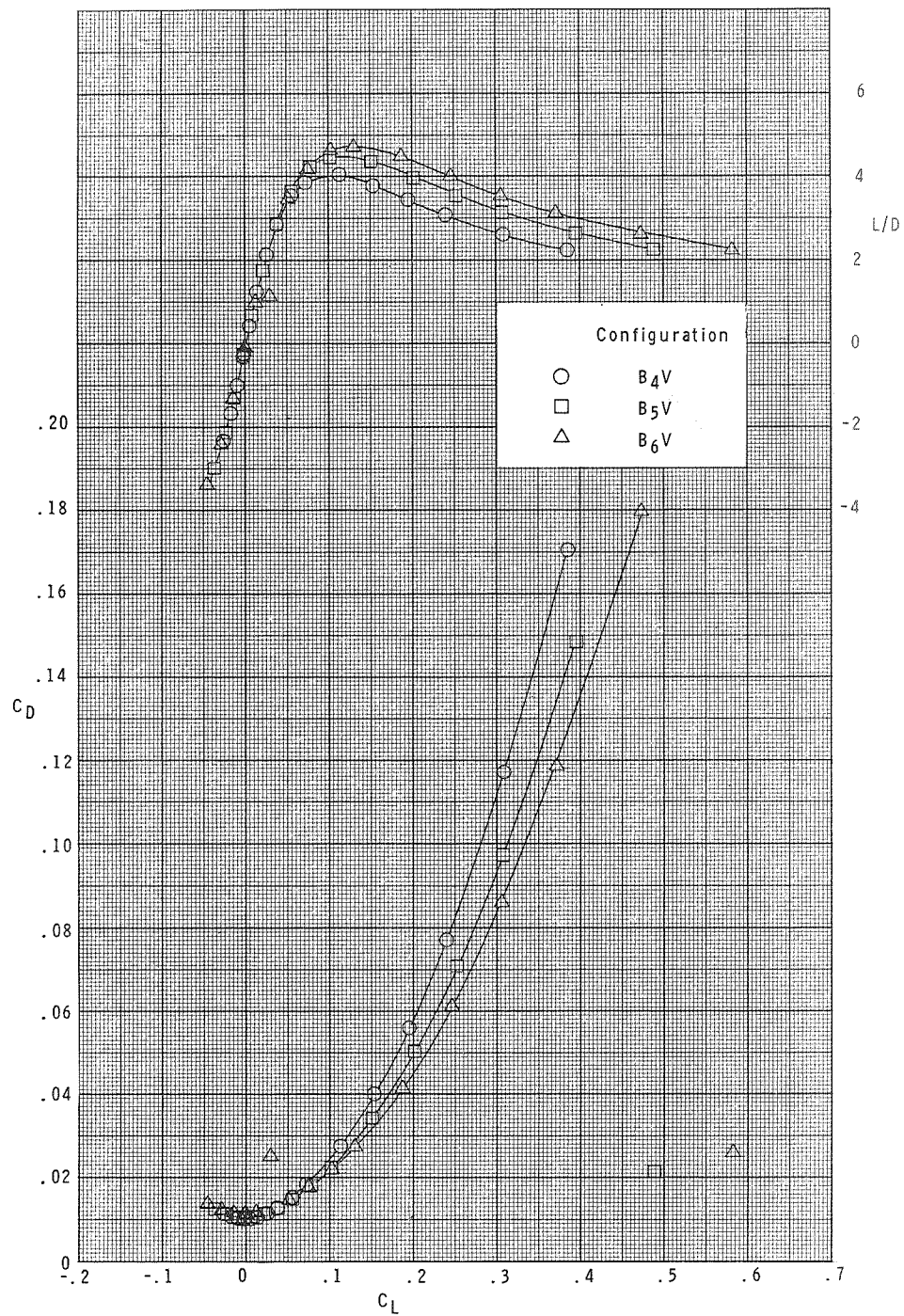
(b)  $M = 2.86$ . Concluded.

Figure 6.- Continued.



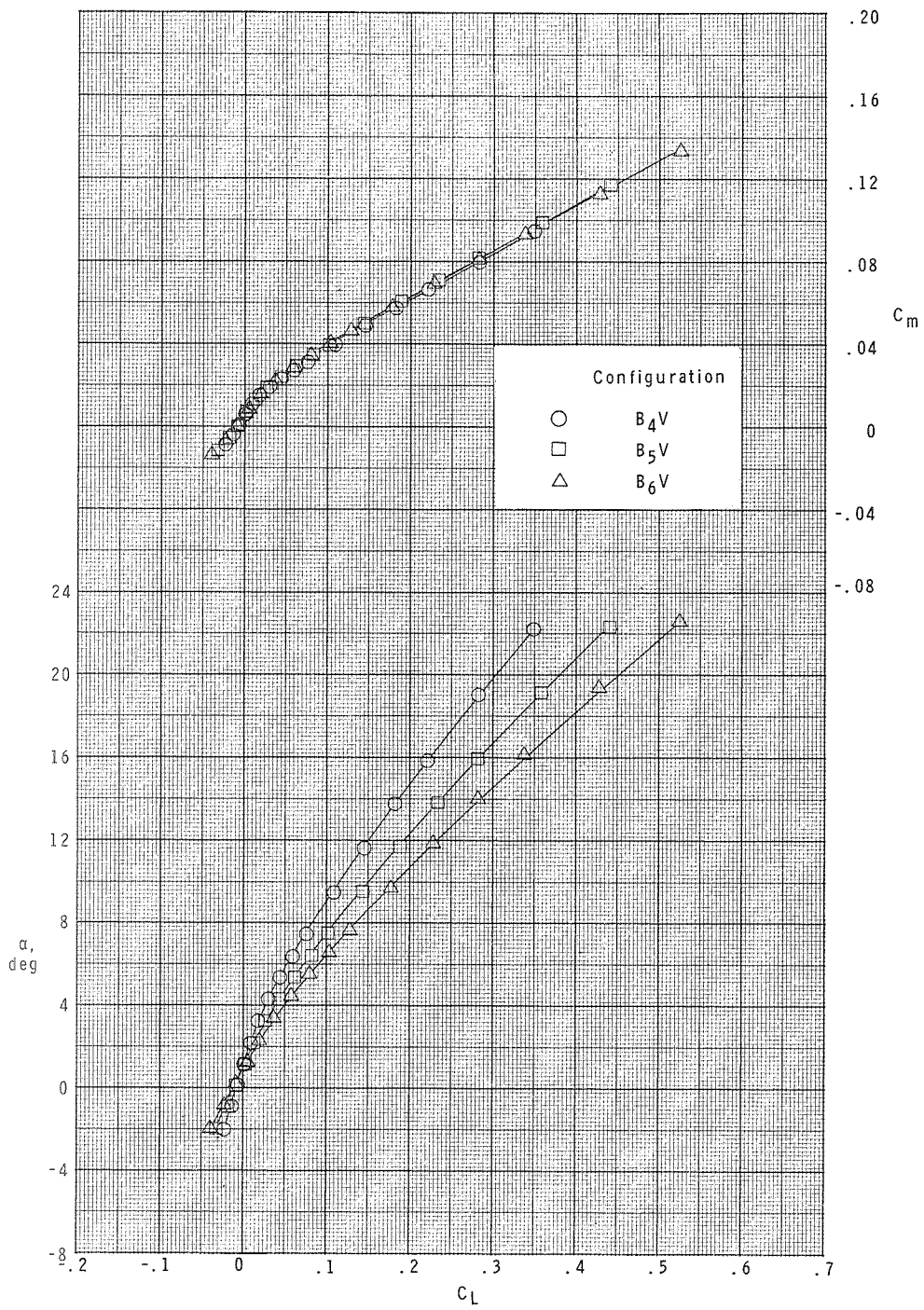
(c)  $M = 3.95$ .

Figure 6.- Continued.



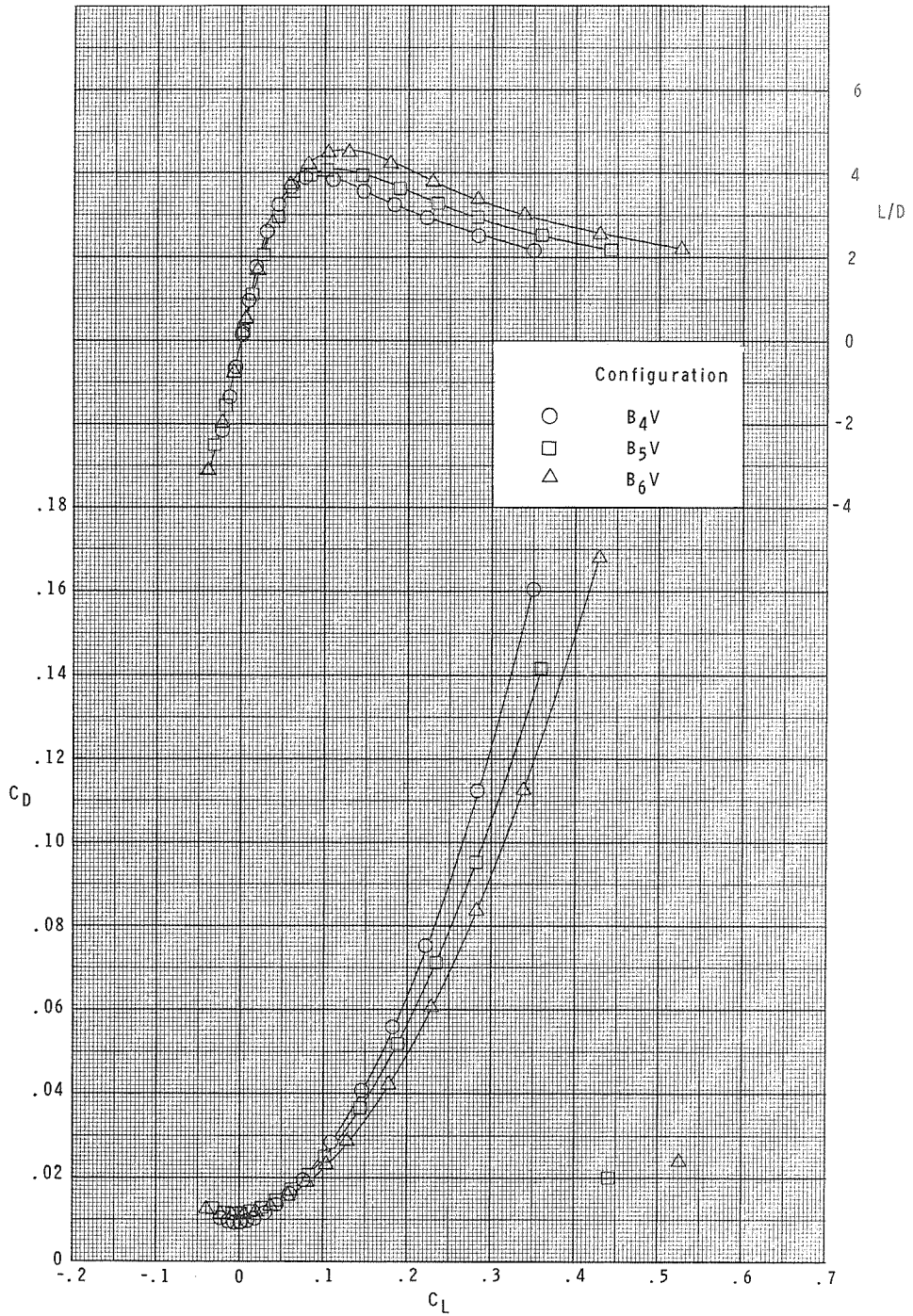
(c)  $M = 3.95$ . Concluded.

Figure 6.- Continued.



(d)  $M = 4.63$ .

Figure 6.- Continued.



(d)  $M = 4.63$ . Concluded.

Figure 6.- Concluded.

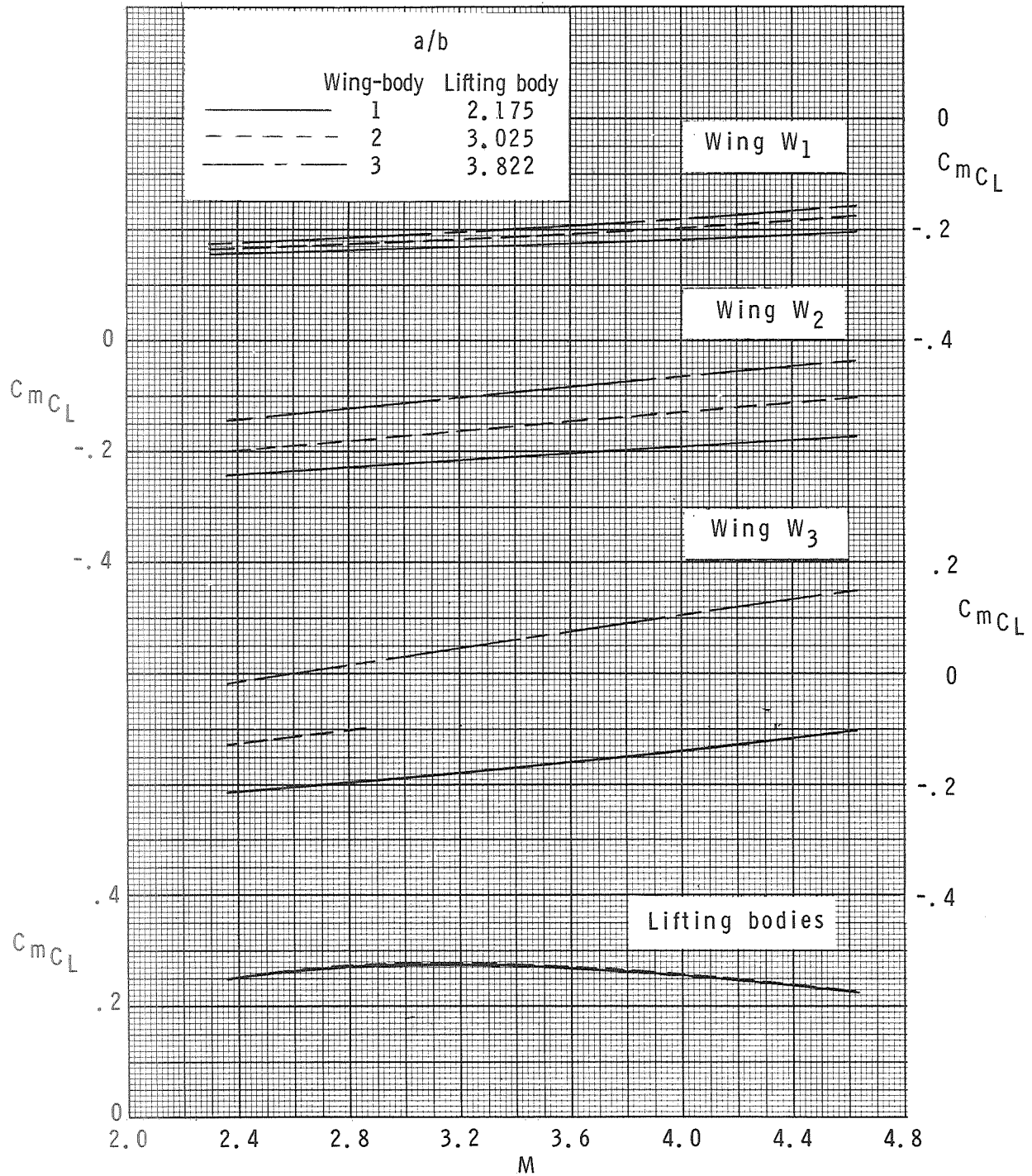


Figure 7.- Summary of static margin.  $\alpha \approx 0^\circ$ .

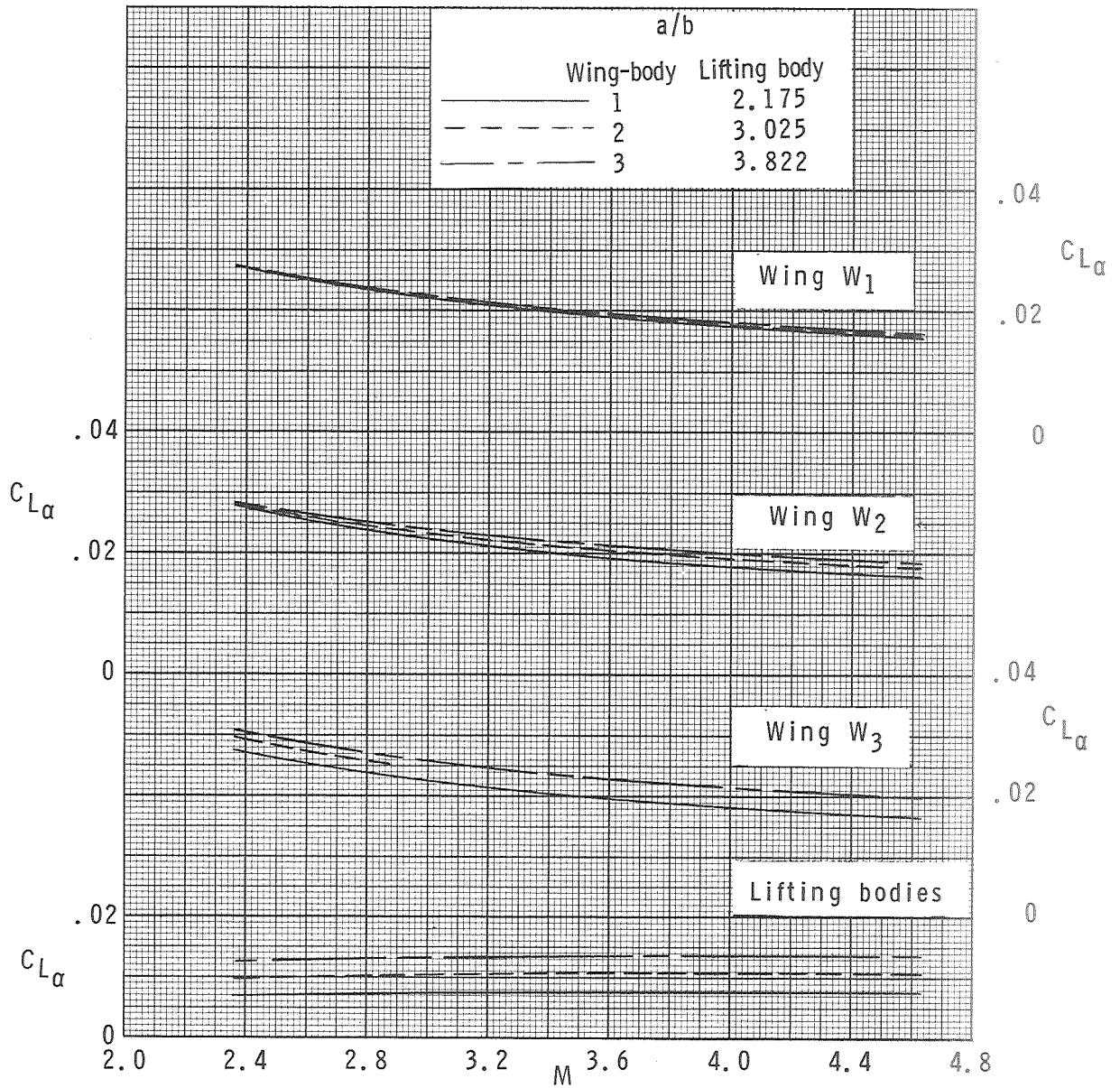


Figure 8.- Summary of lift-curve slope.

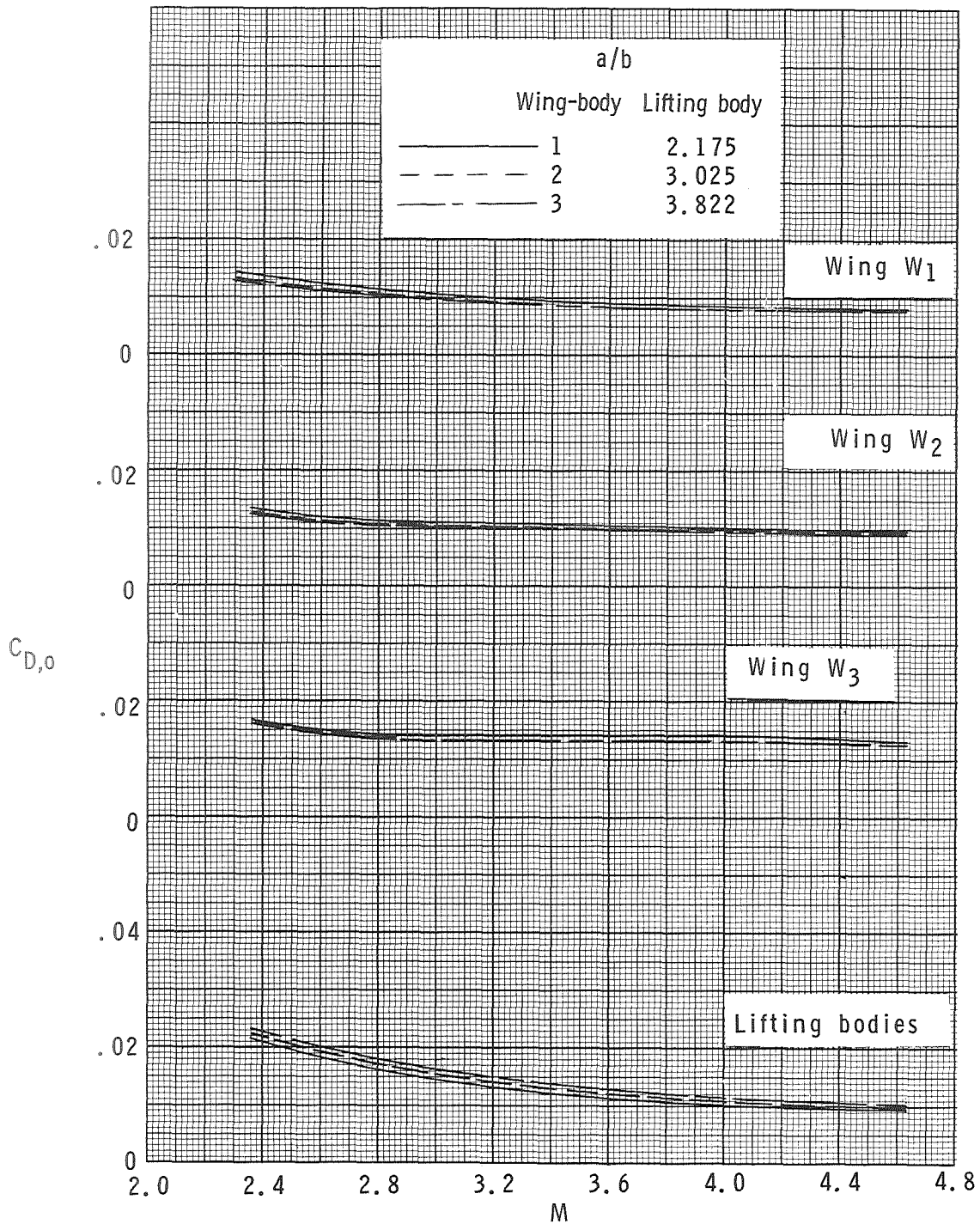


Figure 9.- Summary of minimum drag coefficient.

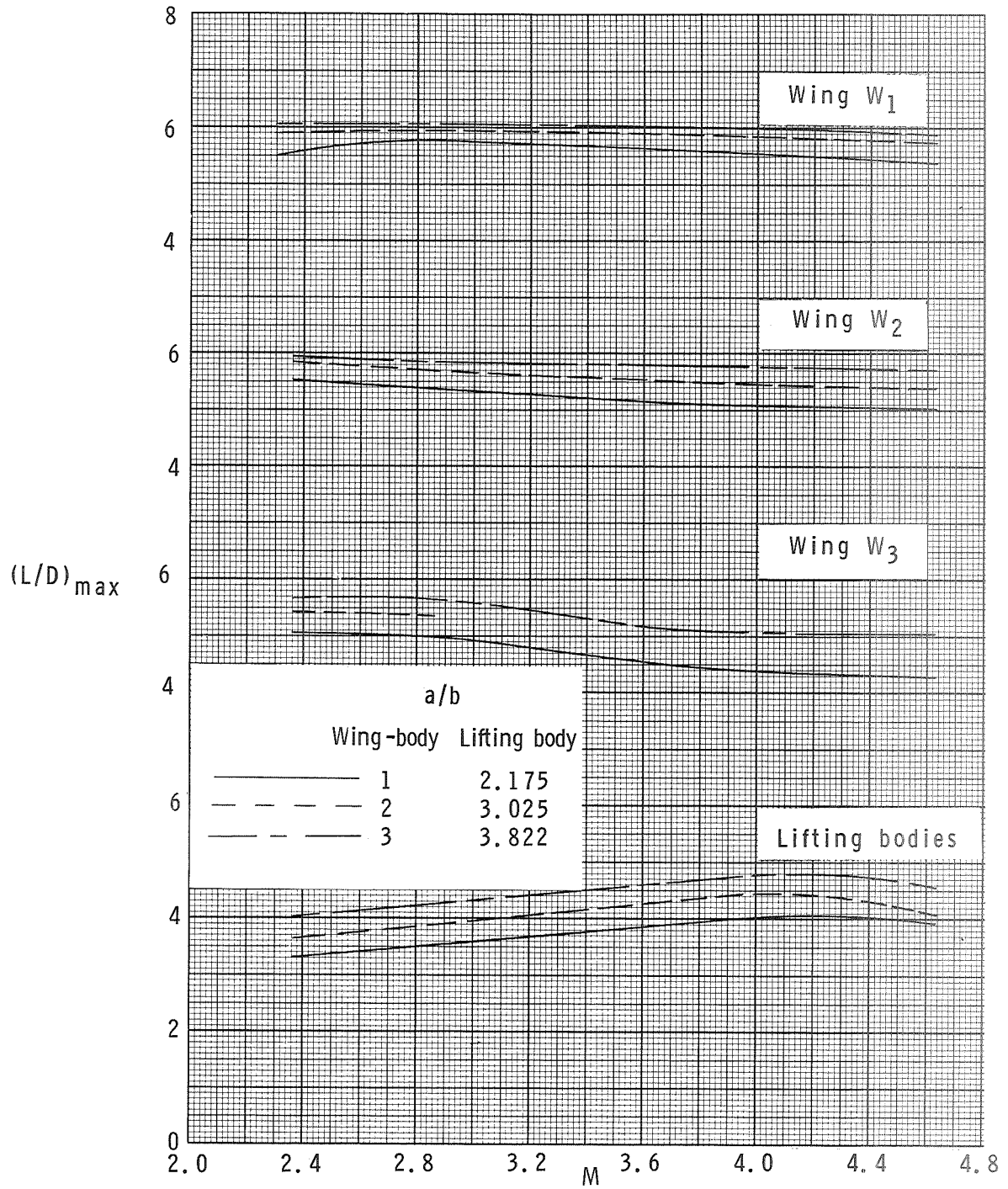
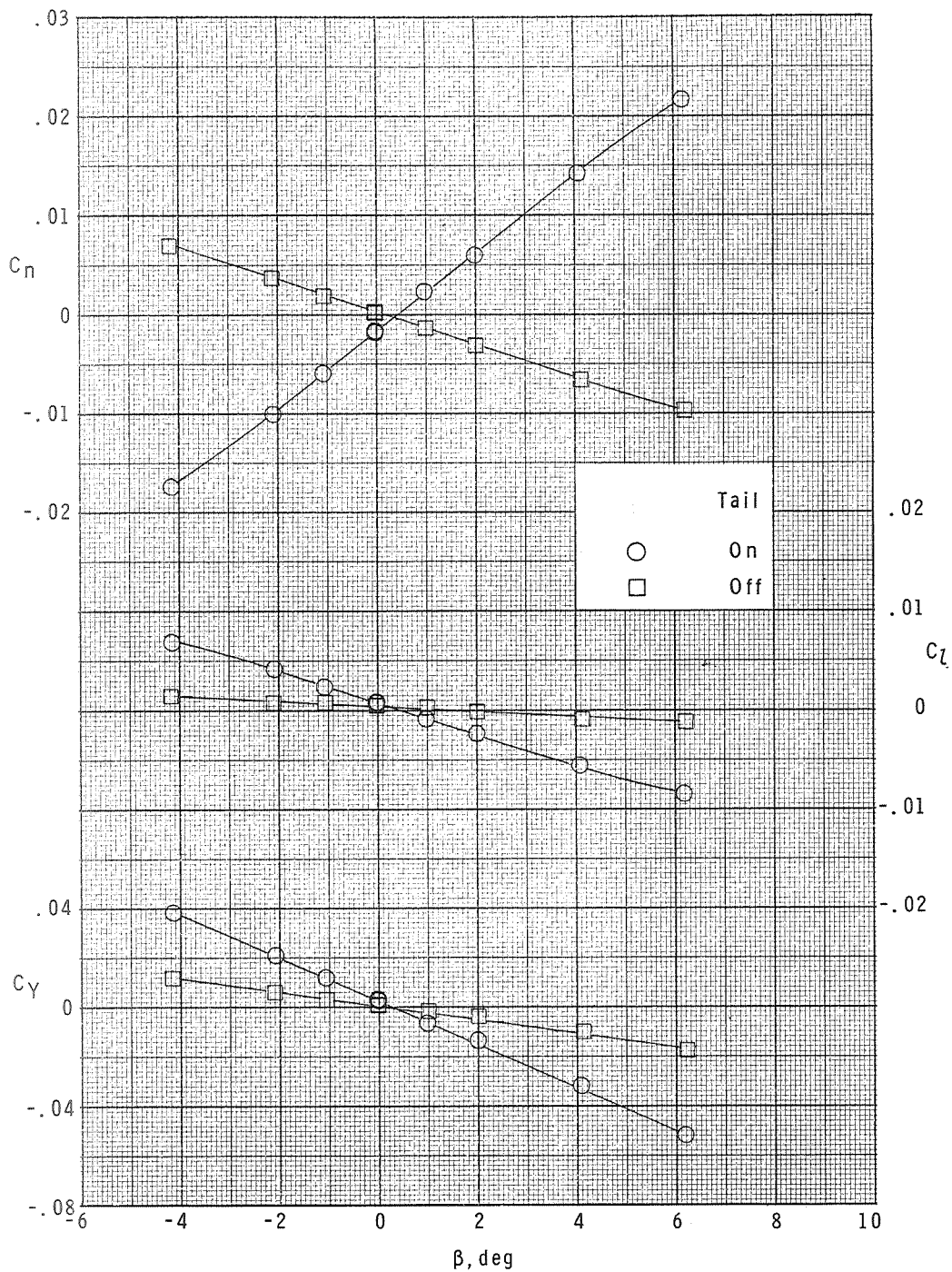
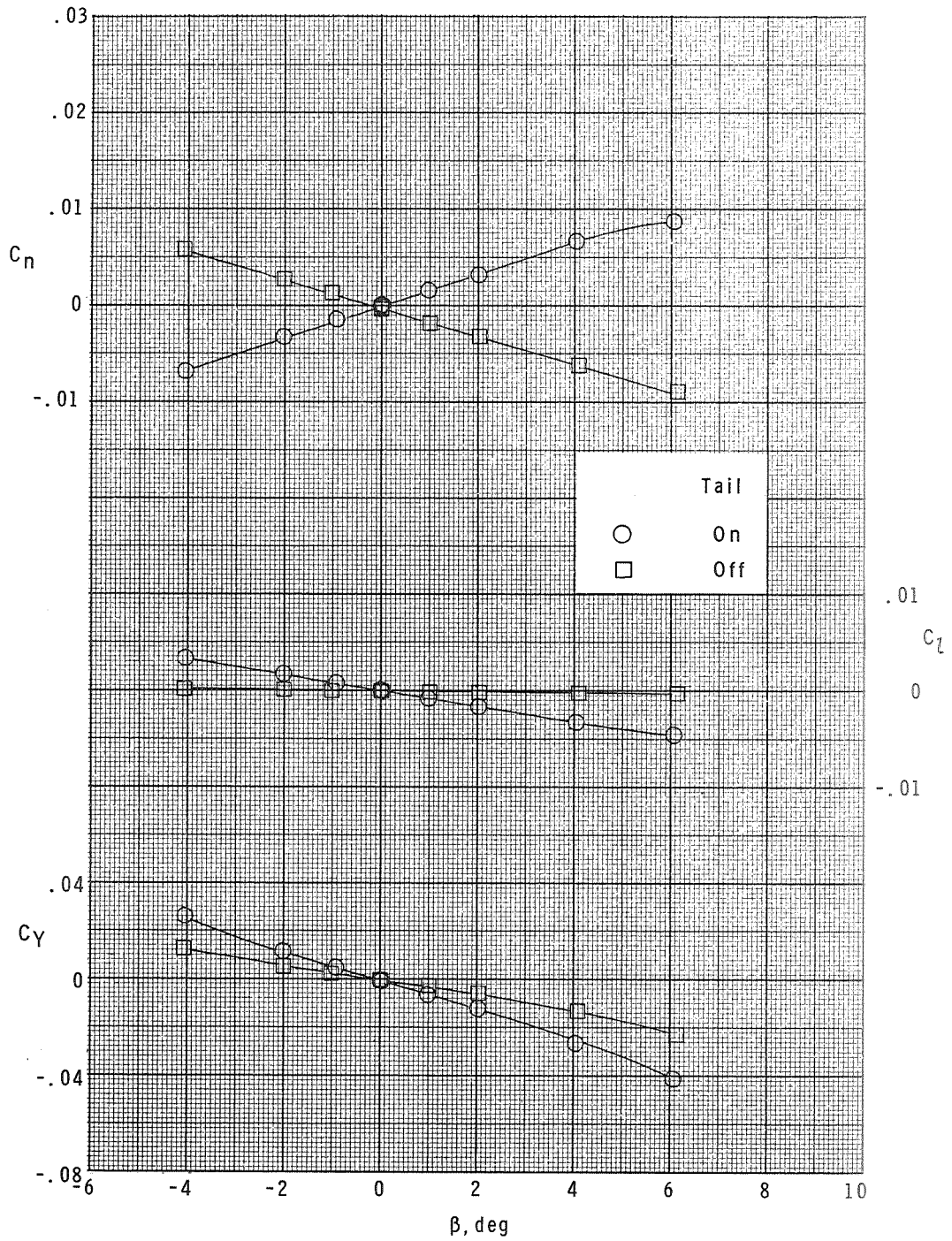


Figure 10.- Summary of maximum lift-drag ratio.



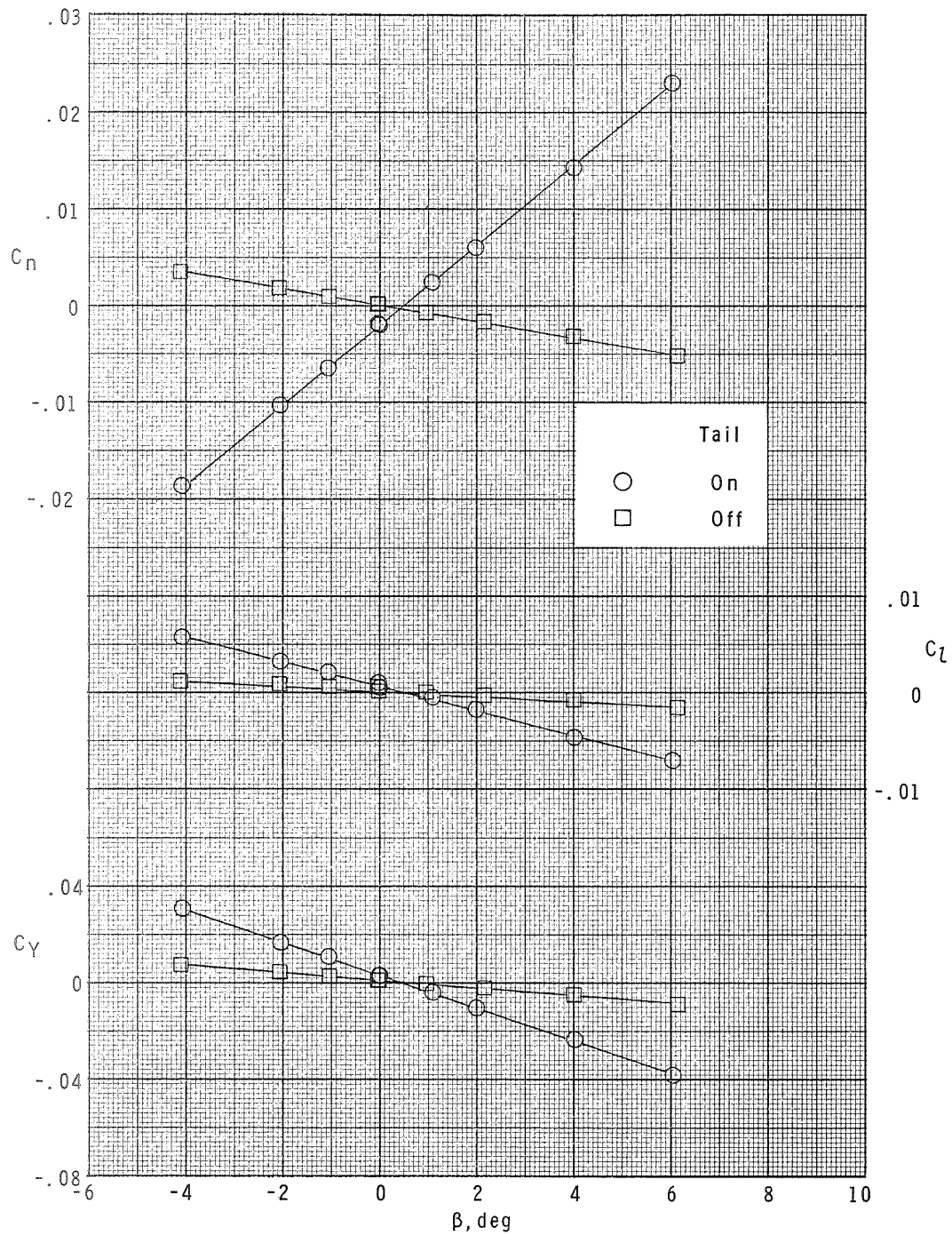
(a)  $M = 2.36$ .

Figure 11.- Lateral aerodynamic characteristics of configuration  $B_1W_2$  with and without vertical tail at  $\alpha = 0^\circ$ .



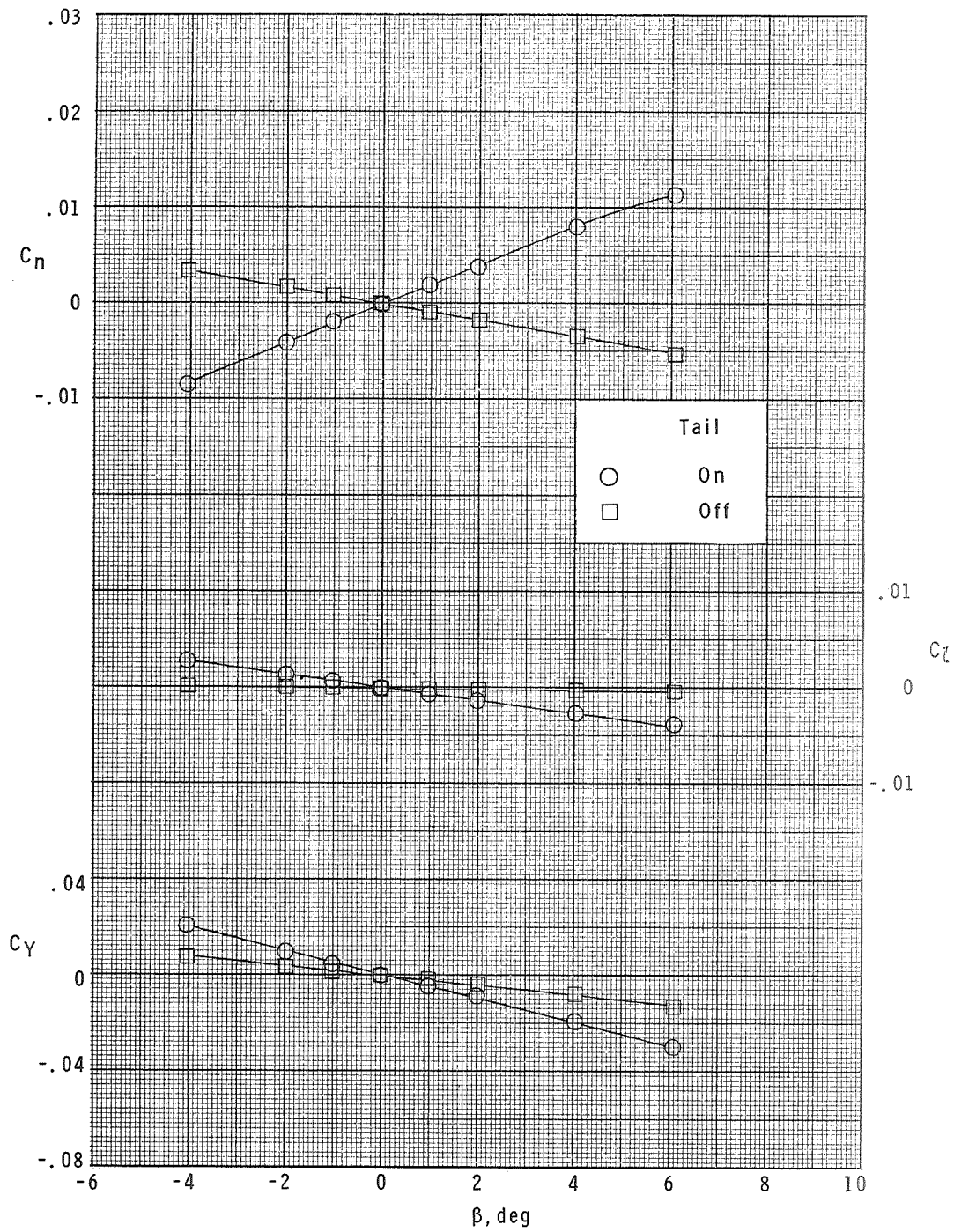
(b)  $M = 4.63$ .

Figure 11.- Concluded.



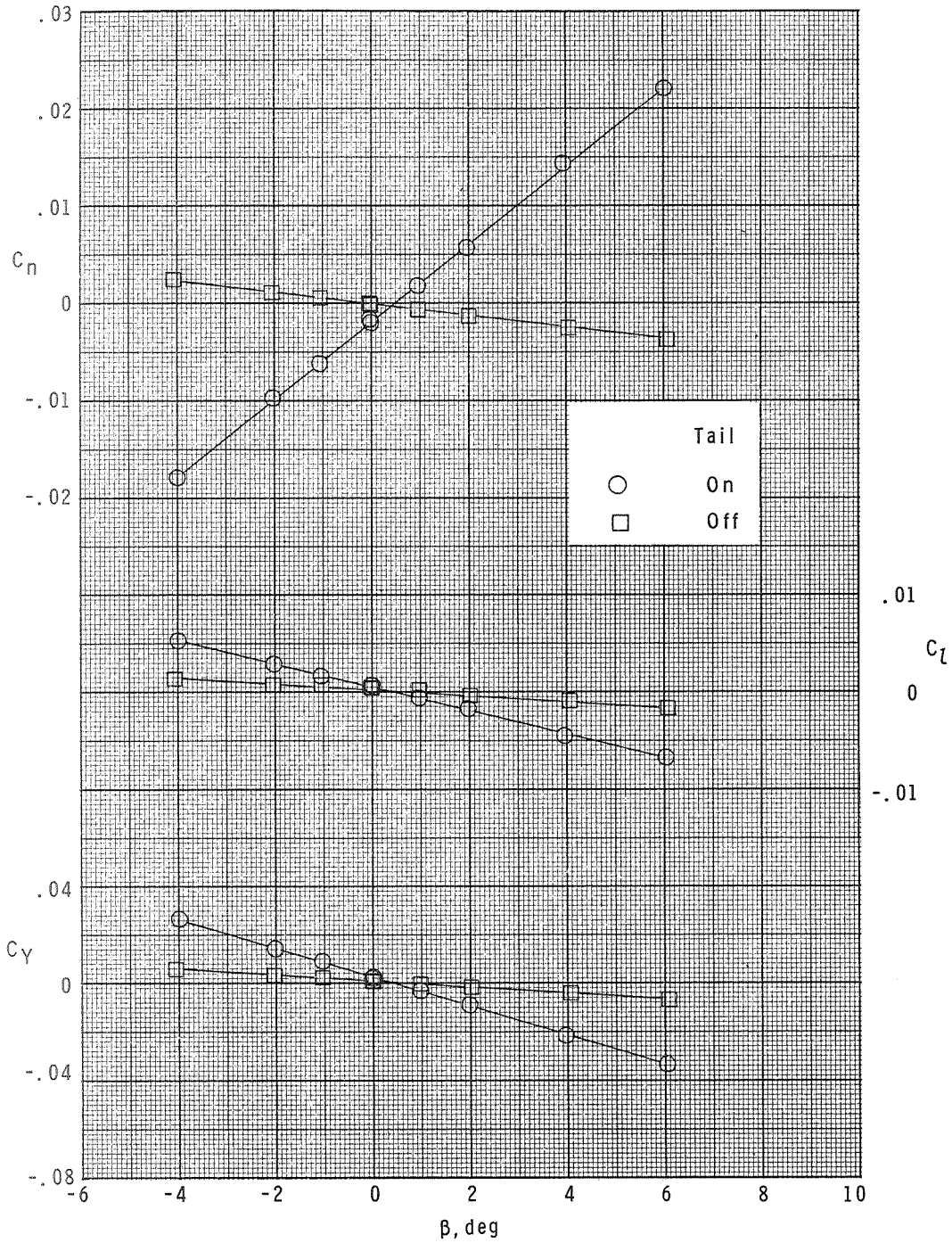
(a)  $M = 2.36$ .

Figure 12.- Lateral aerodynamic characteristics of configuration  $B_2W_2$  with and without vertical tail at  $\alpha = 0^\circ$ .



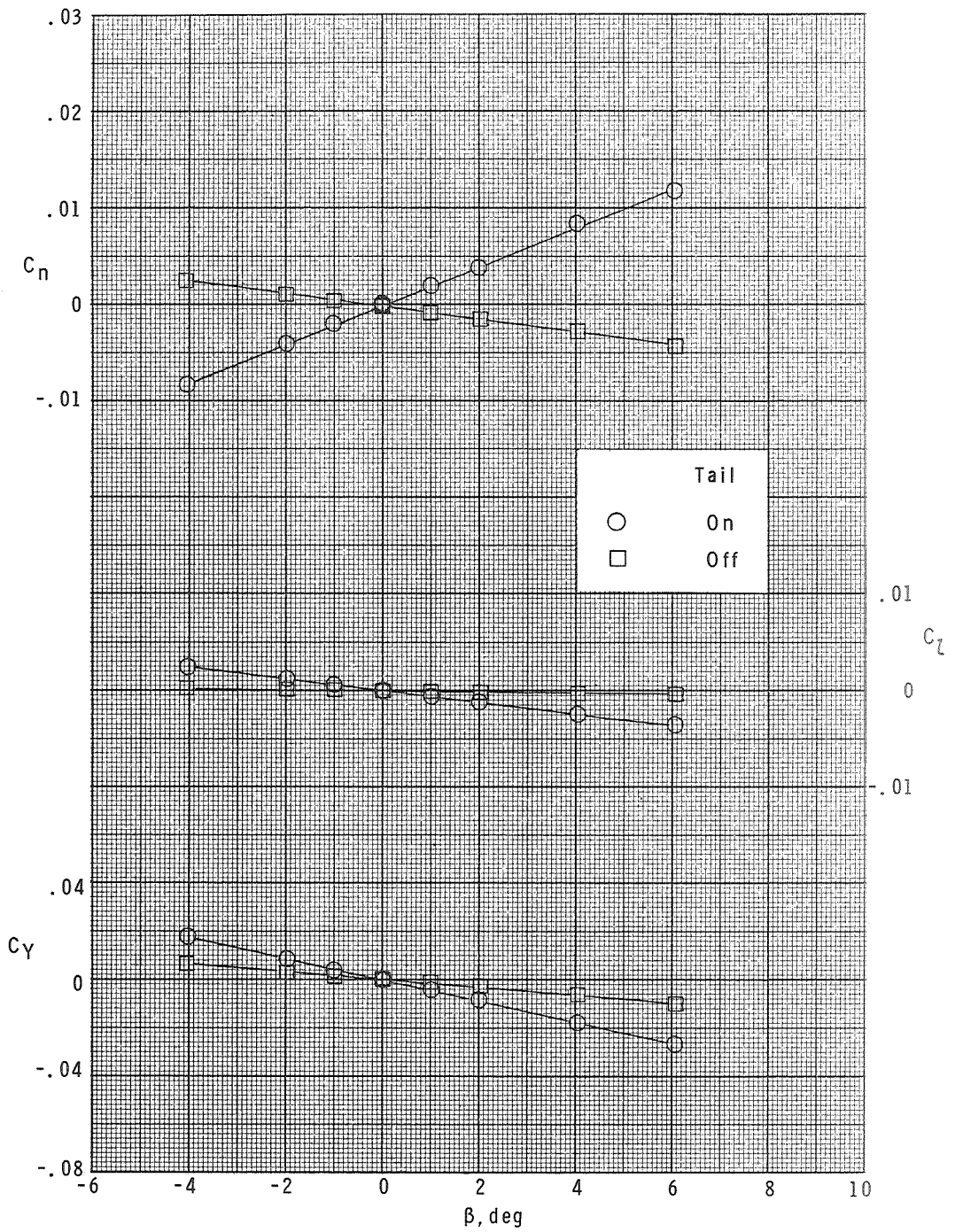
(b)  $M = 4.63$ .

Figure 12.- Concluded.



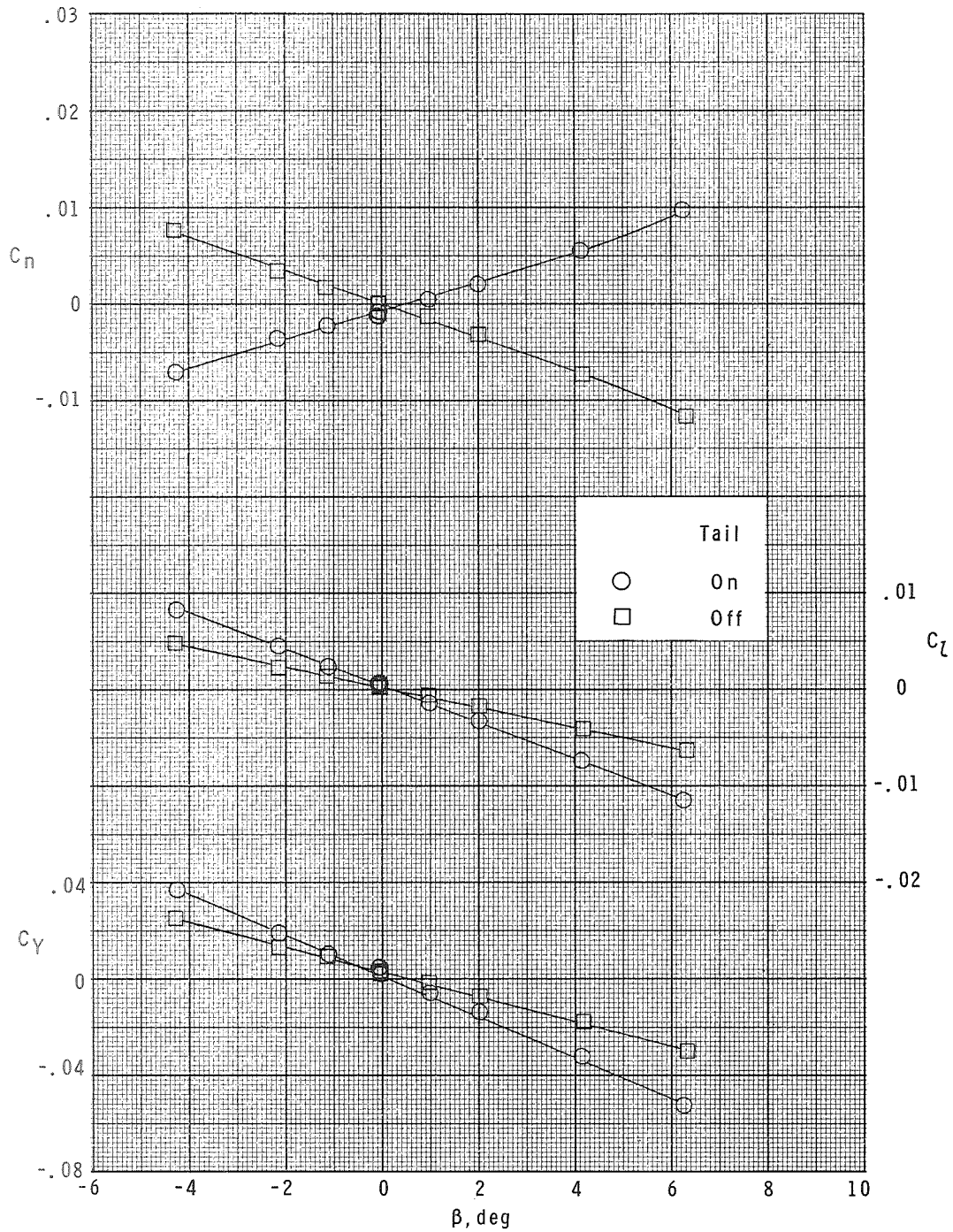
(a)  $M = 2.36$ .

Figure 13.- Lateral aerodynamic characteristics of configuration  $B_3W_2$  with and without vertical tail at  $\alpha = 0^\circ$ .



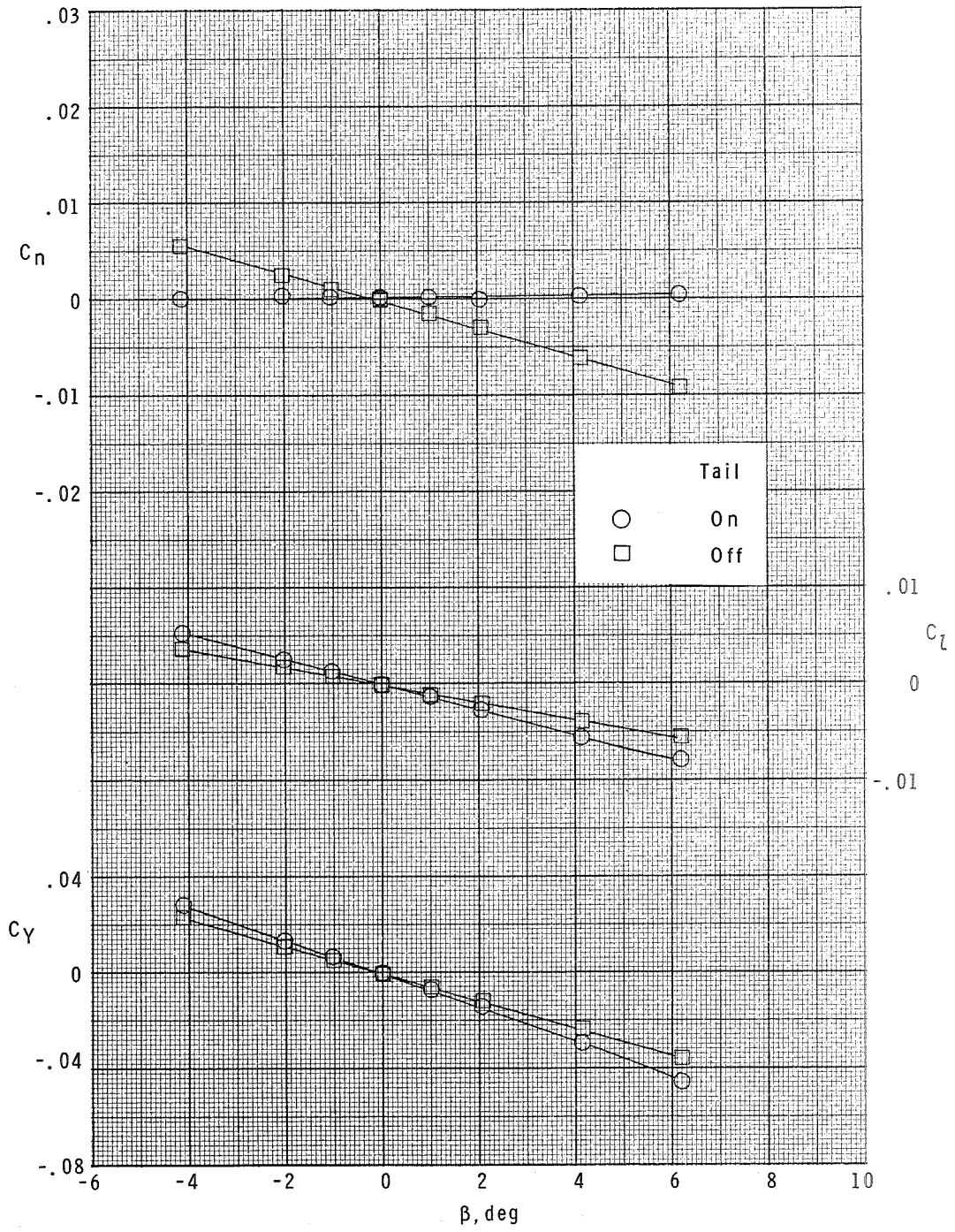
(b)  $M = 4.63$ .

Figure 13.- Concluded.



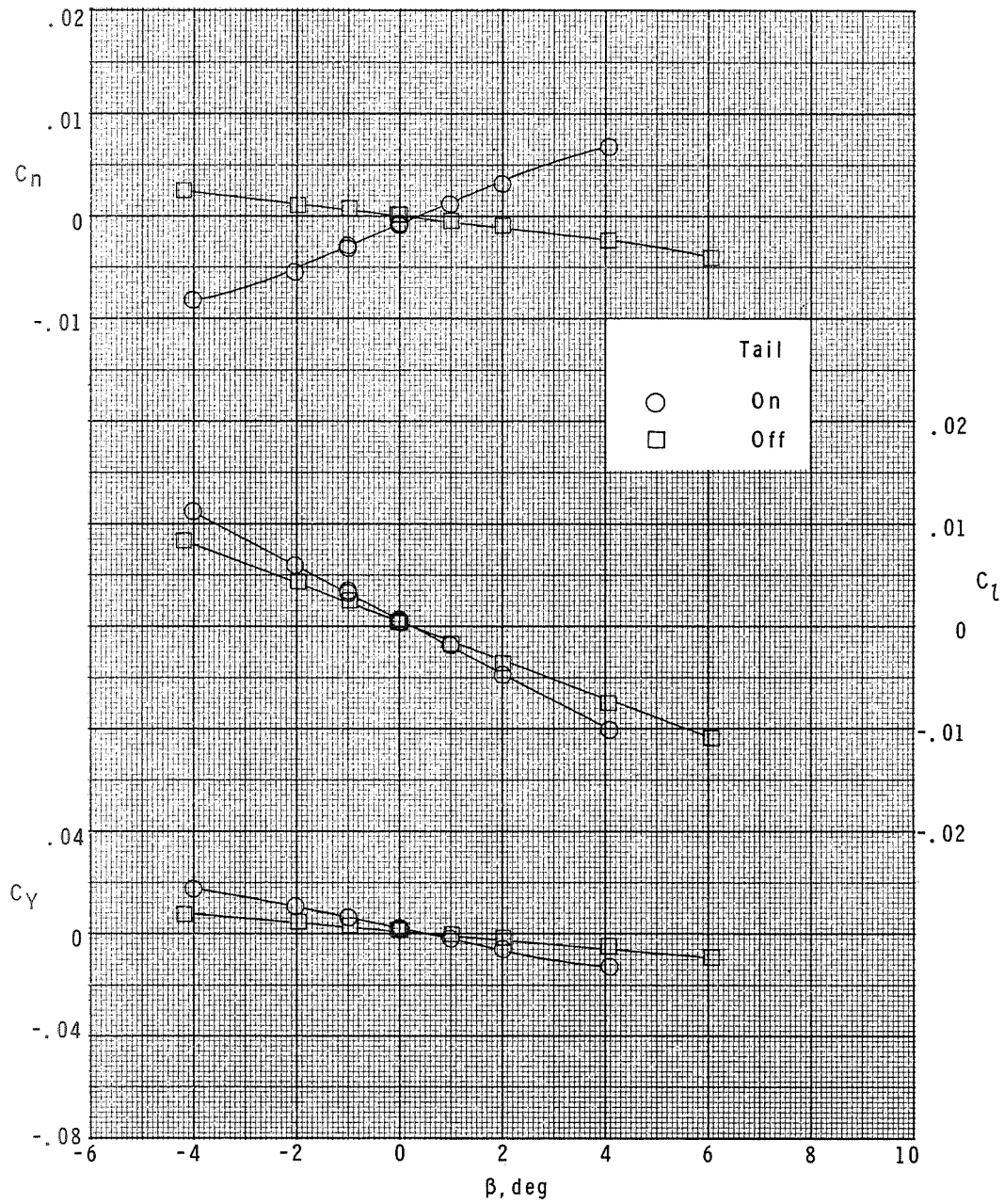
(a)  $M = 2.36$ .

Figure 14.- Lateral aerodynamic characteristics of configuration  $B_1W_2$  with and without vertical tail at  $\alpha = 8^\circ$ .



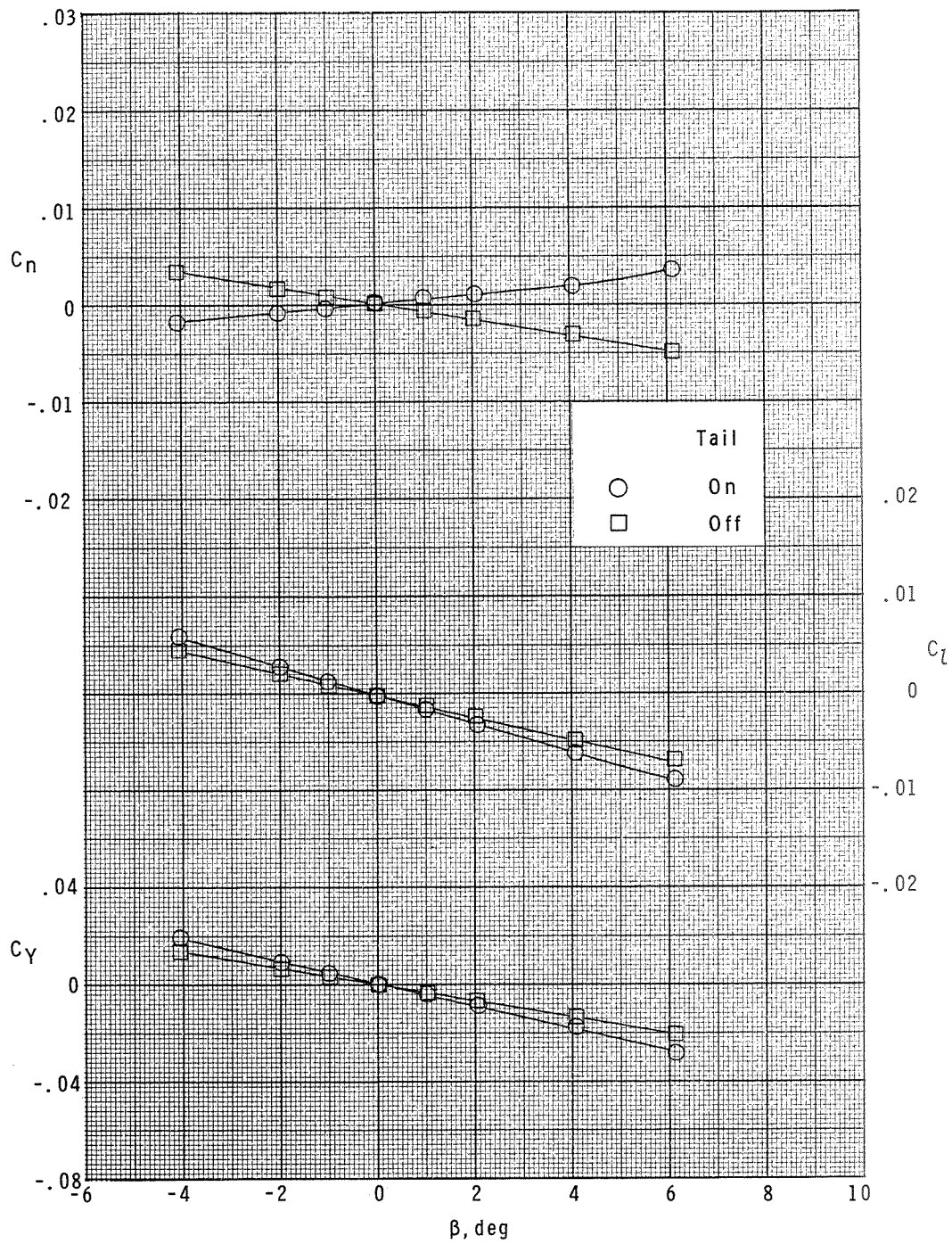
(b)  $M = 4.63$ .

Figure 14.- Concluded.



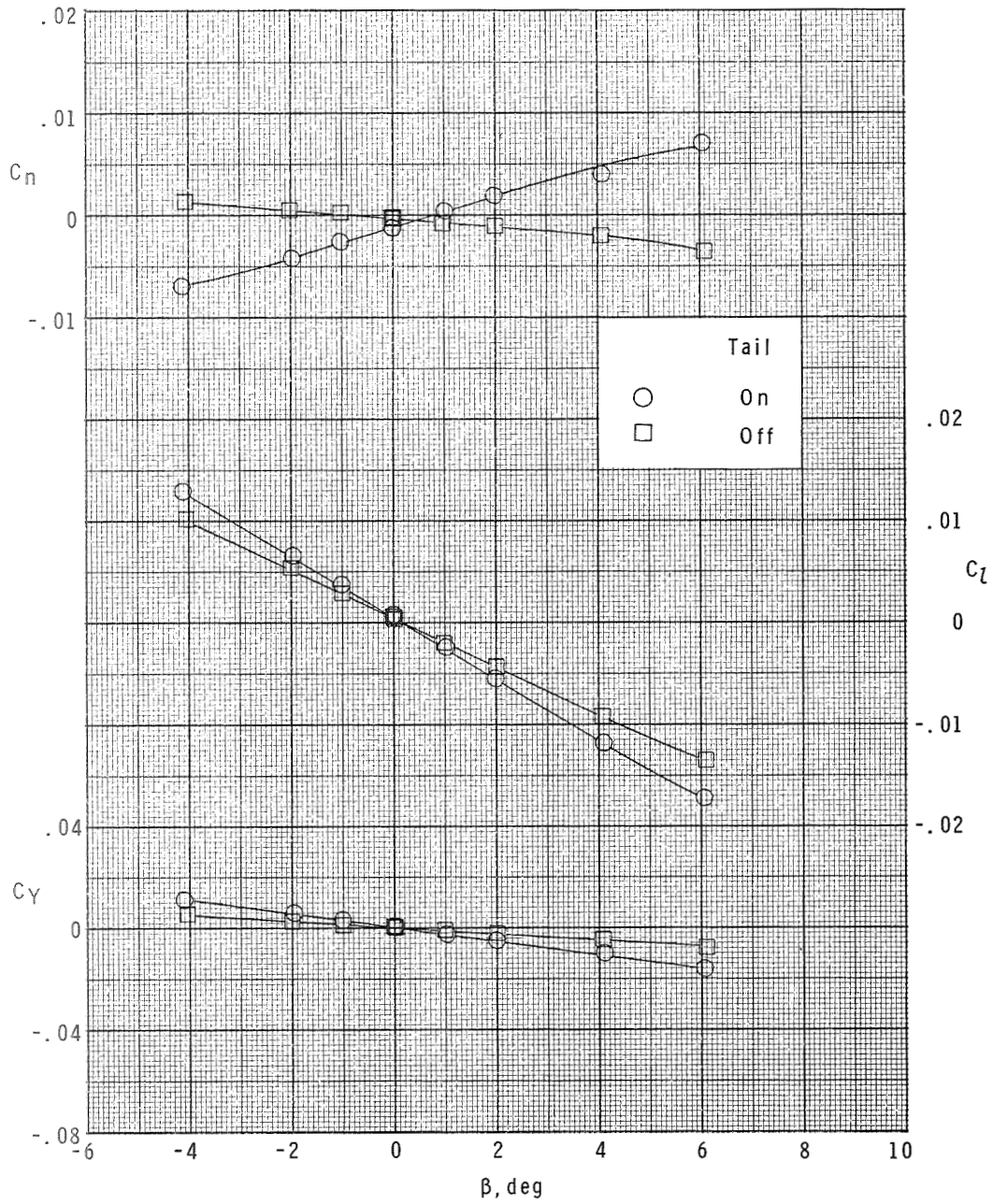
(a)  $M = 2.36$ .

Figure 15.- Lateral aerodynamic characteristics of configuration  $B_2W_2$  with and without vertical tail at  $\alpha = 8^\circ$ .



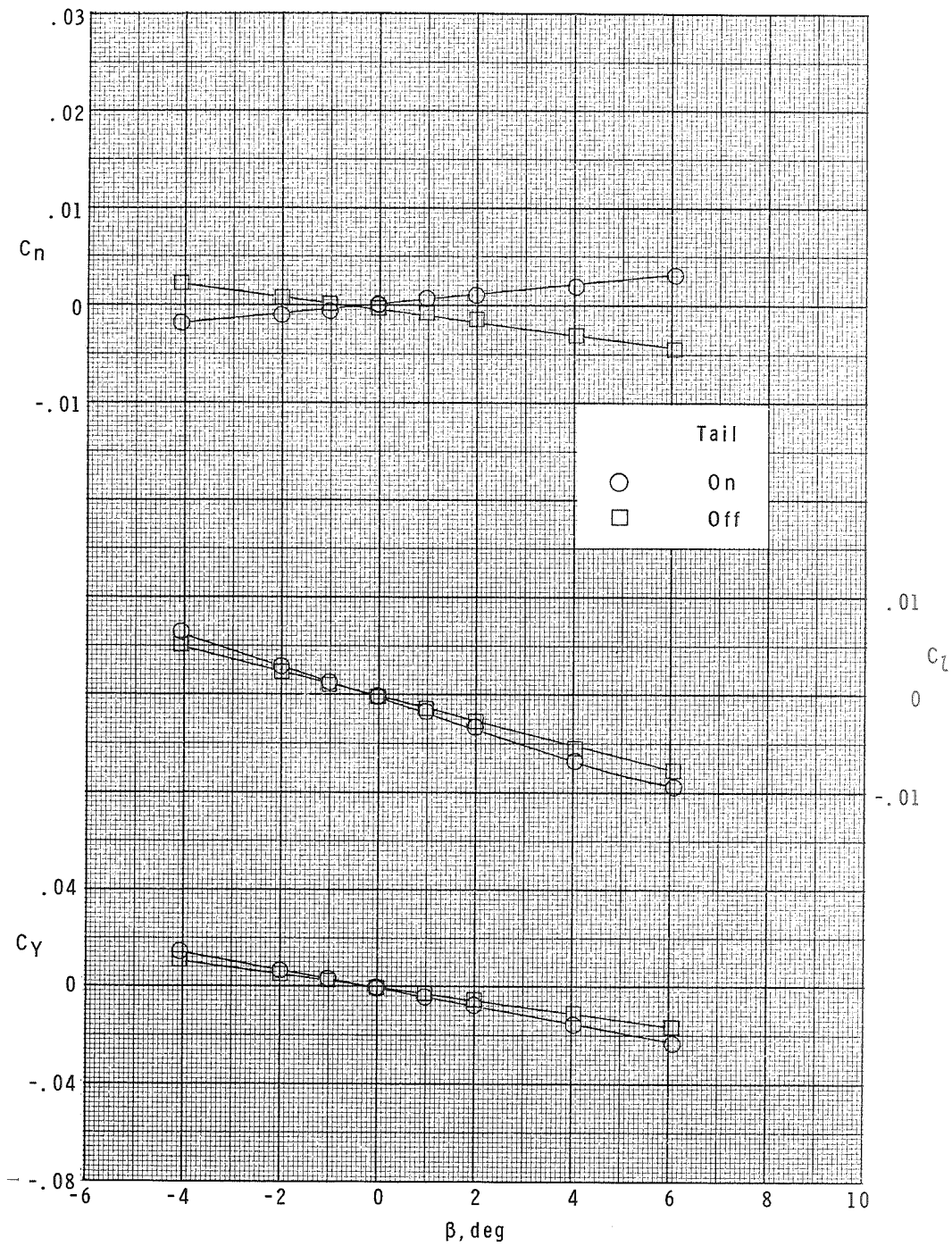
(b)  $M = 4.63$ .

Figure 15.- Concluded.



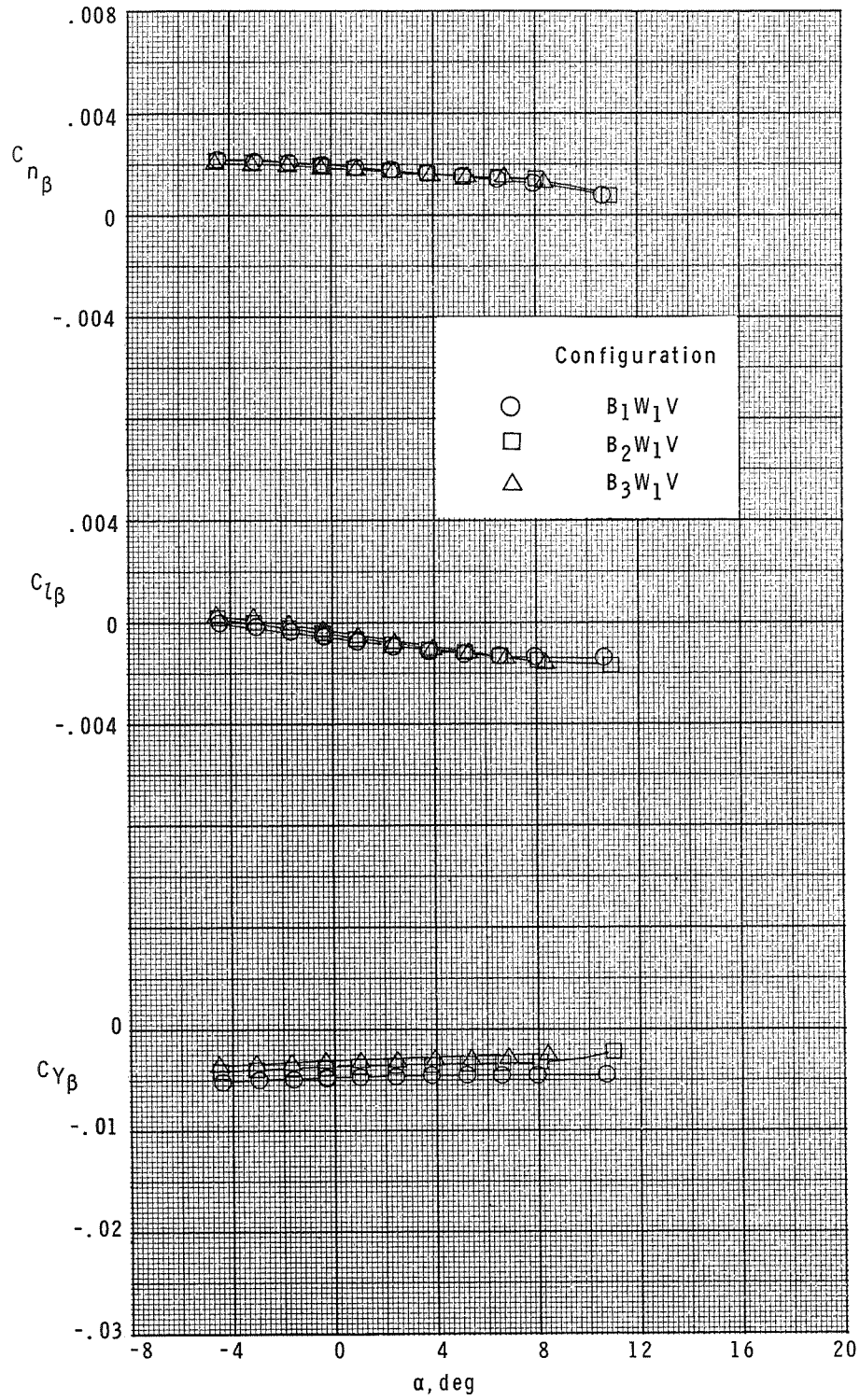
(a)  $M = 2.30$ .

Figure 16.- Lateral aerodynamic characteristics of configuration  $B_3W_2$  with and without vertical tail at  $\alpha = 8^\circ$ .



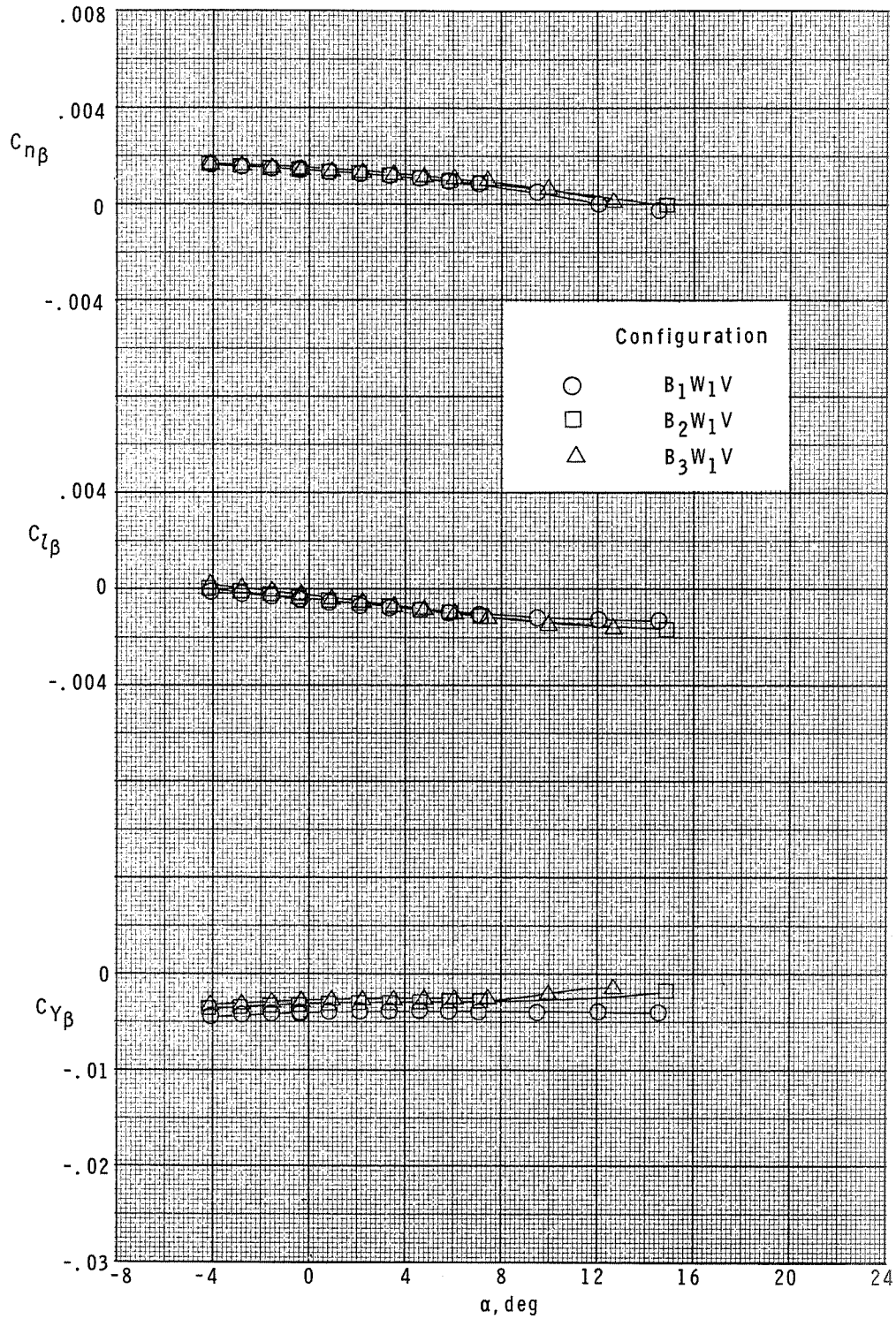
(b)  $M = 4.63$ .

Figure 16.- Concluded.



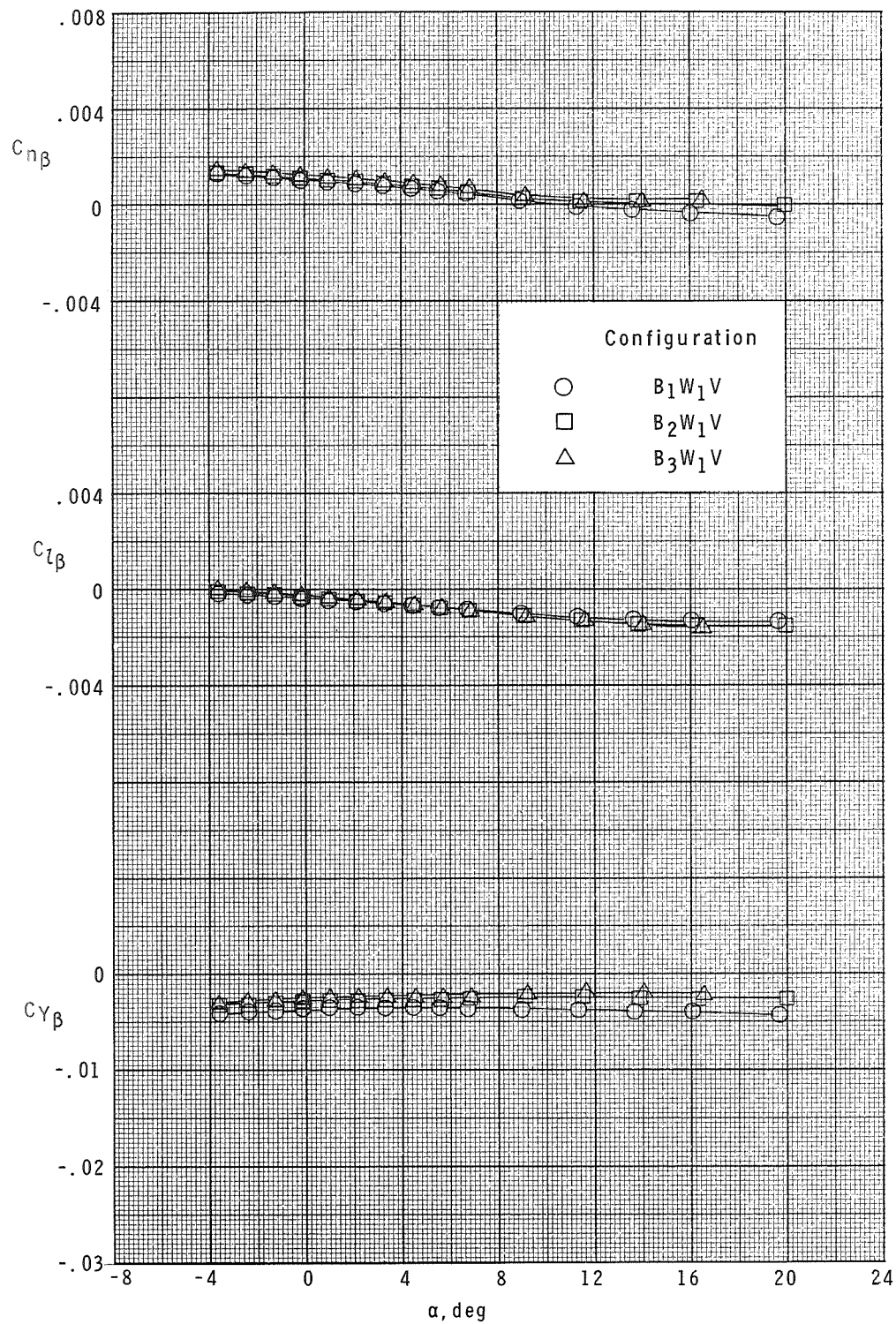
(a) M = 2.30.

Figure 17.- Effect of body shape on lateral stability derivatives of model with large (W<sub>1</sub>) wing.



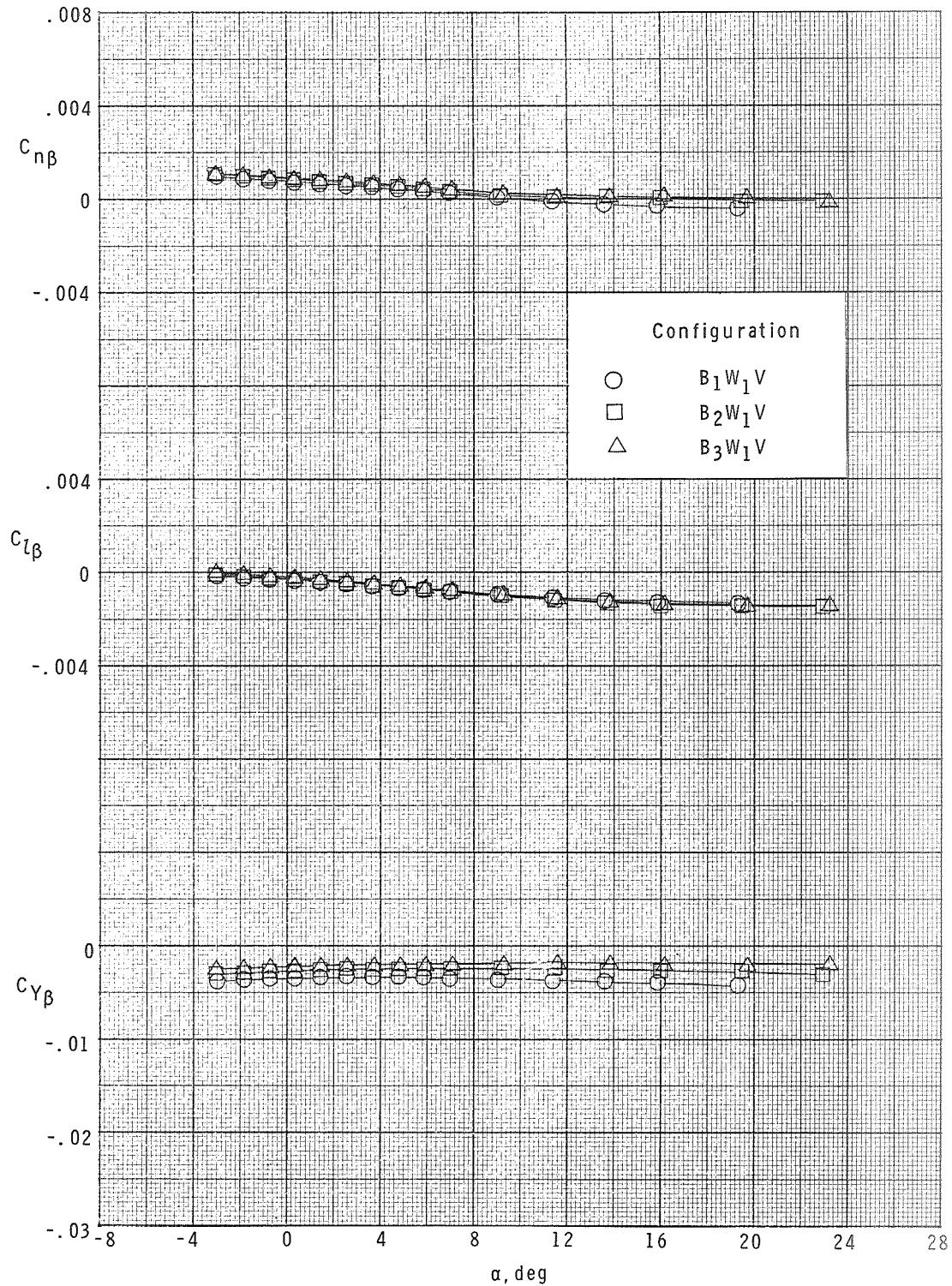
(b)  $M = 2.96$ .

Figure 17.- Continued.



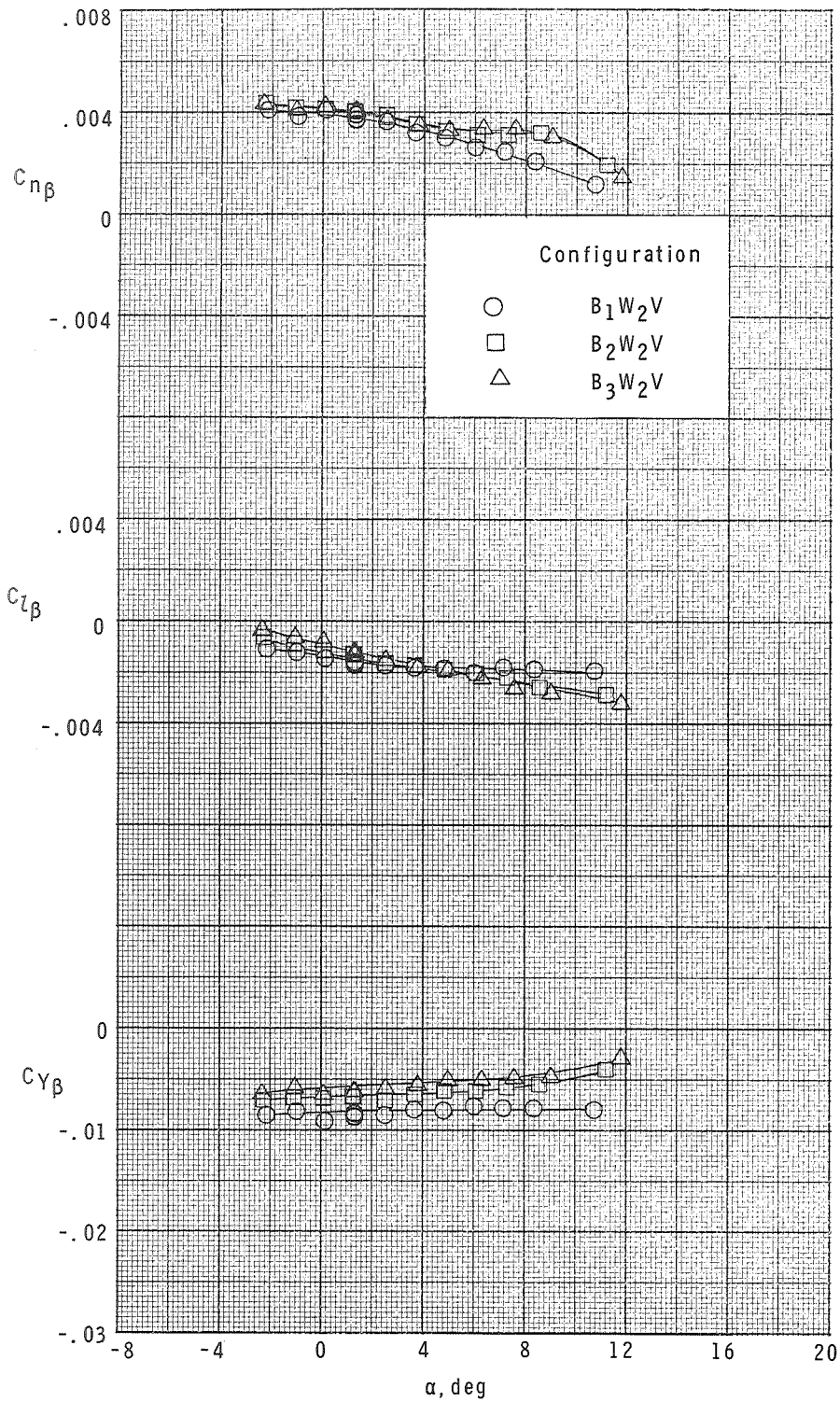
(c)  $M = 3.95$ .

Figure 17.- Continued.



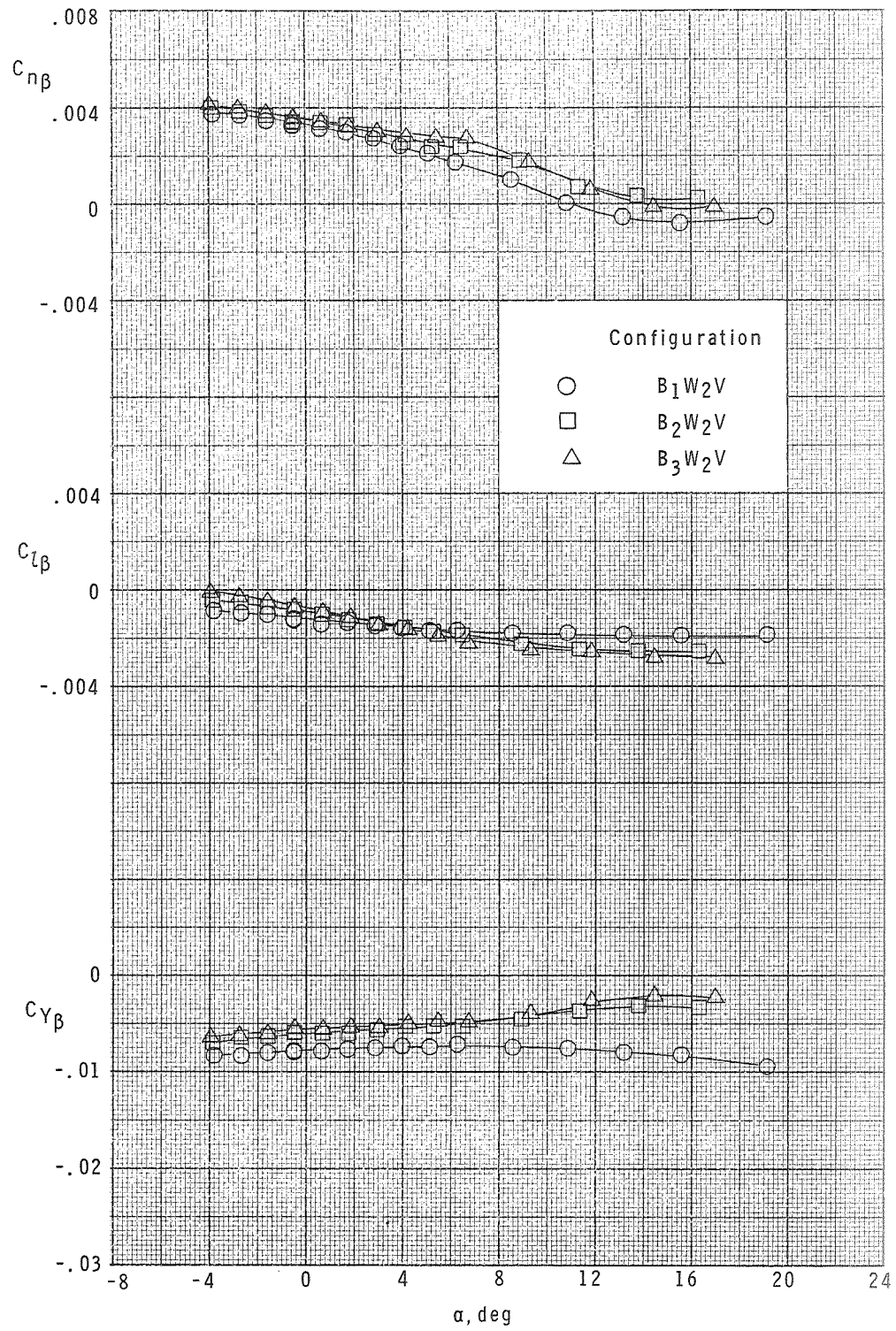
(d)  $M = 4.63$ .

Figure 17.- Concluded.



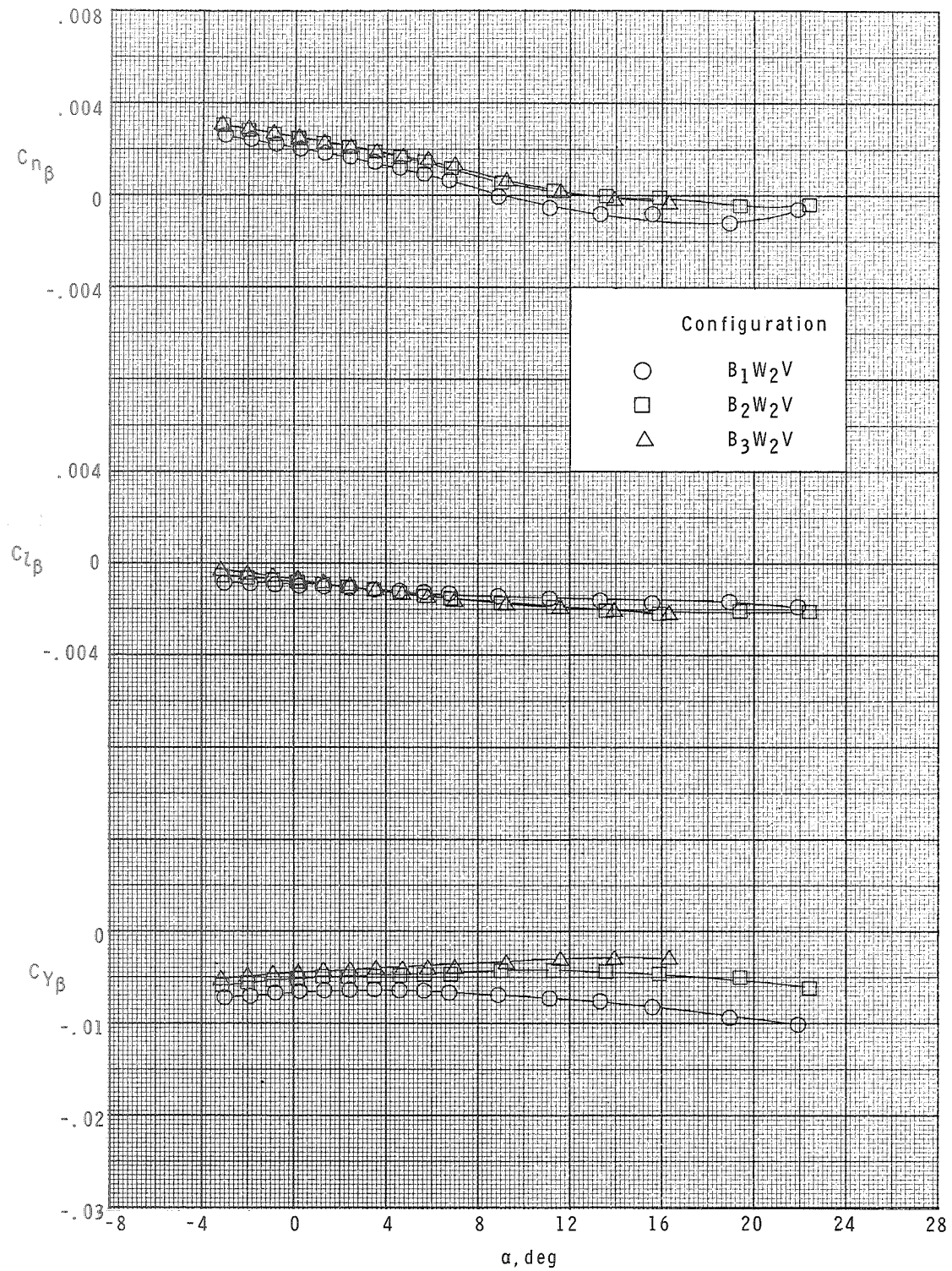
(a)  $M = 2.36$ .

Figure 18.- Effect of body shape on the lateral stability derivatives of model with intermediate-size ( $W_2$ ) wing.



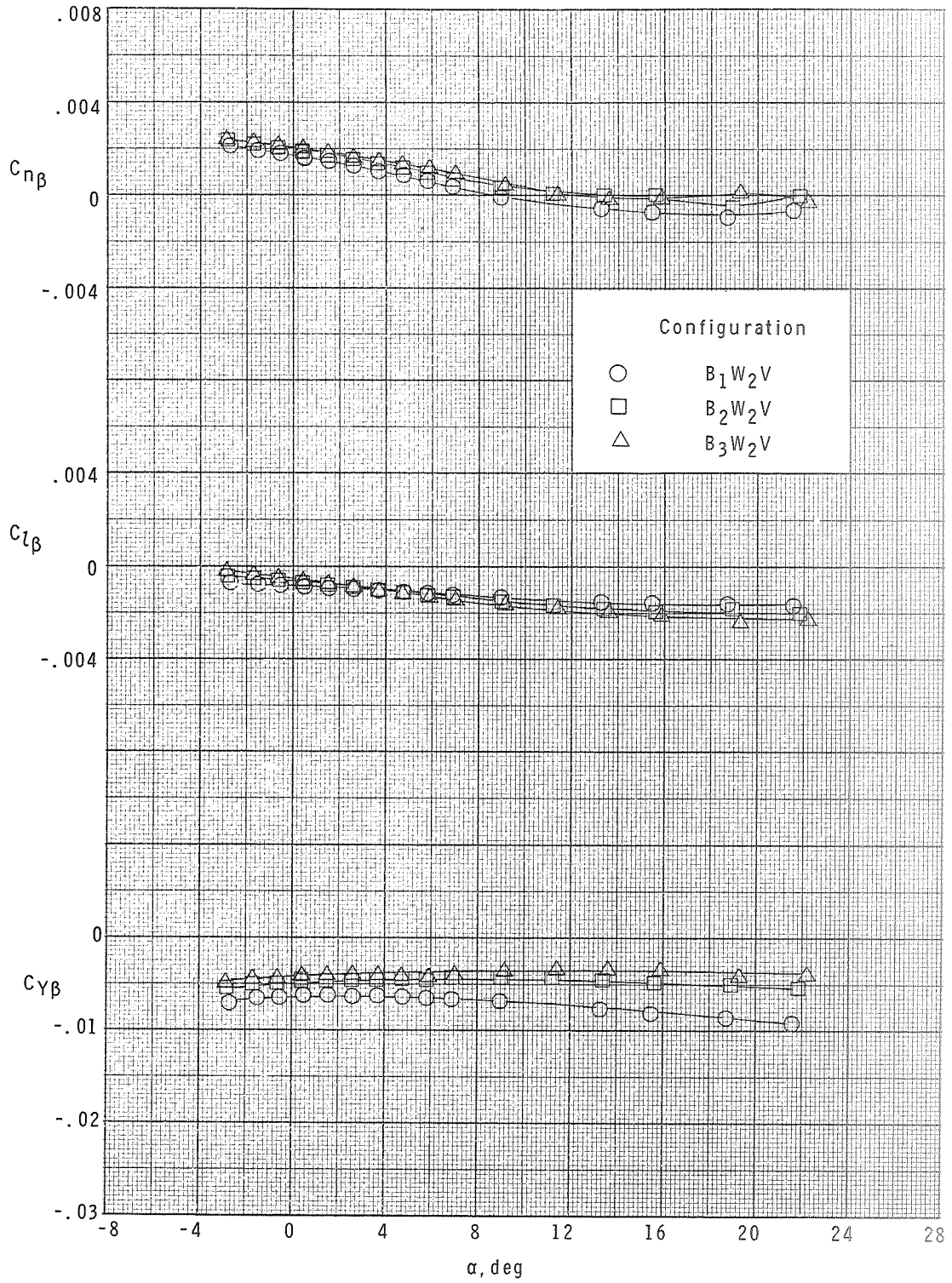
(b)  $M = 2.86$ .

Figure 18.- Continued.



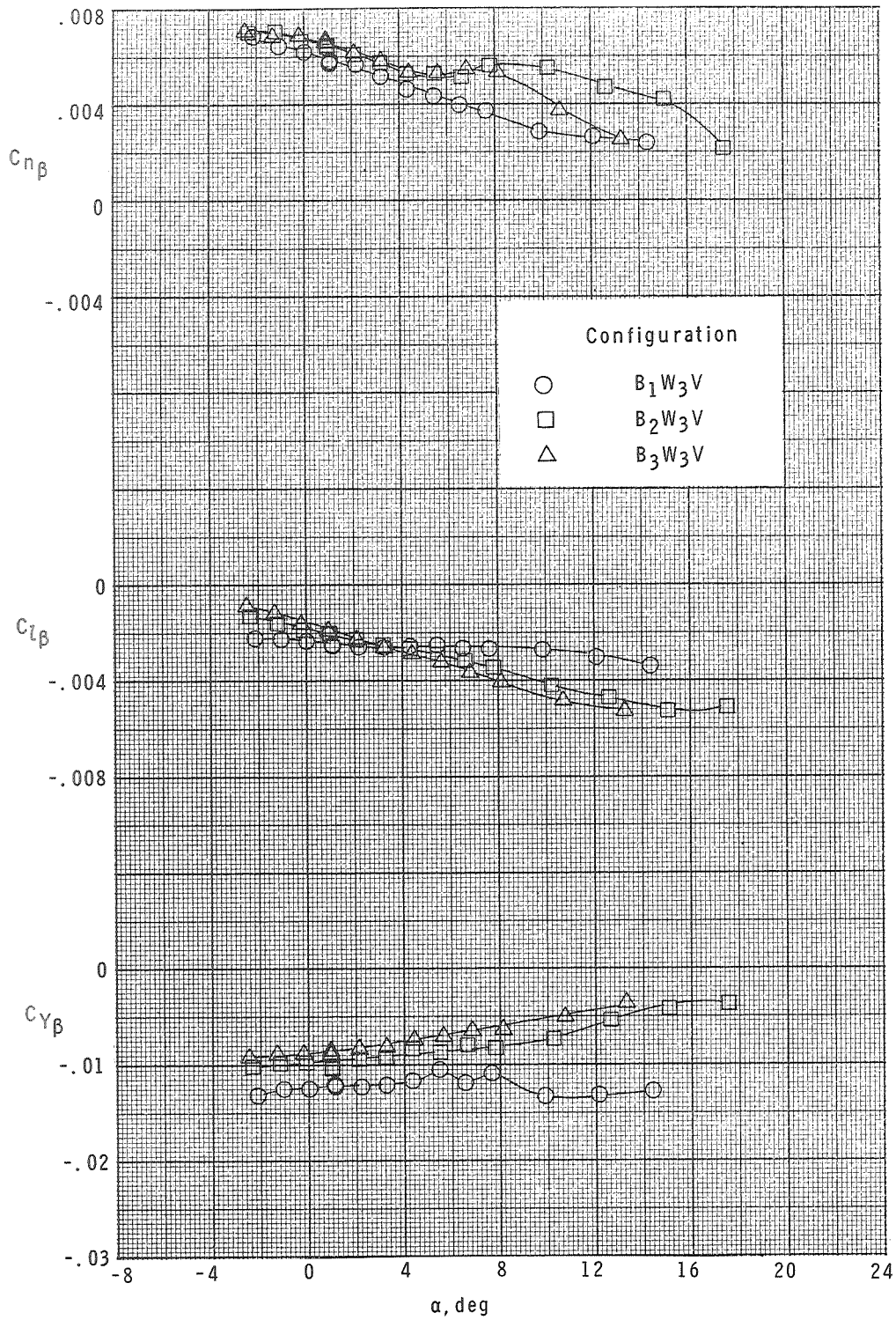
(c)  $M = 3.95$ .

Figure 18.- Continued.



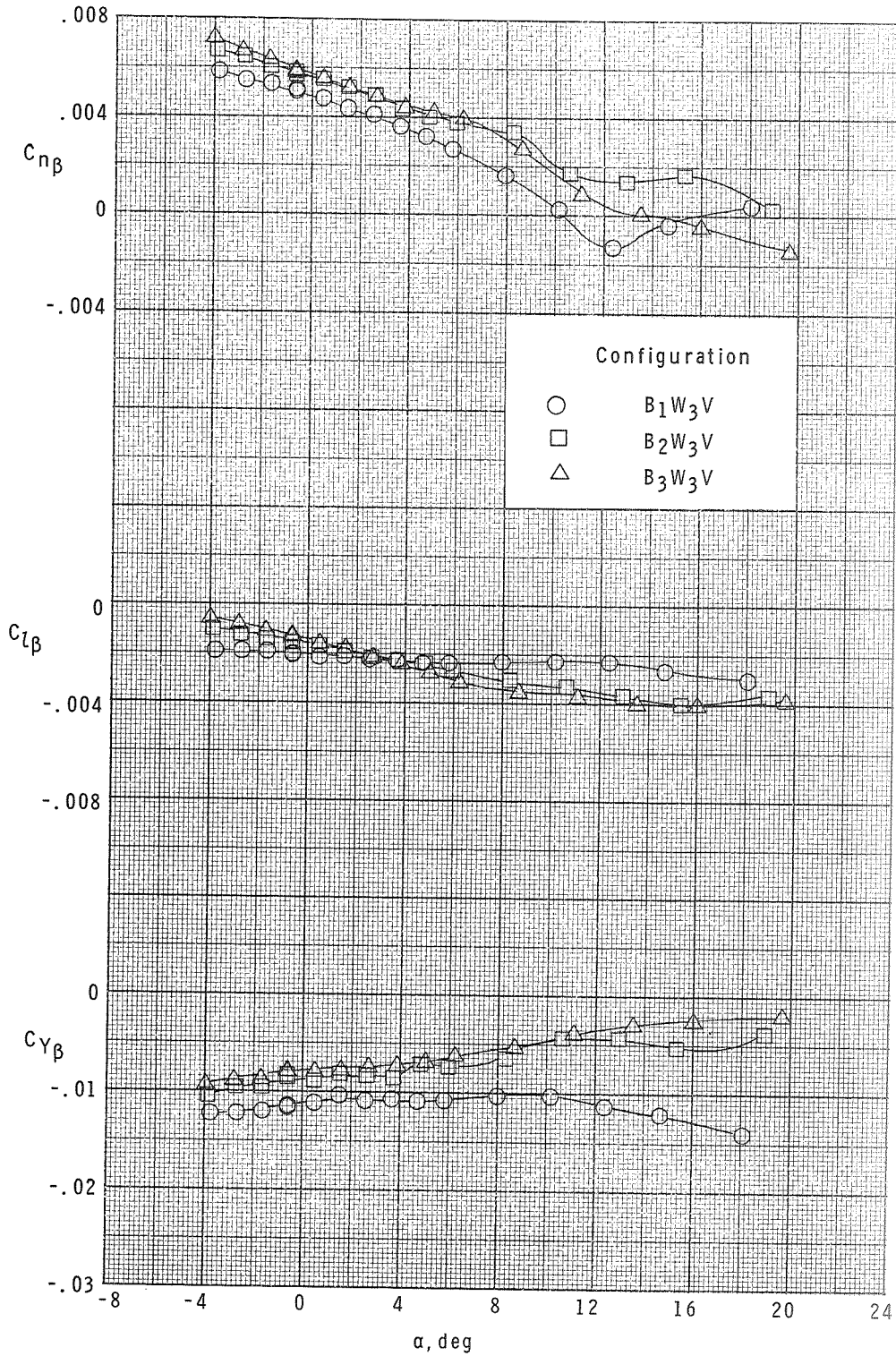
(d)  $M = 4.63$ .

Figure 18.- Concluded.



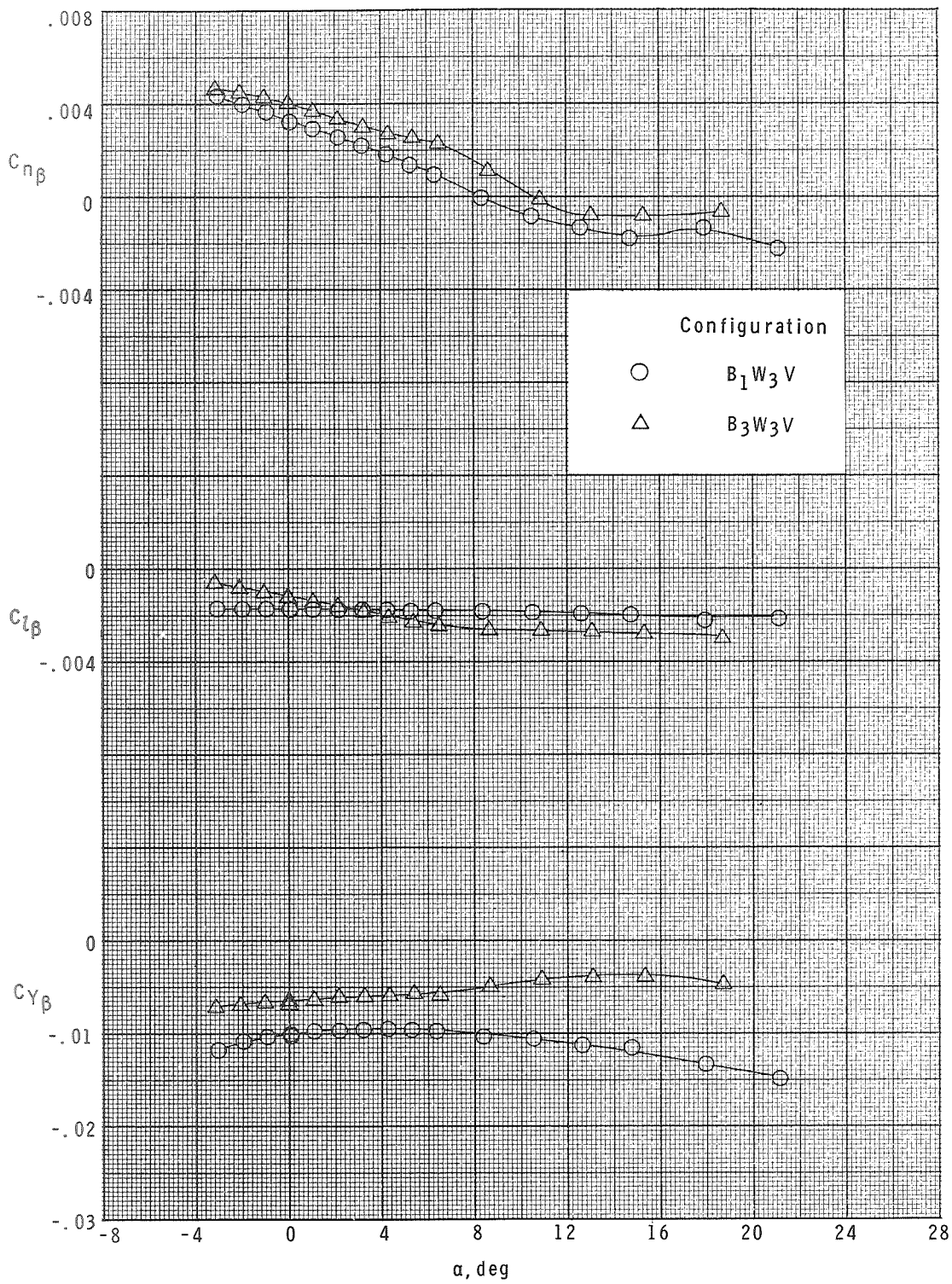
(a)  $M = 2.36$ .

Figure 19.- Effect of body shape on lateral stability derivatives of model with small ( $W_3$ ) wing.



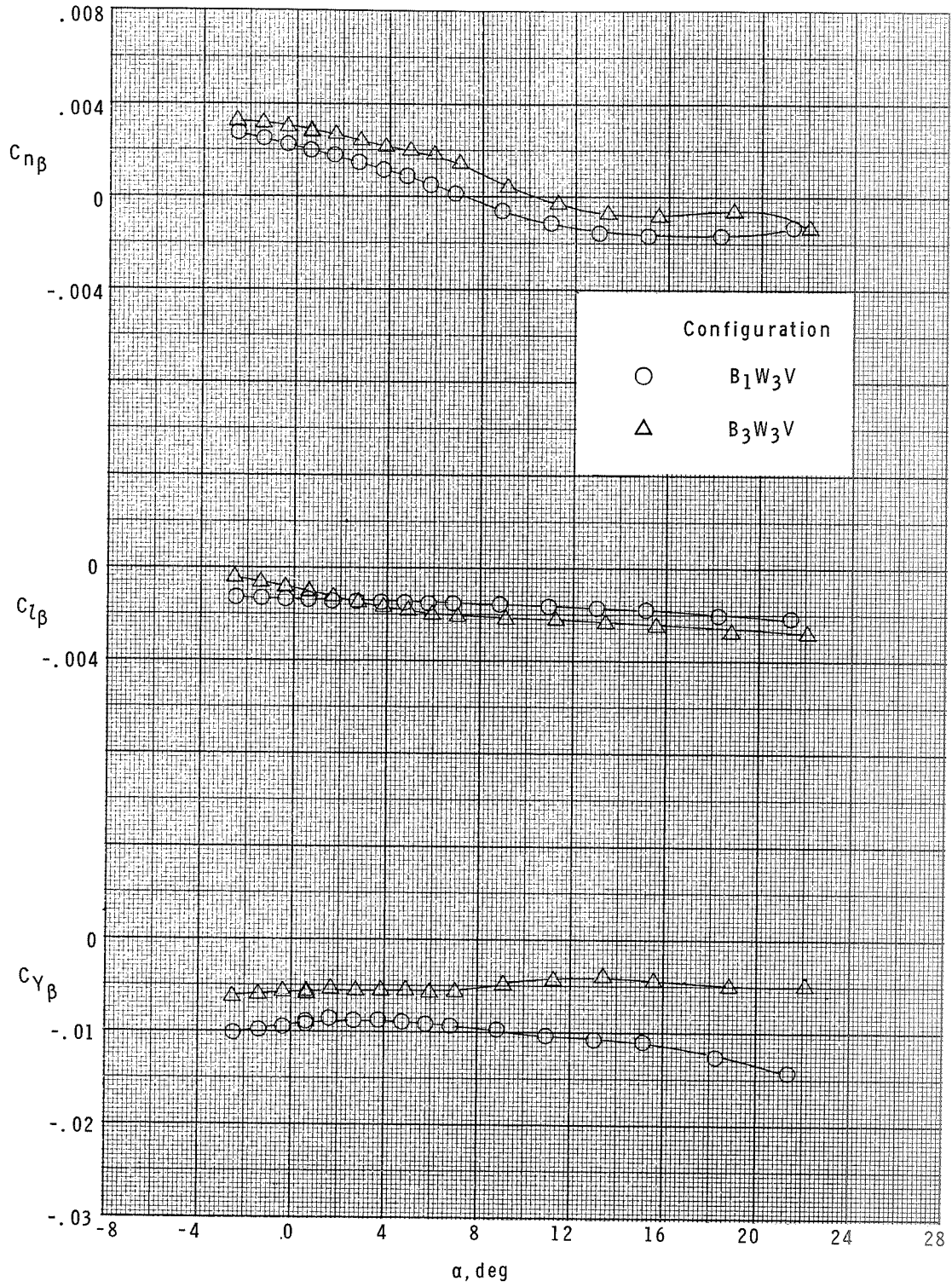
(b)  $M = 2.86$ .

Figure 19.- Continued.



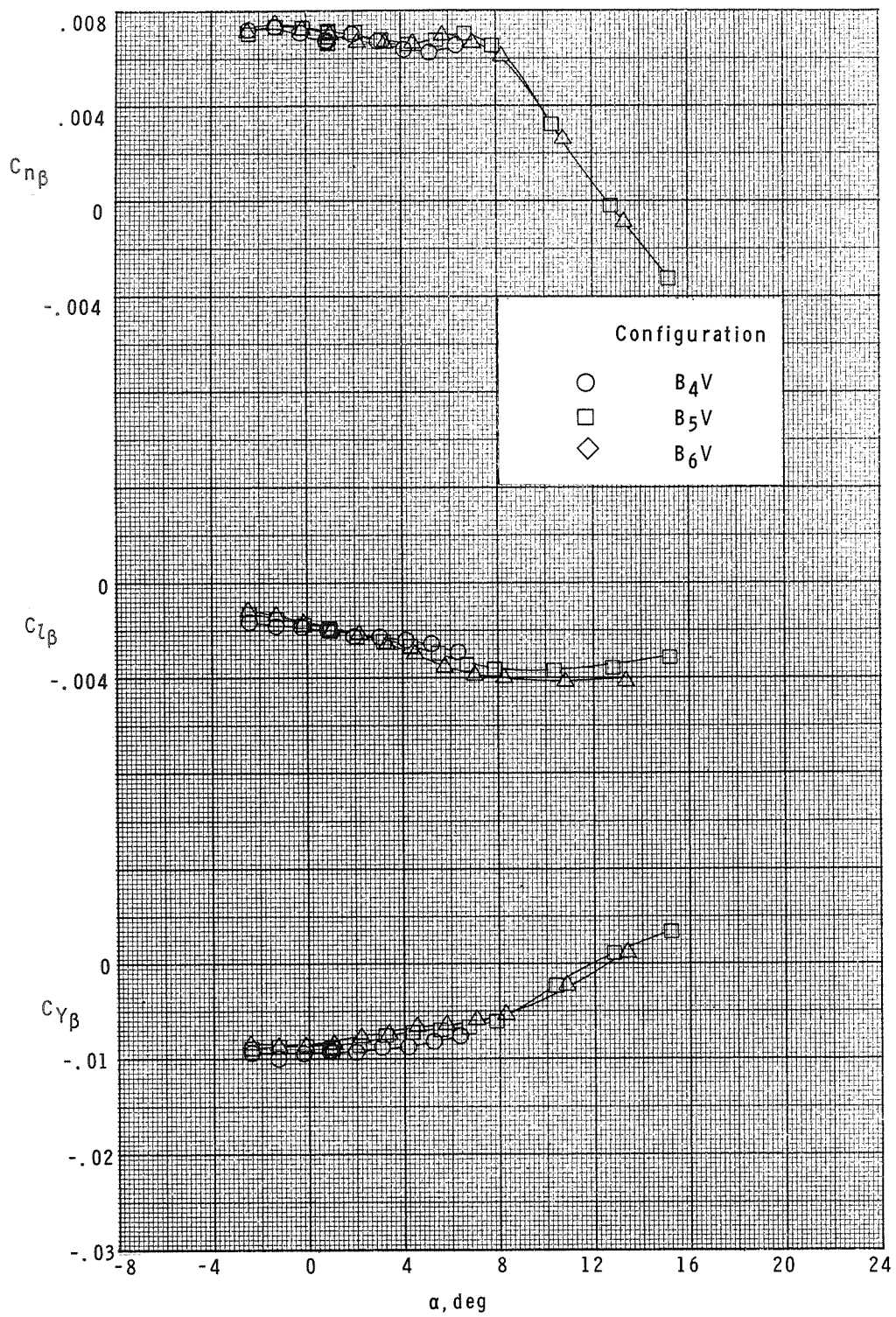
(c)  $M = 3.95$ .

Figure 19.- Continued.



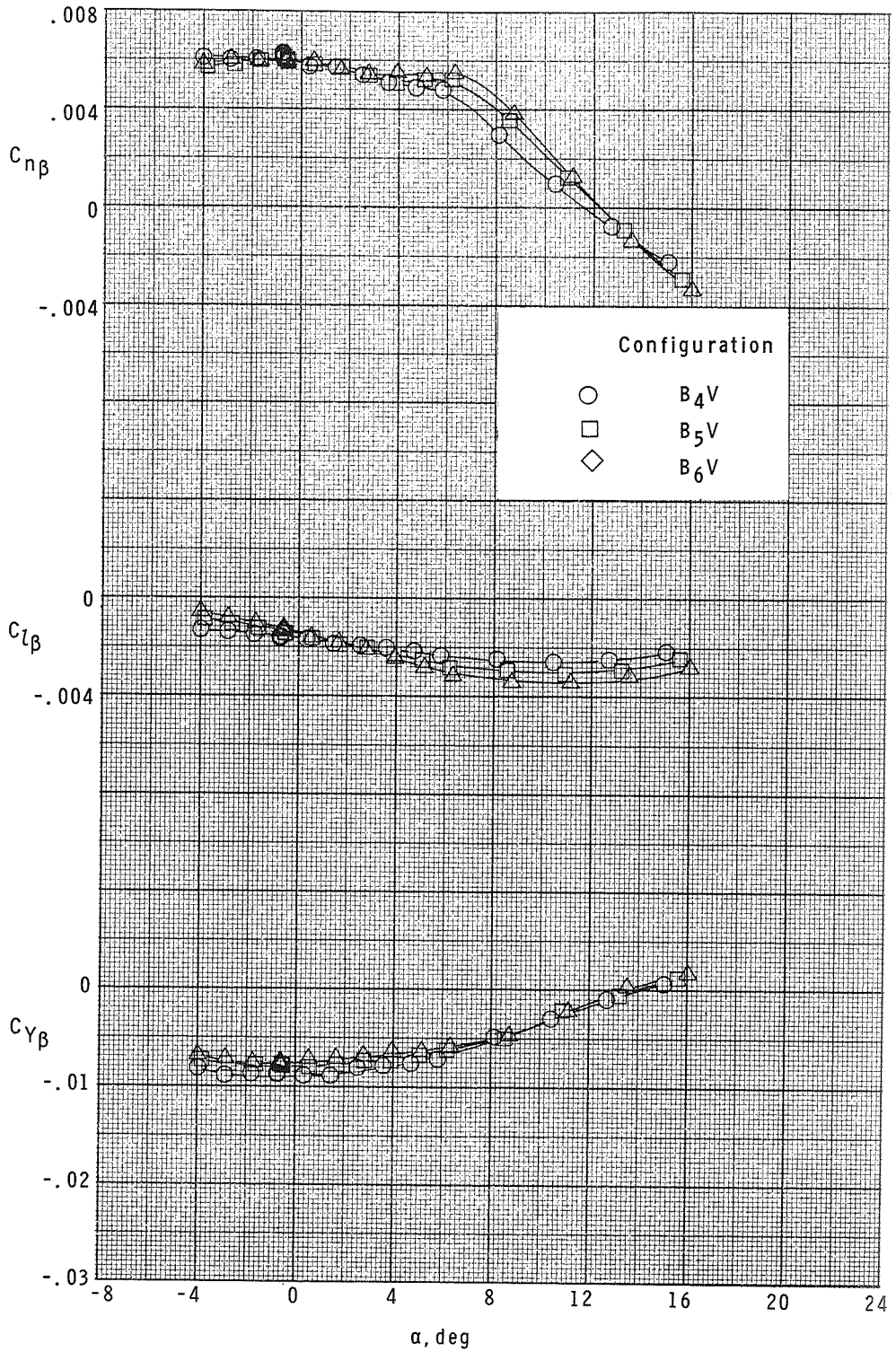
(d)  $M = 4.63$ .

Figure 19.- Concluded.



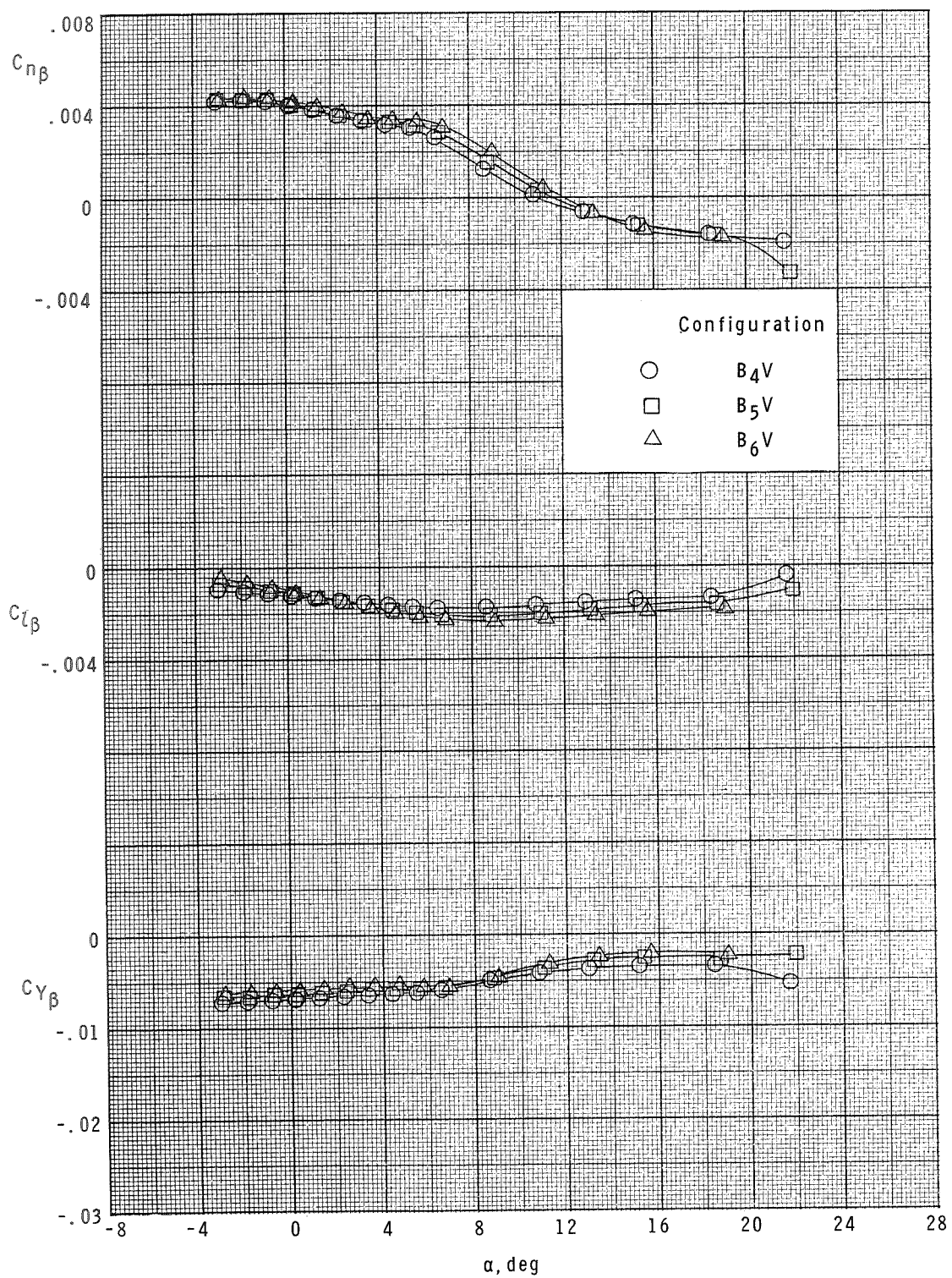
(a)  $M = 2.36$ .

Figure 20.- Effect of body shape on lateral stability derivatives of lifting-body models.



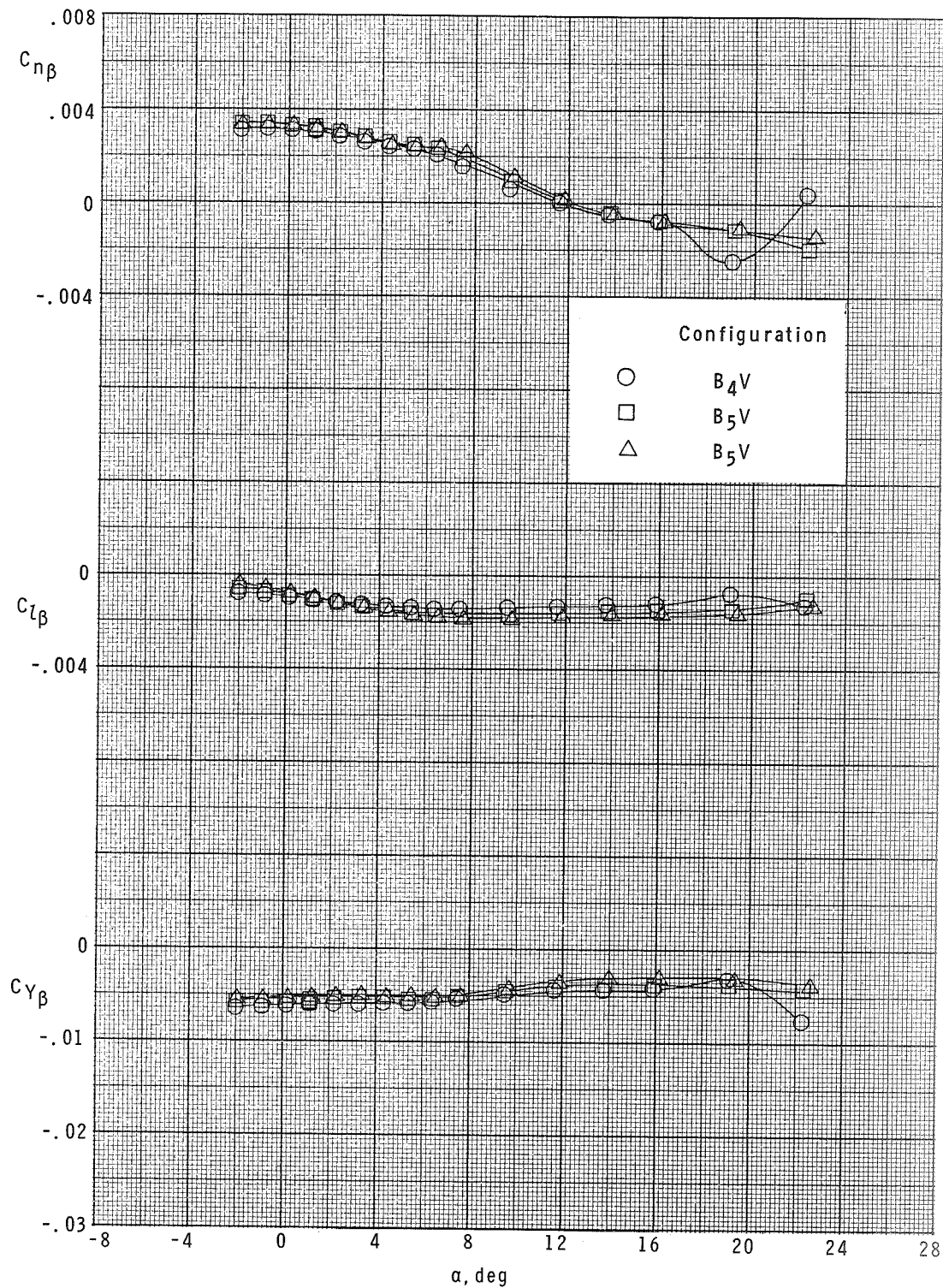
(b)  $M = 2.86$ .

Figure 20.- Continued.



(c)  $M = 3.95$ .

Figure 20.- Continued.



(d)  $M = 4.63$ .

Figure 20.- Concluded.

NATIONAL AERONAUTICS AND SPACE ADMINISTRATION  
WASHINGTON, D. C. 20546

OFFICIAL BUSINESS  
PENALTY FOR PRIVATE USE \$300

FIRST CLASS MAIL



POSTAGE AND FEES PAID  
NATIONAL AERONAUTICS AND  
SPACE ADMINISTRATION

POSTMASTER: If Undeliverable (Section 158  
Postal Manual) Do Not Return

*"The aeronautical and space activities of the United States shall be conducted so as to contribute . . . to the expansion of human knowledge of phenomena in the atmosphere and space. The Administration shall provide for the widest practicable and appropriate dissemination of information concerning its activities and the results thereof."*

— NATIONAL AERONAUTICS AND SPACE ACT OF 1958

## NASA SCIENTIFIC AND TECHNICAL PUBLICATIONS

**TECHNICAL REPORTS:** Scientific and technical information considered important, complete, and a lasting contribution to existing knowledge.

**TECHNICAL NOTES:** Information less broad in scope but nevertheless of importance as a contribution to existing knowledge.

**TECHNICAL MEMORANDUMS:** Information receiving limited distribution because of preliminary data, security classification, or other reasons.

**CONTRACTOR REPORTS:** Scientific and technical information generated under a NASA contract or grant and considered an important contribution to existing knowledge.

**TECHNICAL TRANSLATIONS:** Information published in a foreign language considered to merit NASA distribution in English.

**SPECIAL PUBLICATIONS:** Information derived from or of value to NASA activities. Publications include conference proceedings, monographs, data compilations, handbooks, sourcebooks, and special bibliographies.

**TECHNOLOGY UTILIZATION PUBLICATIONS:** Information on technology used by NASA that may be of particular interest in commercial and other non-aerospace applications. Publications include Tech Briefs, Technology Utilization Reports and Technology Surveys.

*Details on the availability of these publications may be obtained from:*

**SCIENTIFIC AND TECHNICAL INFORMATION OFFICE**

**NATIONAL AERONAUTICS AND SPACE ADMINISTRATION**

Washington, D.C. 20546